Complementary adaptations of bacterial membranes to low temperatures

Dissertation

zur

Erlangung des Doktorgrades (Dr. rer. nat.)

der

Mathematisch-Naturwissenschaftlichen Fakultät

der

Rheinischen Friedrich-Wilhelms-Universität Bonn

vorgelegt von

Alexander Flegler

aus

Taschkent, Usbekistan

Bonn 2022

Angefertigt mit Genehmigung der Mathematisch-Naturwissenschaftlichen Fakultät der
Rheinischen Friedrich-Wilhelms-Universität Bonn

1. Gutachter: Prof. Dr. André Lipski
2. Gutachterin: Priv.-Doz. Dr. Christiane Dahl

Tag der Promotion: 22.06.2022
Erscheinungsjahr: 2022

Eine Hauptursache der Armut in den Wissenschaften ist meist eingebildeter Reichtum.
Es ist nicht ihr Ziel, der unendlichen Weisheit eine Tür zu öffnen,
sondern eine Grenze zu setzen dem unendlichen Irrtum.

– Bertolt Brecht, Leben des Galilei

Table of contents

Summary

The membrane of bacteria is a crucial component that separates the cell from its environment and forms the site of essential functions such as energy generation, nutrient uptake, and sensing. Some bacteria can adapt their membrane to low temperatures by changing the endogenous fatty acid composition to maintain the biologically active liquid-crystalline phase and prevent the transition to the gel phase.

Food preservation by cold storage is indispensable to ensure food stability and safety. However, some food-associated bacteria like the zoonotic pathogen *Listeria monocytogenes* can survive and grow despite low temperatures by adjusting their fatty acid composition via *de novo* biosynthesis. Furthermore, some strains of this species can adapt by an additional, fatty acid-independent mechanism by increasing menaquinone content. Other food-associated bacteria are also thought to adapt to low temperatures by using fatty acid-independent mechanisms and incorporating synthesized carotenoids into their membrane. Therefore, in the present work, in addition to the *de novo* synthesis of fatty acids, the effects of exogenous fatty acids from the food matrix and endogenously produced menaquinones on *Listeria monocytogenes* and of endogenously produced carotenoids from food-associated pigmented bacteria were investigated as cold adaptation mechanisms.

Various supplementation and inhibition experiments, both chemical and molecular, verified the effect of the investigated bacterial membranes' fatty acid-dependent and -independent adaptation to low temperatures. Thus, *Listeria monocytogenes* incorporated exogenous fatty acids into its membrane to maintain membrane fluidization at low temperatures, revealing an unknown mechanism in this pathogen. Furthermore, the menaquinone-dependent membrane fluidization disruption resulted in lower resistance to temperature stress and lower growth rates of *Listeria monocytogenes*. The increased level of the rare C_{50} carotenoid bacterioruberin in the newly discovered food-associated bacterium *Arthrobacter bussei* and its closest relative *Arthrobacter agilis* was confirmed as a fatty acid-independent cold adaptation mechanism. In addition to chemical inhibition experiments, genetic manipulation, creating an adapted CRISPR/Cas system for *Arthrobacter* species, was used as an alternative to studying the effects of the carotenoid. Hence, the present dissertation provides new insights into the cold adaptation mechanisms in human pathogens and novel food-associated bacteria, which sheds light on a little-explored research field

and should be considered for future modeling of food stability and objective against bacterial colonization.

Preliminary remarks

List of abbreviations

AAA	aromatic amino acids	DPH	1,6-diphenyl-1,3,5-hexatriene
ANI	average nucleotide identity	EDTA	ethylenediaminetetraacetic acid
ANOVA	analysis of variance	EFSA	European Food Safety Authority
a_w	water activity	FA	fatty acid
BABR	bisanhydrobacterioruberin	FAME	fatty acids methyl ester
BLAST	Basic Local Alignment Search Tool	FASII	type II fatty acid synthesis
bp	base pair	FFP	farnesyl pyrophosphate
Casi9	catalytically inactive dead Cas9 protein	*G*	grating factor
CDC	conding DNA sequence	GC	gas chromatography
CFU	colony forming units	GGDC	Genome to Genome Distance Calculator
CrtB	phytoene synthase	GGPP	geranylgeranyl pyrophosphate
CrtD	carotenoid-3,4-desaturase	GL1	glycolipid
CrtI	phytoene desaturase (CrtI)	H	polarizer horizontal
CruF	bisanhydrobacterioruberin hydratase	*hdnO*	6-D-hydroxynicotine oxidase gene
dDDH	digital DNA-DNA hybridization	HPLC	high-performance chromatography
DHBABR	dihydrobisanhydrobacterioruberin	Idi	isopentenyl pyrophosphate isomerase
DHIDR	dihydroisopentenyldehydrorhodopin	IDR	isopentenyldehydrorhodopin
DMAPP	dimethylallyl pyrophosphate	IdsA	geranylgeranyl pyrophosphate synthase
DMDS	dimethyl disulfide	IPP	isopentenyl pyrophosphate
DMSO	dimethyl sulfoxide	KEGG	Kyoto Encyclopedia of Genes and Genomes
DNA	deoxyribonucleic acid	L1	unidentified lipid
DPG	diphosphatidylglycerol	LB	lysogeny broth

LPG	lysyl-phosphatidylglycerol
Lye	lycopene elongase
Lye	lycopene elongase/hydratase
M	mean value
m/z	mass-to-charge ratio
MCL	maximum composite likelihood
MDMMG	monoacyldimannosyl-monoacylglycerol
ME	lipid extract from milk
MEP	2-*C*-methyl-D-erythritol 4-phosphate
MK	menaquinone
MLSA	multilocus sequence analysis
MME	lipid extract from minced meat
MS	mass spectrometry
n	number of samples
NaOH	sodium hydroxide
OD	optical density
P60	polysorbate 60
P80	polysorbate 80
PBS	phosphate-buffered saline
PCR	polymerase chain reaction
PG	phosphatidylglycerol
PI	phosphatidylinositoland
PTFE	polytetrafluoroethylene
r	anisotropy
$Ri_{ai\text{-}15/ai\text{-}17}$	ratio of *anteiso*-$C_{15:0}$ to *anteiso*-$C_{17:0}$
SD	standard deviation
SSE	lipid extract from smoked salmon
TE	Tris-EDTA
TLC	thin-layer chromatography
T_m	melting temperature
TMA	1-(4-trimethylammoniumphenyl)
TSA	tryptic soy agar
TSB	tryptic soy broth
UHT	ultra-high temperature processed
UV	ultraviolet
V	polarizer vertical
Vis	visible
WAMT	weighted average melting temperature
YE	yeast extract

List of peer-reviewed publications

Flegler A, Lipski A (2022) Engineered CRISPR/Cas9 system for transcriptional gene silencing in *Arthrobacter* spp. reveals that bacterioruberin is indispensable at low temperatures. Submitted as a Short Communication in *Curr Microbiol*

Flegler A, Iswara J, Mänz AT, Schocke FS, Faßbender WA, Hölzl G, Lipski A (2022) Exogenous fatty acids affect membrane properties and cold adaptation of *Listeria monocytogenes*. *Sci Rep* 12:1499. DOI: 10.1038/s41598-022-05548-6

Flegler A, Lipski A (2022) The C_{50} carotenoid bacterioruberin regulates membrane fluidity in pink-pigmented *Arthrobacter* species. *Arch Microbiol* 204:70. DOI: 10.1007/s00203-021-02719-3

Flegler A, Kombeitz V, Lipski A (2021) Menaquinone-mediated regulation of membrane fluidity is relevant for fitness of *Listeria monocytogenes*. *Arch Microbiol* 203:3353–3336. DOI: 10.1007/s00203-021-02322-6

Flegler A, Runzheimer K, Kombeitz V, Mänz AT, Heidler von Heilborn D, Etzbach L, Schieber A, Hölzl G, Hüttel B, Woehle C, Lipski A (2020) *Arthrobacter bussei* sp. nov., a pink-coloured organism isolated from cheese made of cow's milk. *Int J Syst Evol Microbiol* 70:3027–3036. DOI: 10.1099/ijsem.0.004125

Seel W, Flegler A, Zunabovic-Pichler M, Lipski A (2018) Increased isoprenoid quinone concentration modulates membrane fluidity in *Listeria monocytogenes* at low growth temperatures. *J Bacteriol* 200:e00148-18. DOI: 10.1128/JB.00148-18

Kurth JM, Brito JA, Reuter J, Flegler A, Franke T, Klein EM, Rowe SF, Butt JN, Denkmann K, Pereira IA, Archer M, Dahl C (2016) Electron accepting units of the diheme cytochrome *c* TsdA, a bifunctional thiosulfate dehydrogenase/tetrathionate reductase. *J Biol Chem* 291:24804-24818. DOI: 10.1074/jbc.M116.753863

Conferences

Flegler A, Lipski A (2022) *Listeria monocytogenes* integrates exogenous fatty acids in its membrane (Poster). Annual Conference 2022 of the Association for General and Applied Microbiology in Düsseldorf (20–23 February 2022)

Flegler A, Lipski A (2022) Pink-pigmented *Arthrobacter* species use bacterioruberin to modulate membrane fluidity (Poster). Annual Conference 2022 of the Association for General and Applied Microbiology in Düsseldorf (20–23 February 2022)

Flegler A, Lipski A (2021) Influence of exogenous fatty acids on *Listeria monocytogenes* at low growth temperature (e-Presentation). World Microbe Forum 2021 (20–24 June 2021)

Flegler A, Kombeitz V, Lipski A (2020) Reduced menaquinone concentration decreases resistance against freeze-thaw stress and growth rate in refrigerated milk of *Listeria monocytogenes* (e-Presentation). FEMS Online Conference on Microbiology 2020 (28–31 October 2020)

Flegler A, Kombeitz V, Lipski A (2020) Inhibition of menaquinone synthesis decreases resistance against freeze-thaw stress and growth rate in refrigerated milk of *Listeria monocytogenes* (Poster). Annual Conference 2020 of the Association for General and Applied Microbiology in Leipzig (08–11 March 2020)

Flegler A, Seel W, Lipski A (2018) Inhibition of menaquinone synthesis reveals a new adaptation in membrane fluidity for *Listeria monocytogenes* strains at low temperatures (Poster). FoodMicro 2018 Conference in Berlin (3–6 September 2018)

Flegler A, Seel W, Lipski A (2018) Inhibition of isoprenoid quinone synthesis reveals the function of menaquinones in membrane adaptation to low growth temperatures for *Listeria monocytogenes* (Presentation). Annual Conference 2018 of the Association for General and Applied Microbiology in Wolfsburg (15–18 April 2018)

Chapter 1

General introduction

Of all the natural stress conditions on our planet, cold is probably the most prevalent, at least from the perspective of mesophilic and thermophilic organisms. Habitats for cold-adapted microorganisms constitute a large part of the Earth's surface. Much of the oceans, which cover about 70% of the Earth's surface, have an average temperature of – 1 to 5 °C. The polar regions, including Antarctica and the parts of North America, Europe, and Asia that lie within the Arctic Circle, account for about 20% of the Earth's land area. Alpine regions, including the mountain regions of Europe (Alps), Asia (Himalayas), and America (Rocky Mountains and South American Alps), account for another 5% of the area. Anthropogenically created habitats (e.g., refrigeration and freezing plants) represent only a tiny portion of the potential habitats for cold-adapted organisms but have significant economic relevance. Within these cold habitats, the combination of low temperatures and low availability of liquid water makes these regions extremely inhospitable to all life forms (Gerday & Glansdorff 2007).

Cold-adapted microorganisms are generally divided into two overlapping groups, the psychrophiles and psychrotrophic (or psychrotolerants). This phenotypic distinction was suggested to compare the cardinal growth temperatures of cold-adapted microorganisms. For instance, the minimum, optimum, and maximum growth temperature values are generally in the range of ≤ 0, ≤ 15, and ≤ 20 °C for psychrophilic microorganisms and ≥ 0, ≥ 20, and ≥30 °C for psychrotrophic microorganisms (Morita 1975). Psychrophiles are predominant in marine ecosystems where oceanic waters are permanently cold (< 5 °C), whereas cold-adapted microorganisms isolated from terrestrial environments, which are much more susceptible to extreme temperature fluctuations, are usually considered psychrotolerant (Bölter 2004; Helmke & Weyland 2004). There is no mandatory lower temperature limit for psychrophiles. Active cell processes of microorganisms have already been demonstrated for – 18 °C, and it is assumed that the lower limit could be reached at – 20 °C (Clarke *et al.* 2013; Margesin & Miteva 2011; Merino *et al.* 2019). Most food-relevant microorganisms, which can usually grow at 30 °C and higher, are psychrotolerants or cold-resistant mesophiles due to the fluctuating ambient temperatures to which food is generally exposed (Jay *et al.* 2005). Regarding chilling, the temperature ranges of 4–6 °C (refrigerators) and 10–12 °C (open

refrigerated cabinets) are most important. In this temperature range of 4–12 °C, psychrotrophs can grow at rates only two to four times lower than optimal at 20–30 °C (Russell 2002). In the following context, mesophilic microorganisms are defined according to their optimal growth temperature, but their metabolism exhibits a specific cold resistance so that growth at temperatures between 4 and 12 °C can be observed. Thus, cold-adapted microorganisms are of great importance for the food industry and the associated food safety.

Many foods provide an ideal matrix for various microorganisms due to their high nutrient content and water activity (a_w). The growing, industrialized production of food, significantly the increase in refrigerated and frozen foods, is bringing cold-tolerant bacteria more into the public spotlight (Sun 2016). Refrigeration is the most common way to preserve food, either alone or in combination with other methods such as the addition of preservatives. Cold-tolerant mesophilic microorganisms can pose risks as pathogens, spoilage agents, or toxin producers in the food sector. Therefore, understanding the response of food spoiling and food poisoning microorganisms to the stress caused by low temperatures is essential for developing effective preservation strategies. This knowledge is fundamental in the context of the modern demand for foods to contain fewer preservatives for more natural flavor, and digestibility since many of the significant microorganisms responsible for spoilage (e.g., *Brochothrix thermosphacta*, *Pseudomonas* spp., *Micrococcus* spp.) and poisoning (e.g., *Listeria monocytogenes*, *Yersinia enterocolitica, Campylobacter jejuni*) are psychrotrophic and psychrotolerant, respectively (Russell 2002). A vast growth temperature range characterizes them, often approaching 40 °C, unlike psychrophiles, which have a much narrower range (Margesin & Schinner 1999). Psychrotrophic microorganisms cannot grow as rapidly as psychrophilic microorganisms. Still, they can grow at low temperatures near 0 °C (e.g., 1–3 °C for strains of *L. monocytogenes*) and can proliferate when temperatures rise to room temperatures and, in the case of pathogens, to the human body temperature of 37 °C. This broad thermal capability makes them particularly important for food quality and safety (Russell 2002).

Since microorganisms are in complete thermal equilibrium with their environment, it is reasonable to assume that all structural and functional components of psychrophiles and psychrotolerants have adapted to the demands of low-temperature existence. For example, terrestrial psychrophiles might have to withstand large temperature fluctuations (– 50–25 °C for Antarctic soil organisms), desiccation, low nutrient levels, and high radiation loads, while deep-sea psychrophiles are exposed to constant low temperatures. However, the various adaptive mechanisms are not necessarily universal, as different ecological groups of psychrophiles have evolved mechanisms that suit their particular needs (Casanueva *et al.* 2010).

1 Cold adaptation of the cell membrane in bacteria

The survival of bacteria depends on the homeostasis of membrane lipids and the ability to adjust lipid composition to acclimate the bacterial cell to different environments. Bacterial membranes are composed of proteins embedded in a lipid matrix that closely resembles a phospholipid bilayer. Although there is considerable diversity in phospholipid structures in the bacterial world, most membrane phospholipids are glycerolipids containing two fatty acid chains. These phospholipid acyl chains determine membrane viscosity, affecting essential membrane-associated functions such as passive permeability of hydrophobic molecules, active solute transport, and protein-protein interactions (Zhang & Rock 2008).

Early on, it was discovered that the cytoplasmic membrane is essential for the structural integrity of the cell, separating the inner of the cell from the surroundings and thus forming a diffusion barrier. It consists of a lipid bilayer incorporating various proteins (Danielli & Davson 1935; Gorter & Grendel 1925). These membrane-associated proteins may surface on one half of the lipid layer (peripheral) or span the entire lipid bilayer (integral or transmembrane) and expand the functional spectrum of the cell membrane to include essential functions such as chemotrophic energy production, photosynthesis, cellular respiration, transport, signal transduction, etc. (Cooper & Hausman 2007; Müller-Esterl 2018; Singer & Nicolson 1972). In this context, membrane fluidity represents the parameter to ensure these membrane-associated functions and biological processes (Berg *et al.* 2018; Yoon *et al.* 2015; Zhang & Rock 2008). As a result, membrane modification with the accompanying maintenance of membrane fluidity is among the most important adaptations for growth at low temperatures (Chintalapati *et al.* 2004; Russell 2002; Zhang & Rock 2008). Here, the membrane model used to describe the biomembrane structure is based on the liquid mosaic model (Singer & Nicolson 1972). According to this model, the membrane consists of a lipid bilayer containing proteins in a liquid-crystalline phase. Since then, further insights have been gained, particularly concerning the composition and organization of the membrane. It has been shown that the membrane does not form a homogeneous phase and that microdomains can be present that differ in their composition and properties from the surrounding lipids (Brown and London 1997; Gohrbandt et al. 2022; Jacobson et al. 1995; Simons and Ikonen 1997). Phospholipids, also called

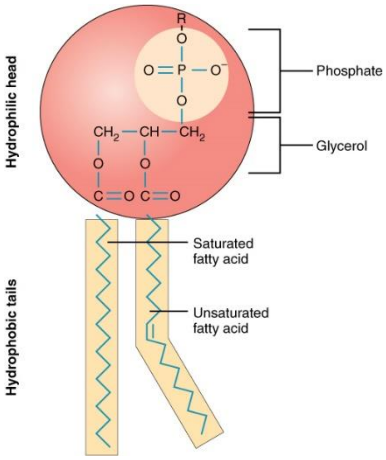

Figure 1.1 The phospholipid molecule consists of a polar phosphate "head," which is hydrophilic and a non-polar lipid "tail," which is hydrophobic. Unsaturated fatty acids result in kinks in the hydrophobic tails. Taken from (Betts *et al.* 2017). Access for free at https://openstax.org/books/anatomy-and-physiology/pages/3-1-the-cell-membrane

phosphatides, are a class of lipids whose molecules have a hydrophilic head with a phosphate group at 3-*sn* and two hydrophobic fatty acid tails esterified to a glycerol molecule at *sn*-1 and *sn*-2 (except in archaea) (Fig. 1.1). Due to their amphiphilic property, they can form lipid bilayers with dynamic structures. The membrane's lateral lipid position and orientation (rotation) can vary. Lateral diffusion is a fast process and constitutes the measure of membrane fluidity. The transfer of lipid from one membrane layer to another is called transverse diffusion or flip-flop and is a prolonged process (Voet *et al.* 2016). Bacteria can actively modulate their membrane fluidity by modifying the fatty acid composition of their lipids. This modification maintains the physiologically optimal fluid phase membrane state, i.e., the liquid-crystalline phase, in response to changing external conditions (Gounot & Russell 1999; Russell 1984; Suutari & Laakso 1994). A decrease in membrane fluidity, and the associated phase transition to a gel phase, leads to reduced growth by disrupting membrane-associated processes, such as electron transport in the respiratory chain, membrane permeability, and substrate transport (Zhang & Rock 2008). To prevent the transition from liquid-crystalline to gel phase at low temperatures, mainly fatty acids with lower melting temperatures are synthesized and incorporated into the membrane.

Lipids can assume various states, thus altering the membrane state itself (Luzzati & Tardieu 1974). Biological membranes can exist in different physical states, distinguished by their lateral organization, molecular order, and mobility of lipid molecules within the bilayer (Eeman & Deleu 2010). The three states of biological membranes are the gel, liquid-crystalline, and disordered membrane phases (Fig. 1.2). The gel phase is also called the solid-ordered phase. The lipids are arranged on a two-dimensional triangular lattice in the membrane plane (Janiak *et al.* 1979). All acyl chains have an *all*-trans configuration and are maximally stretched, resulting in an extremely ordered, compact, and viscous membrane structure. As a result, lateral diffusion of lipids is significantly reduced in this network. The acyl chains of the lipids in the gel phase can be tilted or not tilted to the membrane normal, depending on the degree of hydration. The rise in the tilt angle is accompanied by increased water content (Tardieu *et al.* 1973).

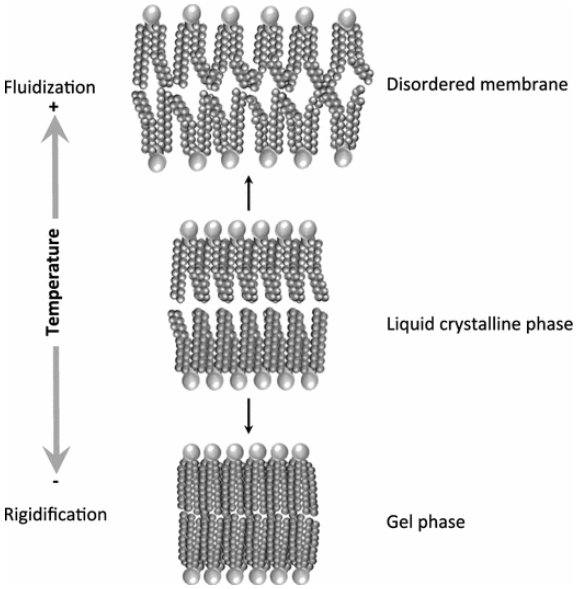

Figure 1.2. Schematic representation of changes in membrane structure and in the behavior of lipid bilayers at low and high temperatures. Low temperatures cause an increase in lipid order and rigidification of membranes, whereas high temperatures cause a decrease in lipid order and fluidization of membranes. Taken from (Los *et al*. 2013)

In the fluid-crystalline phase, also referred to as the liquid-disorder phase, *trans*-Gauche isomerization occurs, resulting in a thinner membrane. Furthermore, the degree of disorder and the distance between adjacent polar head groups increases, the thickness of the membrane decreases, and the planar lattice structure disrupts. Both lateral diffusion and rotation are favored in the liquid-crystalline phase, thus representing the physiologically active form. Therefore, lateral and total diffusion is preferred in this phase, which is the physiologically active form of the biomembrane (Eeman & Deleu 2010; Winter & Noll 2013). Heat shock or elevated temperatures lead to fluidization of the membranes, which in extreme cases can lead to a disintegration of the lipid bilayer (Horváth *et al.* 2012; Vigh *et al.* 1998).

The transition between the gel and liquid-crystalline phases occurs at a specific temperature, known as the thermotropic phase transition or synonymized as the melting temperature (T_m). It describes the temperature required to allow the melting of the membrane lipids and thus the transition of the membrane state from the gel phase to the liquid-crystalline phase and depends on the nature of the hydrophobic moiety (Eeman & Deleu 2010). Since some membrane lipids, such as phosphatidylcholines, have a pretransition temperature due to changes near the polar head group that increase its interaction with the solvent, an additional lamellar phase may occur (Heimburg 2000). For example, phosphatidylethanolamines, which differ from phosphatidylcholines by the polar head group, do not show a pretransition (McIntosh 1980). This phase, called the ripple phase, is characterized by periodic one-dimensional ripples on the surface of the lipid bilayer (Janiak *et al.* 1979). In the presence of non-membrane-forming lipids, such as cholesterol in eukaryotic cell membranes, the lipid bilayer can form an additional lamellar phase, the so-called liquid-ordered phase, which shares the properties of both gel and liquid-crystalline phases (Hjort Ipsen *et al.* 1987). As a result, the liquid-ordered phase exhibits lateral and rotational diffusion similar to the liquid-crystalline phase, but conformational ordering identical to the gel phase (Almeida *et al.* 1993; Filippov *et al.* 2003; Gally *et al.* 1976).

2 Cold adaptation in bacteria using fatty acids

Microorganisms use several mechanisms to alter the properties of their membranes, and thus membrane fluidity, in response to changes in growth temperature. One adaptation has been described as the homeoviscous adaptation and is also referred to as the fatty acid-dependent membrane adaptation in this work (Sinensky 1974). Synthesis and incorporation of fatty acids with lower T_m allow sufficient membrane fluidity at low temperatures (Gounot & Russell 1999; Suutari & Laakso 1994). This adaptation prevents changing from a fluid-disordered state to a solid-ordered gel state, impairing physiological functions and growth (Russell 1984). The membrane's fluidity is

mainly determined by the bound fatty acids of the lipids. As mentioned earlier, the melting temperature of the lipids determined whether the membrane is in the disordered fluid state ($T > T_m$) or the ordered solid-state ($T < T_m$) at a specific temperature and is dependent on the hydrophobic tails of phospholipids. Van der Waals interactions between the cylindrical acyl chains contribute to the tight packing and are effectively supported by electrostatic interactions between the polar head groups (Müller-Esterl 2018). Longer and straight-chained acyl chains form more bonds, so more energy, i.e., a higher temperature, is required for separation. Incorporating fatty acids with lower melting temperatures allows cells to maintain the membrane in the liquid-crystalline phase, thus preserving lateral diffusion within the cell membrane and associated protein functions (Chattopadhyay 2006). Therefore, fatty acids directly affect membrane fluidity (Table 1.1). Membrane fluidity decreases when longer, saturated, *trans*-double bonds or straight-chained fatty acids are present. In contrast, membrane fluidity increases when short, unsaturated, *cis*-double bonds or methyl-branched fatty acids are present (Chintalapati *et al.* 2004; Gounot & Russell 1999; Poger *et al.* 2014).

Table 1.1 Fatty acid changes increase or decrease membrane fluidity in bacteria. Taken from Gounot & Russell (1999).

Increase fluidity		Decrease fluidity
Unsaturation	↔	Saturation
cis double bond	↔	*trans* double bond
Chain shortening	↔	Chain lengthening
Methyl branching	↔	Straight chain
cis-unsaturation	↔	Cyclopropane

Bacteria modulate membrane fluidity, besides fatty acid-dependent *de novo* adaptation, with another variety of strategies, including fatty acid desaturases, changing the size and charge of polar head groups, altering the level of integral membrane proteins, and changing the composition and content of carotenoids (Chintalapati *et al.* 2004). The fatty acid desaturases, which introduce double bonds into fatty acyl chains, comprise a family of enzymes whose representatives are found only in some prokaryotes (Aguilar and Mendoza 2006) and will not be the focus of this work. However, studies have shown that not all of the above strategies have equal effectiveness. For instance, changes in polar head groups are less common and less effective in modifying membrane fluidity (Chintalapati *et al.* 2004; Denich *et al.* 2003; Russell 1998; Suutari & Laakso 1994), and changes by adjusting chain length are only possible in growing cells (Denich *et al.* 2003), this may not be the universal method for modifying membrane fluidity. In addition, proteins and lipid-protein contribute to the overall stability of the membrane bilayer through their interaction with lipids, but the effect itself is dependent on headgroup acylation, membrane fluidity, and membrane thickness, implying that it is not the primary effect on fluidity (Dumas et al. 1999; Epand 1998; Fyfe et al. 2001). Despite the generally accepted dominant endogenously fatty acid-dependent cold adaptation in bacteria, reports showed that some microbial communities did not show sufficient change in fatty acid composition and thus were partially non-compliant with this adaptation. For

example, fatty acids were extracted and identified from Antarctic soils, which showed that the proportion of expected fatty acids with low melting temperatures (unsaturated and *anteiso*-branched fatty acids) was not dominant, and in some samples, even only long degree-chain fatty acids were found (Ganzert *et al.* 2011; Margesin *et al.* 2007).

Further divergent fatty acid adaptations were detected in strains of *L. monocytogenes*. The modification of the fatty acids profile is the primary adaptation of *L. monocytogenes* to low temperatures, with branched fatty acids playing a central role (Annous *et al.* 1997; Mastronicolis *et al.* 1998; Mastronicolis *et al.* 2006; Tatituri *et al.* 2015). A high proportion of branched fatty acids 12-methyltetradecanoic acid (*anteiso*-$C_{15:0}$) and 14-methylhexadecanoic acid (*anteiso*-$C_{17:0}$) characterizes the membrane of *L. monocytogenes* and accounts for at least 85% of all membrane-associated fatty acids (Annous *et al.* 1997; Mastronicolis *et al.* 1998). Furthermore, at low temperatures, the percentage of *anteiso*-$C_{17:0}$ decreases in favor of *anteiso*-$C_{15:0}$, accounting for more than 80% of the total fatty acids. This crucial adaptation maintains the membrane fluidity at low temperatures due to the lower melting point of *anteiso*-$C_{15:0}$ (Seel *et al.* 2018).

Previous studies have described mechanisms in detail by which bacteria assimilate exogenous fatty acids (Black *et al.* 1992; Parsons *et al.* 2011; Yao *et al.* 2015; Yao *et al.* 2016a; Yao *et al.* 2016b). Besides assimilation, bacteria have various mechanisms to incorporate exogenous fatty acids into their phospholipids (Yao & Rock 2017). Since fatty acid biosynthesis is a very energy-consuming process in cell metabolism, exogenous fatty acids could imply an economic benefit (Rock & Jackowski 2002; Yao & Rock 2017; Zhang & Rock 2008). However, since the T_m of phospholipid acyl chains is crucial for regulating membrane fluidity, the energy-saving between the uptake of exogenous fatty acids and the synthesis of endogenous fatty acids must be balanced to ensure the correct biophysical properties of the membrane (Yao & Rock 2017). Most recent studies on the incorporation of exogenous fatty acids into bacteria have been conducted in the course of evaluating the potential importance of exogenous fatty acids for bacterial survival, persistence, virulence, and the development of antibiotics targeting bacterial type II fatty acid synthesis (FASII) (Baker *et al.* 2018; DeMars *et al.* 2020; Hobby *et al.* 2019; Yao & Rock 2017). In addition, some Gram-positive pathogens can incorporate fatty acids from human serum or P80 into their membrane lipids after their fatty acid biosynthesis has been inhibited (Brinster *et al.* 2009). Sarrau *et al.* (2013) showed for *Bacillus cereus* that growth impairment caused by a combination of cold and anaerobic conditions could be compensated by the presence of unsaturated fatty acids from the food or growth medium.

Despite extensive studies on *L. monocytogenes* concerning changes in fatty acid profiles in the membrane after stress, all findings argue against the uptake of exogenous fatty acids in this bacterium (Yao *et al.* 2016b; Yao and Rock 2017). However, the influence of non-synthesizable exogenous fatty acids has not yet been tested at low temperatures, and no information is available on any effects of these fatty acids on *L. monocytogenes*. In contrast, the genes for uptake and incorporation of exogenous fatty acids in *L. monocytogenes* are homologous to those in *S. aureus*. These data suggest that *L. monocytogenes* might use exogenous fatty acids from the environment, and the growth of *L. monocytogenes* may depend on the fatty acid composition of the growth matrix. The incorporation of exogenous fatty acids may either support the adaptation to low growth temperatures of the organism or negatively affect the membrane fluidity depending on the available fatty acids of the growth matrix.

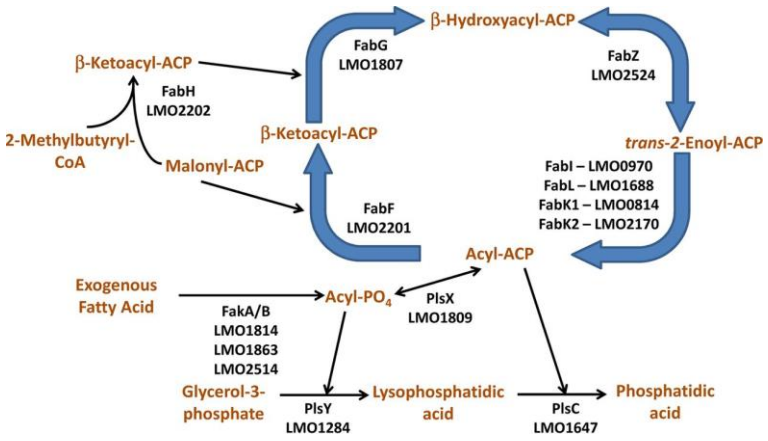

Figure 1.3 Fatty acid synthesis, phospholipid synthesis, and exogenous fatty acid incorporation system of *Listeria monocytogenes*. The locus tags for the genes in *L. monocytogenes* strain EGD-e are annotated below the enzyme symbols. The *L. monocytogenes* genome encodes the same basic type II bacterial fatty acid synthesis, acyltransferase, and exogenous fatty acid incorporation system as the characterized *S. aureus* system. Taken from Yao & Ericson *et al.* (2016b).

3 Cold adaptation in bacteria using quinones

Quinones are ubiquitous lipid-soluble molecules mainly known for their involvement in membrane-bound electron transport in the respiratory chain, including ubiquinones, menaquinones, and dimethylmenaquinones (Nowicka & Kruk 2010; Søballe & Poole 1999). Up to two electrons are transferred successively to the quinone, which simultaneously binds two protons from the inner side of the membrane, ultimately reducing hydroquinone. Upon transfer to the further electron acceptor within the respiratory chain, the hydroquinone is reduced again, and the excess protons are released outside the membrane. Within microorganisms, menaquinones are commonly associated with bacteria and archaea. In addition, ubiquinones can occur alone or combined with menaquinones within the Gram-negative alpha-, beta-, and gamma-proteobacteria (Degli Esposti 2017). As a result, and based on the different lengths and degrees of saturation, isoprenoid quinones are also suitable markers for the chemotaxonomic classification of microorganisms (Collins & Jones 1981; Jeffries *et al.* 1967).

As early as 1970, Hammond & White (1970) concluded that isoprenoid quinones might not be limited to their function of electron transport and handling of oxidative stress, but that other unknown functions must be present in the bacterial membrane. Thus, divergent fatty acid adaptations for different strains within the *L. monocytogenes* species showed a significantly weaker shift toward *anteiso*-branched fatty acids after incubation at 4 °C, suggesting other additional adaptive mechanisms to low temperatures must be present (Mastronicolis *et al.* 1998; Neunlist *et al.* 2005; Nichols *et al.* 2002). In addition to modifying the fatty acid profile, increasing menaquinone-7 (MK-7) content also regulates membrane fluidity of *L. monocytogenes* under low-temperature conditions (Seel *et al.* 2018). The steroid molecule MK-7 could embed parallel with the membrane-forming lipids and induce the previously described liquid-ordered phase state, known as the intercalation of cholesterol in eukaryotic cells (Ohvo-Rekilä 2002; Seel *et al.* 2018). Principally, low temperatures induce an increased production of MK-7 in *L*. *monocytogenes*, thus hindering and expanding the phase transition to a gel-like membrane state to maintain the membrane fluidity. This newly found adaptation mechanism requires less energy than endogenous fatty acid synthesis and is advantageous for growing under nutrient-poor growth conditions (Seel et al., 2018). According to Seel *et al.* (2018), the strains of *L*. *monocytogenes* used different cold adaptation mechanisms. For instance, *L*. *monocytogenes* strain DSM 20600^T and FFH can use both fatty acid modification and synthesis of quinone as the cold adaptation mechanisms. Meanwhile, *L*. *monocytogenes* FFL1 performed the fatty acid modification solely as the cold adaptation mechanism.

4 Cold adaptation in bacteria using carotenoids

The Earth's cryosphere has long been considered too hostile to harbor life. Nevertheless, it is precisely there that countless microorganisms can be found. Moreover, these cold-adapted bacteria and fungi inhabiting cryospheric environments produce various pigments, especially carotenoids, to survive ecological stresses (Sajjad *et al.* 2020). Therefore, the production of carotenoids by microorganisms seems crucial in these habitats (Mueller *et al.* 2005). Carotenoids are natural pigments produced by plants and microorganisms and were firstly isolated by Wackenroder (1831). Currently, carotenoids represent the largest and most diverse known group of natural pigments, and 1183 carotenoid structures are compiled from 702 parent organisms in the Carotenoid Database Japan (Yabuzaki 2017, 2020). The conjugated double bond system of the polyene chain is responsible for the characteristic yellow to red pigmentation due to blue light absorption (Britton 1995). The maximum absorption capacity of carotenoids is ranged from 440 to 520 nm. Most carotenoids (> 95%) consist of eight isoprene units, from which a C_{40} backbone is

assembled, usually with β-cyclization. Further modifications are the hydrogenation of the double bonds or the addition of polar oxygen-containing functional groups. These modifications divide carotenoids into two groups of non-oxygenated carotenes (e.g., β-carotene, lycopene) and oxygen-containing xanthophylls (e.g., lutein, zeaxanthin).

Moreover, carotenoids play a crucial role in the physiological adaptability of Antarctic microorganisms, which respond efficiently to lower temperatures and freeze-thaw cycles (Singh *et al.* 2017). Several studies reported carotenoid-producing bacteria from low-temperature environments (Sajjad *et al.* 2020). However, only a few chemoorganotrophic bacteria can produce C_{30}, C_{45}, or C_{50} carotenoids (Albermann & Beuttler 2016). For example, accumulated C_{50} carotenoid bacterioruberin and glycosylated derivatives were observed in psychrotrophic *Arthrobacter agilis* from an Antarctic sea ice sample. This accumulation of pigments may regulate cellular membrane fluidity at low temperatures (Fong *et al.* 2001).

5 Method to quantify the cold adaptation of the cell membrane

As mentioned previously, the cell's crucial parameter for cold adaptation is the membrane's fluidity. The optimal functionality of the membrane is given in the fluid-disordered phase state. However, high fluidity can also negatively affect membrane integrity (Konings *et al.* 2002; Sohlenkamp and Geiger 2016). Therefore, to measure the direct influence of the different adaptation mechanisms on the membrane, the membrane fluidity should be determined with an appropriate method. Several methods have already been mentioned in the literature for this purpose. These include dynamic differential calorimetry, Fourier transforms infrared spectroscopy, nuclear spin or electron spin resonance, generalized polarization, and fluorescence anisotropy (Denich *et al.* 2003). This work's most important selection criterion was measuring whole cells to directly assert the membrane fluidity, corresponding to the actual membrane. These factors led to the selection of fluorescence anisotropy, a probe-dependent fluorescence measurement. This is incorporated into the membrane before measurement and thus allows measurement on the intact cell, including the cell membrane. The other methods either do not allow measurements on whole living cells, or the fluidity is determined indirectly only due to a distinct phase transition.

Anisotropy measurements could be performed using the fluorescence probes 1,6-diphenyl-1,3,5-hexatriene (DPH) or 1-(4-trimethylammoniumphenyl)-6-phenyl-1,3,5-hexatriene *p*-toluenesulfonate (TMA-DPH) (Cundall *et al.* 1979). DPH and TMA-DPH spontaneously incorporate into the cell membrane of living cells, resulting in intense fluorescence, whereas no fluorescence is observed in the aqueous environment (Illinger *et al.* 1995). This characteristic makes these probes particularly suitable for measuring membrane fluidity based on fluorescence anisotropy. In this case, the mobility of the probe and the surrounding lipids is measured (Harris *et al.* 2002; Winter & Noll 2013). The principle of fluorescence anisotropy measurement is based on the photoselective absorption of the fluorophore by polarized light. The extent of absorption depends on the angle of the transition dipole moment $\overrightarrow{\mu_A}$ of the individual probe to the electric field vector $\vec{E}$ starting from the radiation source. The intense absorption and consequently emission occurs when both vectors are aligned parallel. The exit vector of the emitted photons $\overrightarrow{\mu_A}$ is not congruent to the entrance vector but is also polarized. Accordingly, the strongest fluorescence can be measured for probes at rest, where the angle between $\overrightarrow{\mu_A}$ and $\vec{E}$ changes the least due to the lack of rotation. If the probe is in rotation and has a certain relationship with the fluorescence lifetime, the emitted light will be randomly changed in its orientation. In the aggregate, the emission is now less polarized. The extent of depolarization can be calculated by using vertically polarized light for excitation and detecting the emission intensity vertically (vertical polarization) and horizontally (horizontal polarization) separately (Fig. 1.4). The rotation rate of the probe used behaves in the cell membrane in such a way that as the fluidity increases, the light is continuously depolarized and thus the anisotropy decreases (Lakowicz 2013). Since the fluorescence anisotropy values are inversely proportional to cell membrane fluidity, a high value of anisotropy represents a low value of membrane fluidity (Shinitzky & Barenholz 1978). TMA-DPH was proven to be advantageous over DPH when measuring membrane fluidity, as the former has a vertical orientation in the membrane between the polar and hydrophobic parts.

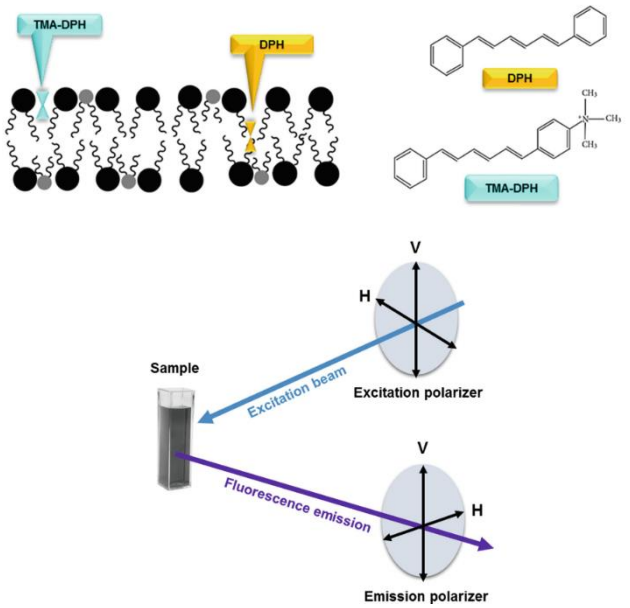

Figure 1.4 Fluorescence anisotropy experiments utilizing membrane-embedded probes. (Top) Schematic structure and localization of the fluorescent probes DPH and TMA-DPH. The scheme shows that owing to its charged group, TMA-DPH is anchored at the lipid-water interface, while DPH is inserted into the hydrophobic core of the bilayer. (Bottom) Diagram of fluorescence polarization. Each polarizer's vertical (V) and horizontal (H) orientation are presented. Taken from Malishev *et al.* (2019).

In contrast, the entirely hydrophobic DPH can also be horizontally-oriented between the two planar membrane layers, giving erroneous measurement results (Malishev et al. 2019).

6 Model organisms

Listeria monocytogenes

L. monocytogenes is a Gram-positive, facultatively anaerobic, intracellular pathogen responsible for listeriosis, a food-borne disease (Fig. 1.5). Listeriosis is a significant cause of many severe cases and deaths from food-borne diseases worldwide (Farber & Peterkin 1991). This food-borne zoonotic disease has a high mortality rate of 25–30%, usually infecting certain groups of people, especially high-risk patients such as elder persons, immunocompromised patients, or pregnant women, but can also affect people who do not have these risk factors (Hamon *et al.* 2006; Hernandez-Milian & Payeras-Cifre 2014). The health burden of outbreaks caused by *L. monocytogenes* in the EU was notable as this pathogen was responsible for 1876 confirmed invasive human cases and caused 780 hospitalizations and 167 deaths. Most of the deaths resulted from consuming fish or fish products and meat or products thereof. Although a decrease in cases was observed at the EU level in 2020, likely due to the impact of the COVID 19 pandemic, listeriosis showed a stable trend during 2016–2020 (EFSA-ECDC 2021). The ability of *L. monocytogenes* to grow at low temperatures allows this bacterium to persist in food processing plants, contaminate food, grow in ready-to-eat food under chilled storage conditions, and thus to the spread of listeriosis (Lopez-Valladares *et al.* 2018). Efforts to control the pathogen are thwarted because *L. monocytogenes* is characterized by its high tolerance to environmental factors such as extreme temperature and osmotic stress (Angelidis *et al.* 2002; Farber & Peterkin 1991; Mead *et al.* 1999). The best-known and investigated characteristic of *L. monocytogenes* is its ability to grow in a vast temperature range from – 2 to 50 °C (Farber & Peterkin 1991; Ko *et al.* 1994; Walker *et al.* 1990). For that reason, the capacity of *L. monocytogenes* to grow at low temperatures seems crucial for its ability to survive in the natural environment for long periods, which is associated with colonization, reproduction, and persistence in the food-processing environment on food-processing equipment (Buchanan *et al.* 2017; Ryser 2007). Recent outbreaks revealed the importance of risk assessment analyses, which must also include the impact of the food matrix on the growth rates and persistence of this organism under low-temperature conditions.

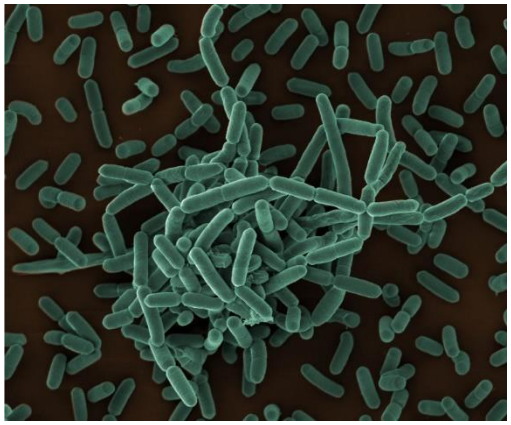

Figure 1.5 Scanning electron microscopy of *Listeria monocytogenes* wildtype EGD. Source: Petra Kaiser/RKI (2021).

Three *L. monocytogenes* strains were used in this work. Two food isolates, FFH and FFL 1, were selected and extended by the corresponding related type strain DSM 20600^T as reference. From previous publications and preliminary data, *L*. *monocytogenes* should utilize exogenous fatty acids. Additionally, some *L. monocytogenes* strains show MK-7 dependent cold adaptation, whose cell fitness interaction still left unanswered questions.

Pink-pigmented *Arthrobacter* species

The genus *Arthrobacter* is one of the numerous microorganisms that can produce pigments. Moreover, the bacteria of this genus have a wide variety of pigment colors and structures, which is quite unusual (Sutthiwong *et al.* 2014). *Arthrobacter* spp. forms a predominant group of microorganisms from various environments such as soil, air, food (e.g., dairy products), water, oil, brine, tobacco leaves, human skin, murals, clinical specimens, wastewater, and activated sludge. For many species of this group, growth at low temperatures and tolerance to high salt concentration is well-known. Therefore, *Arthrobacter* spp. can contaminate milk, dairy products, and other food products (Lipski 2022).

Various bacteria were isolated from food that exhibited temperature-dependent pigmentation in this work. In this context, a pink-pigmented species was isolated and described as *A*. *bussei*, representing a new bacterial species. Furthermore, *A*. *bussei* and the closely related species *Arthrobacter agilis* showed a high content of carotenoids at low temperatures. Thus, both species showed criteria for a fatty acid-independent cold adaptation, which was investigated in-depth.

7 Aims of the thesis

The current research primarily assumes a *de novo* fatty acid-dependent adaptation of the membrane to low temperatures of cold-adapted bacteria. However, *de novo* biosynthesis of fatty acids is very energy- and time-consuming for bacteria. In recent years, cold adaptation has been studied without considering the influence of exogenous fatty acids and membrane-associated lipophilic molecules. Additional cold adaptation mechanisms could bring a distinct advantage to bacteria in this regard. Therefore, this thesis assumes that bacterial cold adaptation is also accomplished by incorporating exogenous fatty acids from the environment or endogenously synthesized lipophilic molecules such as menaquinones and carotenoids into their membrane. Despite the highly complex membranes of bacteria due to a large variety of structure-forming compartments, fatty acids, polar lipids, quinones, and carotenoids were analyzed to obtain reliable and accurate information about the native bacterial membrane profile. Particular attention was paid to the appropriate measurement of membrane fluidity by fluorescence anisotropy. The present study combines approaches of membrane physicochemical elucidation with suitable analyses to assess the consequences of membrane fluidity at the molecular level in bacteria. As a result, alternative bacterial cold adaptation mechanisms in known and novel food-associated bacteria were investigated, revealing their advantages. A better understanding of these adaptation mechanisms and the accurate modeling of the growth in different matrices of food-associated pathogens and spoilage, thus retaining the safety and quality of cold-stored food products providing an overarching comprehension of these bacteria that survive in the largest biosphere. The specific aims of this thesis are as follows (Chapter 2–6).

- Analyses of the covalent incorporation of exogenous fatty acids from the environment into the membrane of *L. monocytogenes* and its impact on cold adaptation (Chapter 2)
- Further insights into the fatty acid-independent cold adaptation mechanism by menaquinones for the fitness and growth of *L*. *monocytogenes* (Chapter 3)
- Isolation and taxonomic characterization of a novel food-associated bacterial species exhibiting intense pigmentation by carotenoids at low temperatures (Chapter 4)
- Investigation of fatty acid-independent cold adaptation mechanisms by carotenoids on the bacterial membrane of pink-pigmented *Arthrobacter sp*. (Chapter 5)
- Further insight into the fatty acid-independent cold adaptation of pink-pigmented *Arthrobacter* sp. on the molecular level by developing an appropriate CRISPR-Cas based gene silencing system (Chapter 6)

References

Aguilar PS, Mendoza D de (2006) Control of fatty acid desaturation: a mechanism conserved from bacteria to humans. *Mol Microbiol* 62:1507–1514

Albermann C, Beuttler H (2016) Synthesis of β-carotene and other important carotenoids with bacteria. In: Vandamme EJ (ed) *Industrial Biotechnology of Vitamins, Biopigments, and Antioxidants*. John Wiley & Sons Incorporated, Weinheim

Almeida PF, Vaz WL, Thompson TE (1993) Percolation and diffusion in three-component lipid bilayers: effect of cholesterol on an equimolar mixture of two phosphatidylcholines. *Biophys J* 64:399–412

Angelidis AS, Smith LT, Hoffman LM, Smith GM (2002) Identification of *opuC* as a chill-activated and osmotically activated carnitine transporter in *Listeria monocytogenes*. *Appl Environ Microbiol* 68:2644–2650

Annous BA, Becker LA, Bayles DO, Labeda DP, Wilkinson BJ (1997) Critical role of anteiso-$C_{15:0}$ fatty acid in the growth of *Listeria monocytogenes* at low temperatures. *Appl Environ Microbiol* 63:3887–3894

Baker LY, Hobby CR, Siv AW, Bible WC, Glennon MS (2018) *Pseudomonas aeruginosa* responds to exogenous polyunsaturated fatty acids (PUFAs) by modifying phospholipid composition, membrane permeability, and phenotypes associated with virulence. *BMC Microbiol* 18:117

Berg JM, Tymoczko JL, Gatto jr. GJ, Stryer L (2018) *Stryer Biochemie*. Springer Spektrum, Berlin

Betts JG, DeSaix P, Johnson E, Johnson JE, Korol O et al. (2013) *Anatomy and Physiology*. OpenStax, Houston

Black PN, DiRusso CC, Metzger AK, Heimert TL (1992) Cloning, sequencing, and expression of the *fadD* gene of *Escherichia coli* encoding acyl coenzyme A synthetase. *J Biol Chem* 267:25513–25520

Bölter M (2004) Ecophysiology of psychrophilic and psychrotolerant microorganisms. *Cell Mol Biol* 50:563–573

Brinster S, Lamberet G, Staels B, Trieu-Cuot P, Gruss A, Poyart C (2009) Type II fatty acid synthesis is not a suitable antibiotic target for Gram-positive pathogens. *Nature* 458:83–86

Britton G (1995) Structure and properties of carotenoids in relation to function. *FASEB J* 9:1551–1558

Brown DA, London E (1997) Structure of detergent-resistant membrane domains: does phase separation occur in biological membranes? *Biochem Biophys Res Commun* 240:1–7

Buchanan RL, Gorris LG, Hayman MM, Jackson TC, Whiting RC (2017) A review of *Listeria monocytogenes*: An update on outbreaks, virulence, dose-response, ecology, and risk assessments. *Food Control* 75:1–13

Casanueva A, Tuffin M, Cary C, Cowan DA (2010) Molecular adaptations to psychrophily: the impact of 'omic' technologies. *Trends Microbiol* 18:374–381

Chattopadhyay MK (2006) Mechanism of bacterial adaptation to low temperature. *J Biosci* 31:157–165

Chintalapati S, Kiran MD, Shivaji S (2004) Role of membrane lipid fatty acids in cold adaptation. *Cell Mol Biol* 50:631–642

Clarke A, Morris GJ, Fonseca F, Murray BJ, Acton E, Price HC (2013) A low temperature limit for life on earth. *PLoS One* 8:e66207

Collins MD, Jones D (1981) Distribution of isoprenoid quinone structural types in bacteria and their taxonomic implication. *Microbiol Rev* 45:316–354.

Cooper GM, Hausman RE (2007) The cell: A molecular approach. *ASM Press*, Washington

Cundall RB, Johnson I, Jones MW, Thomas EW, Munro IH (1979) Photophysical properties of DPH derivatives. *Chem Phys Lett* 64:39–42

Danielli JF, Davson H (1935) A contribution to the theory of permeability of thin films. *J Cell Comp Physiol* 5:495–508

Degli Esposti M (2017) A journey across genomes uncovers the origin of ubiquinone in cyanobacteria. *Genome Biol Evol* 9:3039–3053.

DeMars Z, Singh VK, Bose JL (2020) Exogenous fatty acids remodel *Staphylococcus aureus* lipid composition through fatty acid kinase. *J Bacteriol* 202:e00128–20

Denich T, Beaudette L, Lee H, Trevors J (2003) Effect of selected environmental and physico-chemical factors on bacterial cytoplasmic membranes. *J Microbiol Met* 52:149–182

Dumas F, Lebrun MC, Tocanne J-F (1999) Is the protein/lipid hydrophobic matching principle relevant to membrane organization and functions? *FEBS Lett* 458:271–277.

Eeman M, Deleu M (2010) From biological membranes to biomimetic model membranes. *Biotechnol Agron Soc Environ* 14:691–708

EFSA-ECDC (2021) The European Union One Health 2020 Zoonoses Report. *EFSA J* 19:e06971.

Epand RM (1998) Lipid polymorphism and protein-lipid interactions. *BBA Rev Biomembr* 1376:353–368

Farber JM, Peterkin PI (1991) *Listeria monocytogenes*, a food-borne pathogen. *Microbiol Rev* 55:476–511

Filippov A, Orädd G, Lindblom G (2003) The effect of cholesterol on the lateral diffusion of phospholipids in oriented bilayers. *Biophys J* 84:3079–3086

Fong NJ, Burgess ML, Barrow KD, Glenn DR (2001) Carotenoid accumulation in the psychrotrophic bacterium *Arthrobacter agilis* in response to thermal and salt stress. *Appl Microbiol Biotechnol* 56:750–756

Fyfe PK, McAuley KE, Roszak AW, Isaacs NW, Cogdell RJ, Jones MR (2001) Probing the interface between membrane proteins and membrane lipids by X-ray crystallography. *Trends Biochem Sci* 26:106–112

Gally HU, Seelig A, Seelig J (1976) Cholesterol-induced rod-like motion of fatty acyl chains in lipid bilayers a deuterium magnetic resonance study. *Hoppe Seylers Z Physiol Chem* 357:1447-1450

Ganzert L, Lipski A, Hubberten H-W, Wagner D (2011) The impact of different soil parameters on the community structure of dominant bacteria from nine different soils located on Livingston Island, South Shetland Archipelago, Antarctica. *FEMS Microbiol Ecol* 76:476–491

Gerday C, Glansdorff N (2007) Physiology and Biochemistry of Extremophiles. ASM Press, Washington

Gohrbandt M, Lipski A, Grimshaw JW, Buttress JA, Baig Z et al. (2022) Low membrane fluidity triggers lipid phase separation and protein segregation in living bacteria. EMBO J:e109800.

Gorter E, Grendel F (1925) On bimolecular layers of lipoids on the chromocytes of the blood. *J Exp Med* 41:439–443

Gounot AM, Russell NJ (1999) Physiology of cold-adapted microorganisms. In: Margesin R., Schinner F. (eds) *Cold-adapted organisms: Ecology, physiology, enzymology and molecular biology*. Springer, Berlin Heidelberg.

Hammond RK, White DC (1970) Inhibition of vitamin K_2 and carotenoid synthesis in *Staphylococcus aureus* by diphenylamine. *J Bacteriol* 103:611–615.

Hamon M, Bierne H, Cossart P (2006) *Listeria monocytogenes*: a multifaceted model. *Nat Rev Microbiol* 4:423–434

Harris FM, Best KB, Bell JD (2002) Use of laurdan fluorescence intensity and polarization to distinguish between changes in membrane fluidity and phospholipid order. *BBA Biomembr* 1565:123–128

Heimburg T (2000) A model for the lipid pretransition: coupling of ripple formation with the chain-melting transition. *Biophys J* 78:1154–1165

Helmke E, Weyland H (2004) Psychrophilic versus psychrotolerant bacteria-occurrence and significance in polar and temperate marine habitats. *Cell Mol Biol* 2004 50:553–561

Hernandez-Milian A, Payeras-Cifre A (2014) What is new in listeriosis? *Biomed Res Int* 2014:358051

Hjort Ipsen J, Karlström G, Mourtisen OG, Wennerström H, Zuckermann MJ (1987) Phase equilibria in the phosphatidylcholine-cholesterol system. *BBA Biomembr* 905:162–172

Hobby CR, Herndon JL, Morrow CA, Peters RE, Symes SJK, Giles DK (2019) Exogenous fatty acids alter phospholipid composition, membrane permeability, capacity for biofilm formation, and antimicrobial peptide susceptibility in *Klebsiella pneumoniae*. *Microbiologyopen* 8:e00635

Horváth I, Glatz A, Nakamoto H, Mishkind ML, Munnik T et al. (2012) Heat shock response in photosynthetic organisms: membrane and lipid connections. Prog Lipid Res 51:208–220

Illinger D, Duportail G, Mely Y, Poirel-Morales N et al. (1995) A comparison of the fluorescence properties of TMA-DPH as a probe for plasma membrane and for endocytic membrane. *BBA Biomembr* 1239:58–66.

Jacobson K, Sheets ED, Simson R (1995) Revisiting the fluid mosaic model of membranes. *Science* 268:1441–1442

Janiak MJ, Small DM, Shipley GG (1979) Temperature and compositional dependence of the structure of hydrated dimyristoyl lecithin. *J Biol Chem* 254:6068–6078

Jay JM, Loessner MJ, Golden DA (2005) *Modern food microbiology*. Springer, New York

Jeffries L, Cawthorne MA, Harris M, Diplock AT, Green J, Price SA (1967) Distribution of menaquinones in aerobic Micrococcaceae. *Nature* 215:257-259.

Ko R, Smith LT, Smith GM (1994) Glycine betaine confers enhanced osmotolerance and cryotolerance on *Listeria monocytogenes*. *J Bacteriol* 176:426–431

Konings WN, Albers S-V, Koning S, Driessen AJ (2002) The cell membrane plays a crucial role in survival of bacteria and archaea in extreme environments. *Antonie Van Leeuwenhoek* 81:61–72

Lakowicz JR (2013) *Principles of Fluorescence Spectroscopy*. Springer Science & Business Media

Lipski A (2022) *Arthrobacter* spp. in milk and milk products. In: McSweeney PLH (ed) *Encyclopedia of Dairy Sciences*. Elsevier Science & Technology, San Diego

Lopez-Valladares G, Danielsson-Tham M-L, Tham W (2018) Implicated food products for listeriosis and changes in serovars of *Listeria monocytogenes* affecting humans in recent decades. *Foodborne Pathog Dis* 15:387–397

Los DA, Mironov KS, Allakhverdiev SI (2013) Regulatory role of membrane fluidity in gene expression and physiological functions. *Photosynth Res* 116:489–509.

Luzzati V, Tardieu A (1974) Lipid phases: Structure and structural transitions. *Annu Rev Phys Chem* 25:79–94

Malishev R, Kolusheva S, Jelinek R (2019) Vesicle-based assays to study membrane interactions of amyloid peptides. *Methods Mol* Biol 1873:39–51.

Margesin R, Miteva V (2011) Diversity and ecology of psychrophilic microorganisms. *Res Microbiol* 162:346–361

Margesin R, Schinner F (1999) *Cold-adapted organisms: Ecology, physiology, enzymology and molecular biology*. Springer, Berlin Heidelberg

Margesin R, Neuner G, Storey KB (2007) Cold-loving microbes, plants, and animals-fundamental and applied aspects. *Naturwissenschaften* 94:77–99

Mastronicolis S, German J, Megoulas N, Petrou E, Foka P, Smith G (1998) Influence of cold shock on the fatty-acid composition of different lipid classes of the food-borne pathogen *Listeria monocytogenes*. *Food Microbiol* 15:299–306

Mastronicolis SK, Boura A, Karaliota A, Magiatis P, Arvanitis N et al. (2006) Effect of cold temperature on the composition of different lipid classes of the foodborne pathogen *Listeria monocytogenes*: focus on neutral lipids. *Food Microbiol* 23:184–194

McIntosh TJ (1980) Differences in hydrocarbon chain tilt between hydrated phosphatidylethanolamine and phosphatidylcholine bilayers. A molecular packing model. *Biophys J* 29:237–245

Mead PS, Slutsker L, Dietz V, McCaig LF, Bresee JS et al. (1999) Food-related illness and death in the United States. *Emerg Infect Dis* 5:607–625

Merino N, Aronson HS, Bojanova DP, Feyhl-Buska J, Wong ML et al. (2019) Living at the extremes: Extremophiles and the limits of life in a planetary context. *Front Microbiol* 10:780

Morita RY (1975) Psychrophilic bacteria. *Bacteriol Rev* 39:144–167

Mueller DR, Vincent WF, Bonilla S, Laurion I (2005) Extremotrophs, extremophiles and broadband pigmentation strategies in a high arctic ice shelf ecosystem. *FEMS Microbiol Ecol* 53:73–87

Müller-Esterl W (2018) Struktur und Dynamik biologischer Membranen. In: Müller-Esterl W (ed) *Biochemie*. Springer, Berlin Heidelberg

Neunlist MR, Federighi M, Laroche M, Sohier D, Delattre G et al. (2005) Cellular lipid fatty acid pattern heterogeneity between reference and recent food isolates of *Listeria monocytogenes* as a response to cold stress. *Antonie Van Leeuwenhoek* 88:199–206

Nichols DS, Presser KA, Olley J, Ross T, McMeekin TA (2002) Variation of branched-chain fatty acids marks the normal physiological range for growth in *Listeria monocytogenes*. *Appl Environ Microbiol* 68:2809–2813

Nowicka B, Kruk J (2010) Occurrence, biosynthesis and function of isoprenoid quinones. *BBA* 1797:1587–1605.

Ohvo-Rekilä H (2002) Cholesterol interactions with phospholipids in membranes. *Prog Lipid Res* 41:66–97

Parsons JB, Frank MW, Subramanian C, Saenkham P, Rock CO (2011) Metabolic basis for the differential susceptibility of Gram-positive pathogens to fatty acid synthesis inhibitors. *Proc Natl Acad Sci USA* 108:15378–15383

Poger D, Caron B, Mark AE (2014) Effect of methyl-branched fatty acids on the structure of lipid bilayers. *J Phys Chem B* 118:13838–13848

Rock CO, Jackowski S (2002) Forty years of bacterial fatty acid synthesis. *Biochem Biophys Res Commun* 292:1155–1166

Russell NJ (1984) Mechanisms of thermal adaptation in bacteria: blueprints for survival. *Trends Biochem Sci* 9:108–112

Russell NJ (1998) Molecular adaptations in psychrophilic bacteria: Potential for biotechnological applications. In: Antranikian G (ed) *Biotechnology of Extremophiles*. Springer, Berlin Heidelberg

Russell NJ (2002) Bacterial membranes: the effects of chill storage and food processing. An overview. *Int J Food Microbiol* 79:27–34

Ryser ET (2007) *Listeria, listeriosis, and food safety*. CRC Press, Boca Raton

Sajjad W, Din G, Rafiq M, Iqbal A, Khan S et al. (2020) Pigment production by cold-adapted bacteria and fungi: colorful tale of cryosphere with wide range applications. *Extremophiles* 24:447–473

Sarrau B de, Clavel T, Zwickel N, Despres J, Dupont S et al. (2013) Unsaturated fatty acids from food and in the growth medium improve growth of *Bacillus cereus* under cold and anaerobic conditions. *Food Microbiol* 36:113–122

Seel W, Flegler A, Zunabovic-Pichler M, Lipski A (2018) Increased isoprenoid quinone concentration modulates membrane fluidity in *Listeria monocytogenes* at low growth temperatures. *J Bacteriol* 200:e00148-18

Shinitzky M, Barenholz Y (1978) Fluidity parameters of lipid regions determined by fluorescence polarization. *BBA Rev Biomembr* 515:367–394

Simons K, Ikonen E (1997) Functional rafts in cell membranes. *Nature* 387:569–572

Sinensky M (1974) Homeoviscous adaptation--a homeostatic process that regulates the viscosity of membrane lipids in *Escherichia coli*. *Proc Natl Acad Sci USA* 71:522–525

Singer SJ, Nicolson GL (1972) The fluid mosaic model of the structure of cell membranes. *Science* 175:720–731

Singh A, Krishnan KP, Prabaharan D, Sinha RK (2017) Lipid membrane modulation and pigmentation: A cryoprotection mechanism in Arctic pigmented bacteria. *J Basic Microbiol* 57:770–780

Søballe B, Poole RK (1999) Microbial ubiquinones: multiple roles in respiration, gene regulation and oxidative stress management. *Microbiol* 145:1817–1830.

Sohlenkamp C, Geiger O (2016) Bacterial membrane lipids: diversity in structures and pathways. *FEMS Microbiol Rev* 40:133–159

Sun D-W (2016) *Handbook of Frozen Food Processing and Packaging*. CRC Press, Boca Raton

Sutthiwong N, Fouillaud M, Valla A, Caro Y, Dufossé L (2014) Bacteria belonging to the extremely versatile genus *Arthrobacter* as novel source of natural pigments with extended hue range. *Food Res Int* 65:156–162

Suutari M, Laakso S (1994) Microbial fatty acids and thermal adaptation. *Crit Rev Microbiol* 20:285–328

Tardieu A, Luzzati V, Reman FC (1973) Structure and polymorphism of the hydrocarbon chains of lipids: A study of lecithin-water phases. *J Mol Biol* 75:711–733

Tatituri RVV, Wolf BJ, Brenner MB, Turk J, Hsu F-F (2015) Characterization of polar lipids of *Listeria monocytogenes* by HCD and low-energy CAD linear ion-trap mass spectrometry with electrospray ionization. *Anal Bioanal Chem* 407:2519–2528

Vigh L, Maresca B, Harwood JL (1998) Does the membrane's physical state control the expression of heat shock and other genes? *Trends Biochem Sci* 23:369–374

Voet D, Voet JG, Pratt CW (2016) *Fundamentals of biochemistry: Life at the molecular level*. Wiley, Hoboken

Wackenroder H (1831) Ueber das Oleum radicis Dauci aetherum, das Carotin, den Carotenzucker und den officinellen succus Dauci; so wie auch über das Mannit, welches in dem Möhrensafte durch eine besondere Art der Gährung gebildet wird. *Geigers Magazin der Pharmazie* 33:144-172

Walker SJ, Archer P, Banks JG (1990) Growth of *Listeria monocytogenes* at refrigeration temperatures. *J Appl Bacteriol* 68:157–162

Winter R, Noll F (2013) *Methoden der Biophysikalischen Chemie*. Springer Fachmedien, Wiesbaden

Yabuzaki J (2017) Carotenoids Database: structures, chemical fingerprints and distribution among organisms. *Database* 2017:bax004

Yabuzaki J (2020) Carotenoid Database. http://carotenoiddb.jp/index.html. Accessed 11 January 2022

Yao J, Dodson V, Joshua V, Frank MW, Rock CO (2015): *Chlamydia trachomatis* scavenges host fatty acids for phospholipid synthesis via an acyl-acyl carrier protein synthetase. *J Biol Chem* 290:22163–22173

Yao J, Rock CO (2017) Exogenous fatty acid metabolism in bacteria. *Biochimie* 141:30–39

Yao J, Bruhn DF, Frank MW, Lee RE, Rock CO (2016a) Activation of exogenous fatty acids to acyl-acyl carrier protein cannot bypass FabI inhibition in *Neisseria*. *J Biol Chem* 291:171–181

Yao J, Ericson ME, Frank MW, Rock CO (2016b) Enoyl-acyl carrier protein reductase I (FabI) is essential for the intracellular growth of *Listeria monocytogenes*. *Infect Immun* 84:3597–3607

Yoon Y, Lee H, Lee S, Kim S, Choi K-H (2015) Membrane fluidity-related adaptive response mechanisms of foodborne bacterial pathogens under environmental stresses. *Food Res Int* 72:25–36

Zhang Y-M, Rock CO (2008) Membrane lipid homeostasis in bacteria. *Nat Rev Microbiol* 6:222–233

Chapter 2

Exogenous fatty acids affect membrane properties and cold adaptation of *Listeria monocytogenes*

Listeria monocytogenes is a food-borne pathogen that can grow at very low temperatures close to the freezing point of food and other matrices. Maintaining cytoplasmic membrane fluidity by changing its lipid composition is indispensable for growth at low temperatures. Its dominant adaptation is to shorten the fatty acid chain length and, in some strains, increase in addition the menaquinone content. To date, incorporation of exogenous fatty acid was not reported for *Listeria monocytogenes*. In this study, the membrane fluidity grown under low-temperature conditions was affected by exogenous fatty acids incorporated into the membrane phospholipids of the bacterium. *Listeria monocytogenes* incorporated exogenous fatty acids due to their availability irrespective of their melting points. Incorporation was demonstrated by supplementation of the growth medium with polysorbate 60, polysorbate 80, and food lipid extracts, resulting in a corresponding modification of the membrane fatty acid profile. Incorporated exogenous fatty acids had a clear impact on the fitness of the *Listeria monocytogenes* strains, which was demonstrated by analyses of the membrane fluidity, resistance to freeze-thaw stress, and growth rates. The fatty acid content of the growth medium or the food matrix affects the membrane fluidity and thus proliferation and persistence of *Listeria monocytogenes* in food under low-temperature conditions.

Subjects: Bacteriology; Food microbiology; Pathogens

Flegler A, Iswara J, Mänz AT, Schocke FS, Faßbender WA, Hölzl G, Lipski A (2022) Exogenous fatty acids affect membrane properties and cold adaptation of *Listeria monocytogenes*. *Sci Rep* 12:1499. DOI: 10.1038/s41598-022-05548-6

Author contributions: AF and AL conceived and designed the experiments; AF, JI, ATM, FSS, and WAF. performed the experiments; GH contributed materials/analysis tools; AF analyzed the data, prepared all figures, and wrote the manuscript; AL reviewed and edited the manuscript.

1 Introduction

Listeria monocytogenes (*L. monocytogenes*) is responsible for the food-borne illness listeriosis, which causes a high proportion of severe cases and deaths worldwide (Buchanan *et al.* 2017; Farber and Peterkin 1991; Ryser & Marth 2007). Efforts to control this pathogen, which has a high mortality rate, are thwarted because *L. monocytogenes* is characterized by high tolerance to various environmental factors such as extreme temperatures (Angelidis *et al.* 2002; Farber & Peterkin 1991; Hamon *et al.* 2006; Hernandez-Milian & Payeras-Cifre 2014; Mead *et al.* 1999). The best-known and investigated characteristic of *L. monocytogenes* is its ability to grow in an extensive temperature range of − 1.5–50 °C (Mastronicolis *et al.* 1998; Mastronicolis *et al.* 2006; Saldivar *et al.* 2017; Walker *et al.* 1990). This capacity of *L. monocytogenes* seems crucial for surviving in the natural environment for long periods, associated with colonization, reproduction, and persistence in the food-processing environment and on food-processing equipment (Lopez-Valladares *et al.* 2018). Therefore, recent and recurring outbreaks revealed the importance of risk assessment analyses, which must also include the impact of the food matrix on growth rates and the low-temperature resilience of this organism (Angelo *et al.* 2017; EFSA 2021; Lopez-Valladares *et al.* 2018; Zhang *et al.* 2021).

Exogenous fatty acid metabolism of various food pathogens and other bacterial species has been frequently studied in the context of pathogenicity or colonization of food matrices (Balemans *et al.* 2010; Brinster *et al.* 2009; Parsons *et al.* 2011; De Sarrau *et al.* 2013; Yao *et al.* 2016; Yao & Rock 2015, 2017). However, for temperature adaptation, the modification of the fatty acid profile in *L. monocytogenes* is achieved only by *de novo* synthesis of the branched-chain fatty acids and not by modifying the existing acyl chains (Annous *et al.* 1997; Mastronicolis *et al.* 1998; Mastronicolis *et al.* 2006; Tatituri *et al.* 2015). Although exogenous fatty acids have already been detected in the fatty acid profile of *L. monocytogenes* (Juneja *et al.* 1998), there is no experimental evidence for incorporation in the membrane and the adaptive effect of exogenous fatty acids. Even homologous genes for the uptake and incorporation of exogenous fatty acids are present in *L. monocytogenes*, as in *Staphylococcus aureus* (*S. aureus*) (Yao *et al.* 2016). Incorporating external fatty acids with a low melting point would represent an attractive explanation for the remarkable adaptation of the organism to low temperatures and the successful colonization of refrigerated food.

Here, we uncovered an unknown adaptation mechanism in *L. monocytogenes* by adding exogenous fatty acids. *L. monocytogenes* can non-selectively utilize and incorporate exogenous fatty acids into the polar lipids of the cell membrane from the environment in addition to *de novo* synthesis of fatty acids. The utilization has a negative or positive effect on the adaptation of the membrane to low growth temperatures. Correct acyl chain composition of the membrane is crucial for

the survival of *L. monocytogenes* in the environment, and modification of this composition by exogenous fatty acids affects the fitness of this bacterium. This observation reveals a so far unconsidered impact of the lipid composition of the growth matrix on the growth and robustness of *L. monocytogenes* under low-temperature conditions. The potentially beneficial effect of food lipids on *L. monocytogenes* membranes may explain the successful colonization of many fatty food matrices stored under low-temperature conditions.

2 Results

Listeria monocytogenes covalently incorporates exogenous fatty acids into its membrane

Food matrices usually contain fatty acids ester-linked to triglycerides or polar lipids such as phospholipids or glycolipids. Therefore, in this study, we used polysorbate 60 (P60) and polysorbate 80 (P80) as well as lipid extracts from milk (ME), minced meat (MME), and smoked salmon (SSE) as supplements. Before the cultivation experiments, we analyzed fatty acid composition for tryptic soy broth-yeast extract medium (TSB-YE) without and with supplementation. P60 was used as a source for octadecanoic acid ($C_{18:0}$) and P80 as a source for *cis*-9-octadecenoic acid ($C_{18:1}$ *cis* 9). Both fatty acids could not be synthesized by *L. monocytogenes* and represent lipids with a high and a low melting temperature (T_m), 69.3 °C for $C_{18:0}$ and 12.8 °C for $C_{18:1}$ *cis* 9. We used supplementation with D-sorbitol to control for the effects of the sorbitan moiety of the polysorbate additions. The results for D-sorbitol controls coincide with those from cultures without any supplement. D-sorbitol was considered not to affect fatty acid profiles, membrane fluidity, or cell fitness. In addition, supplementation did not affect the medium's water activity (a_w) and pH. We cultivated three *L. monocytogenes* strains at 6 and 37 °C in TSB-YE without or with supplementation and analyzed the impact on the bacterial fatty acids composition.

The dominant fatty acids of the TSB-YE supplemented with P60 were 54.4 ± 0.9% $C_{18:0}$ and 46.6 ± 0.6% hexadecanoic acid ($C_{16:0}$), TSB-YE supplemented with P80 consisted of 75.3 ± 0.5% $C_{18:1}$ *cis* 9, 18.7 ± 0.3% $C_{16:0}$ and 6 ± 0.3 *cis*-9-hexadecenoic acid ($C_{16:1}$ *cis* 9), and TSB-YE supplemented with P60P80 were 49.0 ± 0.7% $C_{18:1}$ *cis* 9, 29.2 ± 0.2% $C_{16:0}$, and 21.8 ± 1.0% $C_{18:0}$, respectively. We could detect no fatty acids in the TSB-YE without supplementation and with D-sorbitol supplementation. After growth in the previously analyzed growth media, all *L. monocytogenes* strains showed a branched-chain fatty acid profile at 6 and 37 °C growth temperature (Tables 2.1, 3.2).

The dominating fatty acids of all strains were 12 methyltetradecanoic acid (*anteiso*-$C_{15:0}$), 14-methylhexadecanoic acid (*anteiso*-$C_{17:0}$), and 13-methyltetradecanoic acid (*iso*-$C_{15:0}$), at both growth temperatures. The three branched-chain fatty acids accounted for at least 96% of the total fatty acids in all strains when grown in TSB-YE without supplementation at 6 or 37 °C, respectively (Tables 2.1, 2.2). All strains significantly reduced the three branched-chain fatty acids after cultivation at 6, and 37 °C in TSB-YE supplemented with P60, with P80, or with P60P80. Additionally, the fatty acid profile presents the exogenous fatty acids $C_{16:0}$, $C_{18:0}$, and $C_{18:1}$ *cis* 9. For all strains, the content of $C_{16:0}$ and $C_{18:0}$ was nearly 42–59% (6 °C), and 8–12% (37 °C) after supplementation with P60, of $C_{16:0}$ and $C_{18:1}$ *cis* 9 was nearly 16–20% (6 °C), and 6–8% (37 °C) after supplementation with P80, and of $C_{16:0}$, $C_{18:0}$ and $C_{18:1}$ *cis* 9 was nearly 37–50% (6 °C) and 7–9% (37 °C) after supplementation with P60P80. Calculation of the weighted average melting temperature (WAMT) based on all detected fatty acids for each profile demonstrated that the supplemented fatty acids affected the membrane melting temperature. During the growth of the tested strains, the proportion of exogenous fatty acids in cell extracts increased with an increasing optical density at 625 nm (OD_{625}) at both incubation temperatures indicating the accumulation of exogenous fatty acids in the bacterial membrane (data not shown).

The three dominant fatty acids of the TSB-YE supplemented with milk extract (ME) were 25.6 ± 0.5% $C_{16:0}$, 18.8 ± 0.2% $C_{18:1}$ *cis* 9, and 15.0 ± 0.2% tetradecanoic acid ($C_{14:0}$), of TSB-YE supplemented with minced meat extract (MME) were 36.7 ± 5.0% $C_{18:1}$ *cis* 9, 28.3 ± 0.2% $C_{16:0}$, and 11.8 ± 2.1% $C_{18:0}$, and of TSB-YE supplemented with smoked salmon extract (SSE) were 16.2 ± 1.7% *cis*-9,12-octadecadienoic acid ($C_{18:2}$ *cis* 9,12), 15.5 ± 4.0% $C_{18:1}$ *cis* 9, and 14.3 ± 1.2% $C_{16:0}$ (Table 2.2). After growth in the presence of lipid extracts from food, fatty acid profiles of all *L. monocytogenes* strains contained exogenous fatty acids from the supplemented food extracts. After growth in TSB-YE supplemented with ME, with MME, or with SSE, all strains showed a reduction of branched-chain fatty acids and the presence of exogenous fatty acids. In all three strains, the exogenous fatty acids dodecanoic acid ($C_{12:0}$), $C_{14:0}$, $C_{16:1}$ *cis* 9, $C_{16:0}$, $C_{18:2}$ *cis* 9,12, $C_{18:1}$ *cis* 9, *cis*-11-octadecadienoic acid ($C_{18:1}$ *cis* 11), $C_{18:0}$, *cis*-5,8,11,14,17-eicosapentaenoic acid ($C_{20:5}$), and *cis*-4,7,10,13,16,19-docosahexaenoic acid ($C_{22:6}$) of the food lipid extracts were detected (Table 2.2). The content of exogenous fatty acids in the total fatty acid profile was about 10–22% after supplementation with ME, about 10–25% after supplementation with MME, and about 12–28% after supplementation with SSE for all strains at 6 °C growth temperature.

Table 2.1 Fatty acid (FA) composition, weighted-average melting temperature (WAMT), the ratio of *anteiso*-$C_{15:0}$ to *anteiso*-$C_{17:0}$ ($Ri_{ai\text{-}15/ai\text{-}17}$), and menaquinone-7 (MK-7) content. *Listeria monocytogenes* strains DSM 20600^T, FFH, and FFL1 grown at 6 °C in tryptic soy broth-yeast extract medium without supplementation (TSB-YE), with 0.1% (wt/vol) polysorbate 60 (P60), with 0.05% (wt/vol) each of polysorbate 60 and polysorbate 80 (P60 P80), and with 0.1% (wt/vol) polysorbate 80 (P80). Values are means ± standard deviation (n = 3). Asterisks represent p values (*p < 0.001, **p < 0.0001, ***p < 0.00001, ****p < 0.000001) compared to cultures in TSB-YE without supplementation.

Parameter	**DSM 20600^T**				**FFH**				**FFL1**			
	TSB-YE	P60	P60P80	P80	TSB-YE	P60	P60P80	P80	TSB-YE	P60	P60P80	P80
FA (%)												
anteiso-$C_{13:0}$	n.d.	6.9 ± 0.9**	n.d.	n.d.	n.d.	0.2 ± 0.2	n.d.	n.d.	n.d.	0.7 ± 0.1	n.d.	n.d.
iso-$C_{14:0}$	0.8 ± 0.3	0.4 ± 0.3	n.d.	0.2 ± 0.2	n.d.	0.7 ± 0.2	0.2 ± 0.2	n.d.	1.2 ± 0.2	1.3 ± 0.2	0.9 ± 0.2	1.3 ± 1.3
$C_{14:0}$	n.d.	0.5 ± 0.4	n.d.	n.d.	n.d.	0.3 ± 0.1	n.d.	n.d.	0.4 ± 0.3	0.3 ± 0.1	0.2 ± 0.0	0.1 ± 0.1
iso-$C_{15:0}$	8.8 ± 1.7	1.5 ± 0.4***	3.5 ± 0.6*	4.9 ± 1.0	9.7 ± 1.7	4.3 ± 0.5***	3.4 ± 0.6****	2.9 ± 0.5****	5.3 ± 0.2	5.0 ± 0.5	4.7 ± 0.7	6.9 ± 3.2
anteiso-$C_{15:0}$	82.6 ± 2.8	30.9 ± 3.6****	41.4 ± 5.4****	67.1 ± 8.9****	85.1 ± 0.6	39.6 ± 5.3****	37.9 ± 2.9****	68.8 ± 3.5****	88.5 ± 0.5	36.8 ± 1.6****	45.5 ± 1.7****	66.1 ± 10.3****
iso-$C_{16:0}$	0.7 ± 0.2	n.d.	n.d.	0.2 ± 0.2	0.3 ± 0.3	1.1 ± 0.1	0.6 ± 0.1	0.1 ± 0.1	1.1 ± 0.9	1.5 ± 0.4	1.2 ± 0.2	0.8 ± 0.7
$C_{16:0}$	n.d.	42.0 ± 1.6****	14.3 ± 3.6****	2.5 ± 0.9	n.d.	21.3 ± 0.8****	17.4 ± 1.6****	1.9 ± 0.8	0.2 ± 0.2	22.7 ± 0.5****	12.1 ± 1.4****	2.9 ± 2.6
anteiso-$C_{17:0}$	7.1 ± 0.8	1.8 ± 0.4**	7.5 ± 1.0	8.0 ± 1.7	4.9 ± 1.8	11.3 ± 1.5****	8.0 ± 0.6	9.6 ± 0.6**	3.4 ± 1.4	9.5 ± 0.7***	10.5 ± 0.7****	8.6 ± 0.2**
$C_{18:1}$ *cis* 9	n.d.	n.d.	14.8 ± 2.4****	17.1 ± 5.3****	n.d.	n.d.	14.4 ± 0.9****	16.7 ± 3.1****	n.d.	n.d.	15.5 ± 0.7****	12.8 ± 3.0****
$C_{18:0}$	n.d.	16.7 ± 4.9****	18.6 ± 5.6****	n.d.	n.d.	21.0 ± 5.3****	18.0 ± 3.7****	n.d.	n.d.	22.3 ± 2.9****	9.5 ± 2.6****	n.d.
WAMT (°C)	27.9 ± 0.7	47.2 ± 2.6****	38.2 ± 3.9****	25.6 ± 0.4	27.4 ± 0.1	45.0 ± 2.3****	39.5 ± 2.1****	25.0 ± 0.2	26.9 ± 0.3	46.3 ± 1.1****	34.6 ± 1.4****	27.3 ± 2.3
$Ri_{ai\text{-}15/ai\text{-}17}$	11.6	16.7	5.6	7.5	17.3	3.5	4.7	7.2	26.4	3.9	4.3	7.7
MK-7 (nmol g^{-1})	213 ± 12	213 ± 7	188 ± 19*	175 ± 16***	181 ± 9	178 ± 7	170 ± 4	135 ± 5****	89 ± 5	139 ± 2****	135 ± 8****	90 ± 8

Table 2.2 Fatty acid (FA) composition, weighted-average melting temperature (WAMT), and the ratio of *anteiso*-$C_{15:0}$ to *anteiso*-$C_{17:0}$ ($Ri_{ai\text{-}15/ai\text{-}17}$). *Listeria monocytogenes* strains DSM 20600^T, FFH, and FFL 1 grown at 37 °C in tryptic soy broth-yeast extract medium without supplementation (TSB-YE), with 0.1% (wt/vol) polysorbate 60 (P60), with 0.05% (wt/vol) each of polysorbate 60 and polysorbate 80 (P60P80), and with 0.1% (wt/vol) polysorbate 80 (P80). Values are means ± standard deviation (n = 3). Asterisks represent p values (*p < 0.001, **p < 0.0001, ***p < 0.00001, ****p < 0.000001) compared to cultures in TSB-YE without supplementation.

Parameter	**DSM 20600^T**				**FFH**				**FFL 1**			
	TSB-YE	P60	P60P80	P80	TSB-YE	P60	P60P80	P80	TSB-YE	P60	P60P80	P80
FA (%)												
iso-C_{14}:0	n.d.	0.4 ± 0.1	n.d.	n.d.	0.2 ± 0.0	0.4 ± 0.1	n.d.	n.d.	0.2 ± 0.0	0.5 ± 0.1	n.d.	n.d.
$C_{14:0}$	n.d.	n.d.	n.d.	n.d.	n.d.	0.4 ± 0.4	n.d.	n.d.	n.d.	0.2 ± 0.2	n.d.	n.d.
iso-$C_{15:0}$	3.9 ± 0.1	6.0 ± 0.2****	5.8 ± 0.1***	5.8 ± 0.0***	9.3 ± 0.6	6.5 ± 0.2****	6.5 ± 0.1****	6.5 ± 0.0****	6.5 ± 0.2	5.7 ± 0.3	6.6 ± 0.0	6.3 ± 0.1
anteiso-$C_{15:0}$	60.2 ± 1.1	40.6 ± 0.3****	39.7 ± 0.4****	40.0 ± 0.6****	52.5 ± 1.9	38.0 ± 1.1****	38.7 ± 0.2****	37.8 ± 0.4****	49.6 ± 1.6	38.6 ± 0.7****	39.8 ± 0.2****	39.4 ± 0.4****
iso-$C_{16:0}$	1.7 ± 0.1	2.7 ± 0.1	2.6 ± 0.0	2.6 ± 0.1	2.5 ± 0.3	3.0 ± 0.1	2.8 ± 0.2	3.3 ± 0.1	3.6 ± 0.2	3.6 ± 0.2	3.4 ± 0.1	3.8 ± 0.1
$C_{16:0}$	0.6 ± 0.1	6.7 ± 0.3****	3.8 ± 0.1****	2.7 ± 0.2****	1.3 ± 0.3	10.5 ± 0.5****	5.7 ± 0.2****	4.1 ± 0.0****	1.3 ± 0.1	7.6 ± 1.5****	4.6 ± 0.2****	3.6 ± 0.3****
Iso-$C_{17:0}$	1.3 ± 0.1	3.1 ± 0.0***	3.5 ± 0.1****	3.4 ± 0.1****	2.4 ± 0.3	3.6 ± 0.1**	4.0 ± 0.1***	4.2 ± 0.1****	1.4 ± 0.2	3.2 ± 0.2**	3.4 ± 0.0***	3.3 ± 0.2***
anteiso-$C_{17:0}$	32.3 ± 0.9	39.0 ± 0.1****	41.2 ± 0.2****	42.2 ± 0.7****	31.9 ± 0.7	36.1 ± 1.0****	38.7 ± 0.4****	40.4 ± 0.2****	37.5 ± 0.9	36.1 ± 0.7*	39.4 ± 0.0***	40.2 ± 0.2****
$C_{18:1}$ cis 9	n.d.	n.d.	2.5 ± 0.0****	3.4 ± 0.2****	n.d.	n.d.	3.1 ± 0.3****	3.6 ± 0.1****	n.d.	n.d.	2.5 ± 0.2****	3.3 ± 0.3****
$C_{18:0}$	n.d.	1.5 ± 0.3**	0.8 ± 0.2	n.d.	n.d.	1.5 ± 0.3	0.5 ± 0.1***	n.d.	n.d.	4.5 ± 2.1****	0.4 ± 0.0	n.d.
WAMT (°C)	30.2 ± 0.5	34.4 ± 0.1****	32.7 ± 0.2****	31.9 ± 0.0****	32.1 ± 0.6	35.7 ± 0.3****	33.0 ± 0.2*	32.5 ± 0.0	32.5 ± 0.4	36.1 ± 0.6****	33.1 ± 0.1	32.7 ± 0.1
$Ri_{ai\text{-}15/ai\text{-}17}$	1.9	1.0	1.0	0.9	1.6	1.1	1.0	0.9	1.3	1.1	1.0	1.0

Because the cells' menaquinone-7 (MK-7) content was previously associated with membrane fluidity under low-temperature conditions, we analyzed this lipid for all cultures grown at 6 °C (Table 3.1). *L. monocytogenes* strain DSM 20600^T, FFH, and FFL 1 had an MK-7 content of 213 ± 12, 181 ± 9, and 89 ± 5 nmol g^{-1}, respectively, after growth in TSB-YE at 6 °C (Table 2.1). This MK-7 content is in accord with previous findings that the former two strains increase their production under low-temperature growth conditions, but the latter strain does not (Seel *et al.* 2018). After growth in TSB-YE supplemented with P80, strains DSM 20600^T and FFH had significantly lower MK-7 content of 175 ± 16 and 135 ± 5 nmol g^{-1}, respectively, while strain FFL 1 showed unchanged MK-7 content of 90 ± 8 nmol g^{-1}. After growth in TSB-YE supplemented with P60 or P60P80, strain FFL 1 was the only strain that significantly increased MK-7 content of 139 ± 2 and 135 ± 8 nmol g^{-1}, respectively. For the other two strains, supplementation with P60 or P60P80 did not increase the MK-7 content. Thus, supplementation with exogenous fatty acids also affects the fatty acid synthesis of *L. monocytogenes*. We used the ratio of *anteiso*-$C_{15:0}$ to *anteiso*-$C_{17:0}$ ($Ri_{ai\text{-}15/ai\text{-}17}$) to assess the impact of exogenous fatty acids on the profile of endogenously synthesized fatty acids. For all supplemented cultures, except one, we noticed the decrease of the $Ri_{ai\text{-}15/ai\text{-}17}$. Strain *L. monocytogenes* DSM 20600^T grown at 6 °C and supplemented with P60 was the only exception. Thus, the WAMT of the total fatty acid profiles was not primarily determined by the shift of the $Ri_{ai\text{-}15/ai\text{-}17}$ but by the T_m of the incorporated exogenous fatty acids (Table 2.1–2.3).

We could confirm the active incorporation of exogenous fatty acids in the bacterial cell membrane of *L. monocytogenes*. Polar lipids were extracted from all strains grown at 6 °C in TSB-YE supplemented with P80 and analyzed with quadrupole time-of-flight mass spectrometry (Q-TOF MS). Phosphatidylglycerol (PG)-$C_{30:0}$ (*m/z* 693.47) and lysyl-phosphatidylglycerol (LPG)-$C_{30:0}$ (*m/z* 821.56) were identified in all strains as main molecular species and contained only *iso*/*anteiso*-$C_{15:0}$ fatty acids (*m/z* 241.21) as derived from the total and the MS/MS spectra (Fig. 2.1a–d). Two other main species, PG-$C_{33:1}$ (*m/z* 733.50) and LPG-$C_{33:1}$ (*m/z* 861.59), were detected (Fig. 2.1a, b), which were absent in strains grown without supplementation. The fragmentation patterns in the MS/MS spectra of the two lipids confirm the presence of $C_{15:0}$ and, in addition, $C_{18:1}$ as derived from the fragments with *m/z* 241.21 and *m/z* 281.24, respectively (Fig 2.1e, f). These results confirm the incorporation of the exogenous fatty acid $C_{18:1}$ into phospholipids in *L. monocytogenes*. We could not observe the incorporation of two $C_{18:1}$ per lipid molecule. Other phospholipids' fatty acids were $C_{17:0}$ (native) and $C_{16:0}$ (supplemented). $C_{16:0}$, $C_{17:0,}$ and $C_{18:1}$ were observed only in combination with $C_{15:0}$ in the different lipid species but not among each other. Incorporation of $C_{18:0}$ into PG and LPG was also observed. $C_{16:0}$, $C_{18:0,}$ and $C_{18:1}$ could not be detected in strains grown without supplementation. $C_{18:1}$ was not detectable in the two glycolipids, monoglycosyldiacylglycerol and

Table 2.3 Fatty acid (FA) composition, weighted-average melting temperature (WAMT), and the ratio of *anteiso*-$C_{15:0}$ to *anteiso*-$C_{17:0}$ ($Ri_{ai\text{-}15/ai\text{-}17}$). Tryptic soy broth-yeast extract medium supplemented with food lipid extracts and *Listeria monocytogenes* strains DSM 20600^T, FFH, and FFL 1 grown at 6 °C on tryptic soy agar-yeast extract medium supplemented with 0.1% (wt/vol) milk extract (ME), with 0.1% (wt/vol) minced meat extract (MME) or with 0.1% (wt/vol) smoked salmon extract (SSE). Values are means ± standard deviation (*n* = 3).

Parameter	**Food lipid**			**DSM 20600^T**			**FFH**			**FFL 1**		
	ME	MME	SSE	ME	MME	SSE	ME	MME	SSE	ME	MME	SSE
FA (%)												
$C_{12:0}$	7.0 ± 0.4			0.7 ± 0.0			0.4 ± 0.1			0.9 ± 0.2		
$C_{14:0}$	15.0 ± 0.2	3.5 ± 0.6	7.0 ± 0.8	2.1 ± 0.4	0.7 ± 0.1	1.0 ± 0.2	2.6 ± 0.4	0.8 ± 0.3	0.9 ± 0.2	3.7 ± 1.1	0.7 ± 0.0	1.0 ± 0.2
iso-$C_{15:0}$				8.7 ± 0.6	10.9 ± 0.1	10.3 ± 2.1	6.6 ± 0.2	5.8 ± 0.6	5.8 ± 1.6	5.8 ± 0.3	5.8 ± 0.6	5.6 ± 1.7
anteiso-$C_{15:0}$				71.0 ± 0.4	66.6 ± 1.1	66.1 ± 0.9	71.1 ± 0.7	66.3 ± 0.2	57.8 ± 10.0	60.8 ± 7.9	56.8 ± 1.1	55.9 ± 9.8
$C_{16:1}$ *cis* 9	2.0 ± 0.0	5.2 ± 0.9	6.2 ± 0.6	1.0 ± 0.1	0.3 ± 0.0	0.3 ± 0.1	0.7 ± 0.0	0.4 ± 0.0	1.6 ± 1.5	1.0 ± 0.0	1.2 ± 0.2	1.6 ± 1.3
iso-$C_{16:0}$				0.3 ± 0.1	1.7 ± 0.2	1.2 ± 0.1	0.3 ± 0.2	0.8 ± 0.1	0.8 ± 0.2	0.5 ± 0.1	0.7 ± 0.0	1.1 ± 0.4
$C_{16:0}$	25.6 ± 0.5	28.3 ± 0.2	14.3 ± 1.2	2.7 ± 0.0	2.2 ± 0.1	5.0 ± 2.1	3.2 ± 0.6	3.9 ± 0.5	10.1 ± 5.6	7.8 ± 3.2	6.1 ± 0.0	10.1 ± 5.2
iso-$C_{17:0}$				0.4 ± 0.0	0.4 ± 0.0	0.4 ± 0.1	0.4 ± 0.1	0.4 ± 0.0	0.3 ± 0.1	0.4 ± 0.1	0.3 ± 0.0	0.3 ± 0.1
anteiso-$C_{17:0}$				8.6 ± 0.4	10.7 ± 1.1	10.0 ± 0.4	10.2 ± 0.5	11.3 ± 0.3	9.9 ± 3.0	9.2 ± 0.3	11.3 ± 0.3	11.0 ± 1.4
$C_{18:2}$ *cis* 9,12	3.0 ± 0.1	9.6 ± 1.7	16.2 ± 1.7	0.3 ± 0.1	1.5 ± 0.0	0.7 ± 0.1	0.3 ± 0.0	1.8 ± 0.0	3.6 ± 3.5	0.6 ± 0.1	2.7 ± 0.0	3.7 ± 2.5
$C_{18:1}$ *cis* 9	18.4 ± 0.2	36.7 ± 5.0	15.5 ± 4.0	2.1 ± 0.2	2.3 ± 0.0	1.1 ± 0.3	2.0 ± 0.2	4.6 ± 0.0	5.3 ± 4.9	5.2 ± 1.8	9.7 ± 0.0	5.6 ± 3.5
$C_{18:1}$ *cis* 11	1.3 ± 0.0	4.8 ± 0.8	2.5 ± 0.4		0.2 ± 0.0	0.2 ± 0.1		0.2 ± 0.0	1.6 ± 1.2		0.7 ± 0.0	1.2 ± 1.1
$C_{18:0}$	10.0 ± 0.2	11.8 ± 2.1	2.8 ± 0.3	0.7 ± 0.5	0.8 ± 0.0	1.3 ± 1.0	0.9 ± 0.5	2.6 ± 0.0	1.2 ± 0.7	2.7 ± 1.7	3.1 ± 0.0	1.0 ± 0.5
$C_{20:5}$			6.2 ± 1.4			0.3 ± 0.0			0.5 ± 0.3			0.5 ± 0.4
$C_{22:6}$			10.5 ± 0.4			0.9 ± 0.3			0.8 ± 0.5			1.3 ± 0.6
WAMT (°C)				29.0 ± 0.8	29.4 ± 1.0	30.0 ± 3.5	29.1 ± 1.6	29.0 ± 1.0	28.9 ± 8.8	31.3 ± 6.4	28.9 ± 0.7	28.6 ± 7.6
$Ri_{ai\text{-}15/ai\text{-}17}$				8.3	6.2	6.6	7.0	5.9	5.8	6.6	5.0	5.1

diglycosyldiacylglycerol, found in the tested strains (data not shown), indicating a preference for incorporation of exogenous fatty acids into phospholipids.

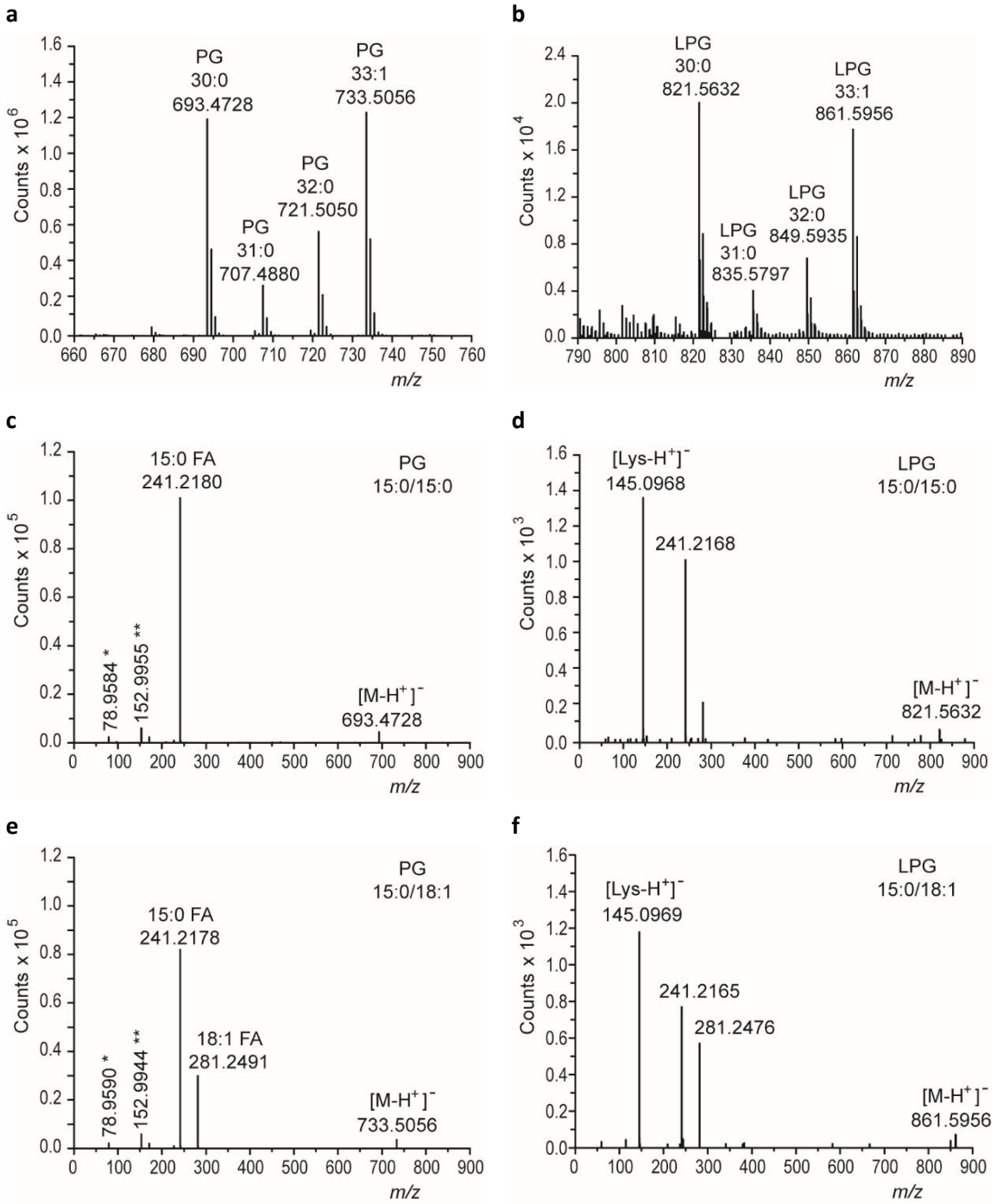

Figure 2.1 Analysis of polar lipids by quadrupole time-of-flight mass spectrometry. Phosphatidylglycerol (PG) and lysyl-phosphatidylglycerol (LPG) were detected in lipid extracts from cells of *Listeria monocytogenes* strain DSM 20600^T cells grown at 6 °C on tryptic soy agar-yeast extract medium supplemented with 0.1% (wt/vol) polysorbate 80. The lipids were measured in the negative ion mode. Different molecular species of PG (a) and LPG (b) can be observed in the total ion spectra. Characteristic fragments in the MS/MS spectra of the respective lipids allow the detection of single fatty acids as indicated in the figure (c–f). Further fragments are characteristic for PG derived from the phosphite anion *$[PO_3]^-$ and the glycerolphosphate **$[GroP]^-$ head group. Fragmentation of LPG results in detecting a fragment (*m/z* 145.09) derived from a deprotonated lysyl residue $[Lys\text{-}H^+]^-$ (Atila *et al.* 2016, Zhou *et al.* 2016).

The incorporation of exogenous fatty acids alters membrane fluidity and support cold adaptation

We measured changes in the lateral diffusion capability of the cytoplasmic membranes induced by supplementation with P80 or SSE after growth at 6 °C based on trimethylammonium diphenylhexatriene (TMA-DPH) anisotropy (Fig. 2.2). The data showed an apparent discrepancy between cells grown with and without exogenous fatty acid supplementation. Supplementation with an exogenous fatty acid source during growth at 6 °C resulted in a higher fluidity of the membranes for all *L. monocytogenes* strains in a temperature range between 5 and 15 °C. The difference between supplemented and non-supplemented strains is > Δ0.010 at these low temperatures. At higher temperatures, membrane fluidity increased steadily until TMA-DPH anisotropy values for all three strains approximate each other at temperatures of 20 °C and above. *L. monocytogenes* strains grown at 6 °C in TSB-YE with P80 or SSE as an exogenous source of fatty acids showed a significantly smaller TMA-DPH anisotropy change over the entire measuring range, which indicates a broad transition phase. Strain FFL 1 showed the most considerable effect from all three strains. Growth with P80 and SSE increased cell membrane fluidity and a broader transition phase than strains without supplementation by exogenous fatty acids. This is because these supplements provide fatty acids with low T_m. Long-term incubations for up to 48 h of non-growing cells suspended in Ringer's solution with P80 at 6 °C showed no effect on membrane fluidity (Fig. 2.3). These results indicated the dependency of membrane effects on growing, biochemically active cells but not on the mere abiotic association of P80 with the cell membrane. In addition, for this long-term incubation, $C_{18:1}$ could not be detected in the cells' fatty acid profile, indicating that fatty acid profile analyses show only incorporated fatty acids but no fatty acids bound to polysorbate.

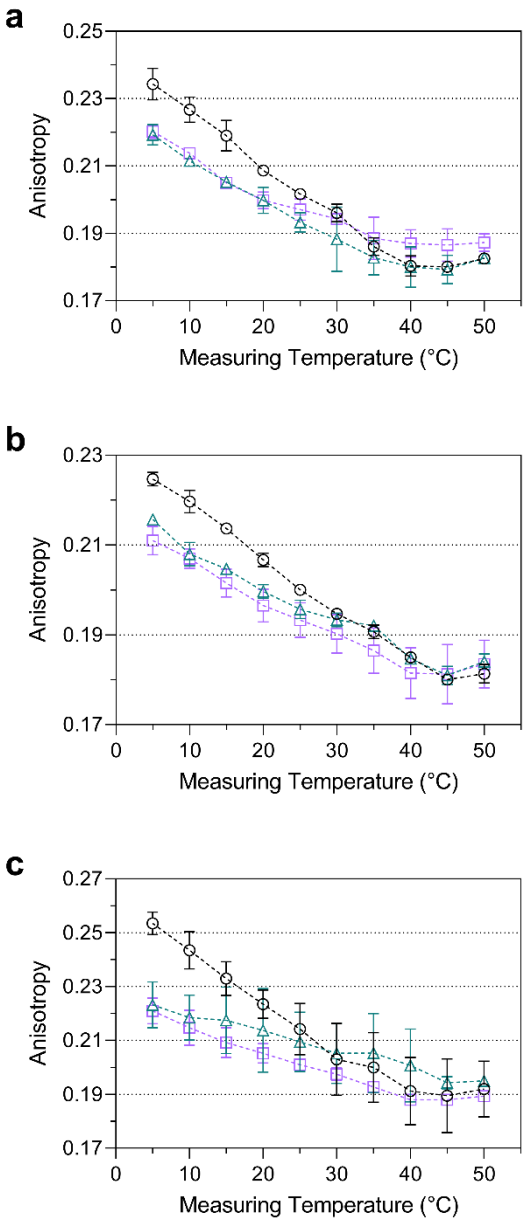

Figure 2.2 Analysis of membrane fluidity by TMA-DPH anisotropy. *Listeria monocytogenes* strains DSM 20600^T (a), FFH (b), and FFL 1 (c) grown at 6 °C in tryptic soy broth-yeast extract medium without supplementation (○), with 0.1% (wt/vol) of polysorbate 80 (△), and with 0.1% (wt/vol) salmon lipid extract (□). Values are means ± standard deviation (n = 3).

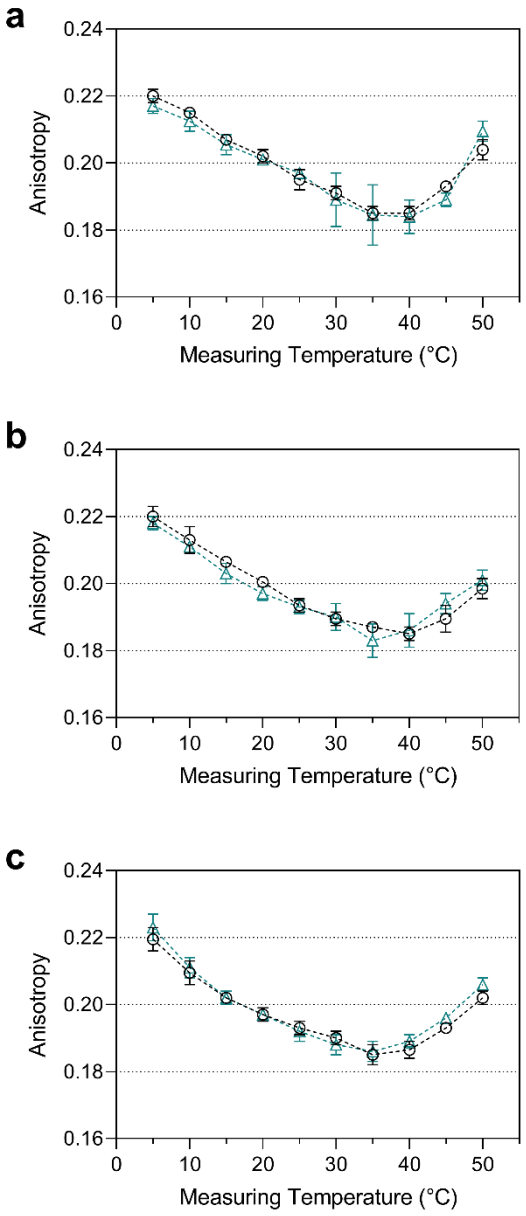

Figure 2.3 Time-dependent analysis of membrane fluidity by TMA-DPH anisotropy. *Listeria monocytogenes* strain DSM 20600^T incubated at 6 °C after 1 h (a), 24 h (b), and 48 h (b) in Ringer's solution without supplementation (○) and with 0.1% (wt/vol) of polysorbate 80 (△). Values are means ± standard deviation (n = 2).

Exogenous fatty acids affect resistance to freeze-thaw stress and growth rates

We applied a freeze-thaw stress test as an indicator of membrane integrity. This test showed a positive and a negative impact of exogenous fatty acids sources on cell resistance depending on the supplement (Fig. 2.4). After growth at 6 °C and subjected to freeze-thaw stress, all *L. monocytogenes* strains showed a significant decrease of log_{10}-reduction of CFU mL^{-1} if supplemented with P60, P80, or SSE compared to non-supplemented TSB-YE. Strains DSM 20600^T and FFL 1 grown in TSB-YE with P60 and all strains grown in TSB-YE with P80 showed significantly decreased log_{10}-reduction after freeze-thaw stress compared to cultures in un-supplemented TSB-YE. Thus, supplementation with exogenous fatty acids can positively affect cell fitness, regardless of the T_m of the incorporated fatty acids. The highest resistance against freeze-thaw stress was observed for strain DSM 20600^T after growth in TSB-YE with P60 and for strains FFH and FFL 1 after growth in TSB-YE with P80 or SSE. Supplementation with SSE produced the exact extent of log_{10}-reduction of CFU mL^{-1} as supplementation with P80 for all strains.

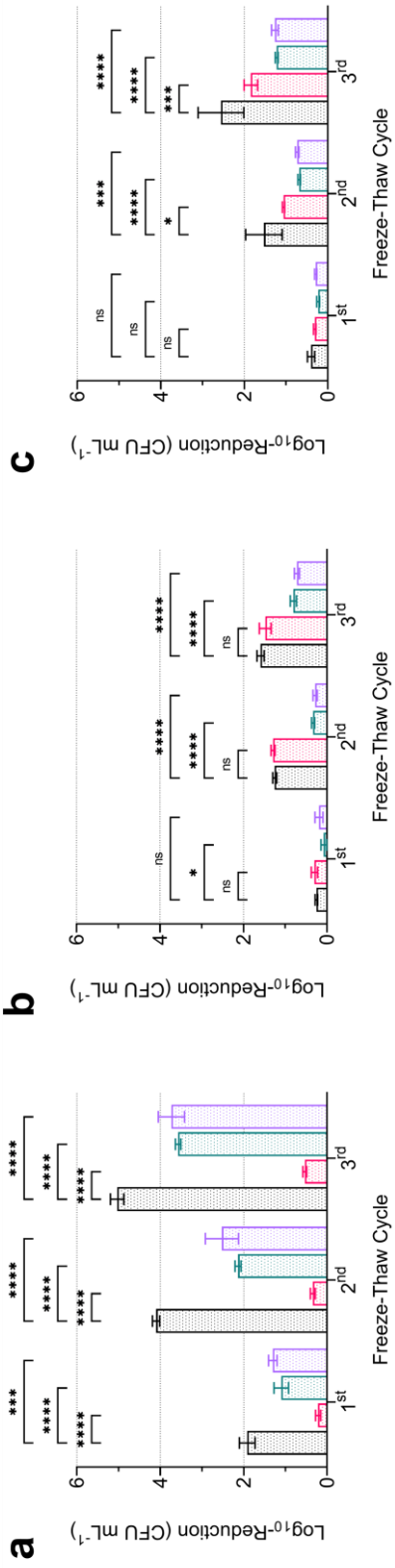

Figure 2.4 Logarithmic reduction of viable cell counts after freeze-thaw stress test. *Listeria monocytogenes* strains DSM 20600T (A), FFH (B), and FFL 1 (C) grown at 6 °C in tryptic soy broth-yeast extract medium (TSB-YE) without supplementation (black), with 0.1% (wt/vol) polysorbate 60 (red), with 0.1% (wt/vol) polysorbate 80 (green), and with 0.1% (wt/vol) salmon lipid extract (indigo) after one, two and three freeze-thaw cycles (each 24 h) relative to the initial cell count. Values are means ± standard deviation (n = 3). Asterisks represent p values (*p < 0.001, **p < 0.0001, ***p < 0.00001, ****p < 0.000001) compared to cultures in TSB-YE without supplementation.

The supplementation experiments showed a clear impact on growth rates of the tested *L. monocytogenes* strains at 6 and 37 °C (Fig. 2.5). The growth rates at 6 °C were reduced after supplementation with P60 and increased after supplementation with P80, compared to non-supplemented controls. The growth rates decreased from 0.034 to 0.010, 0.048 to 0.013, and 0.048

to 0.017 after supplementation with P60 and increased to 0.047, 0.072, and 0.061 after supplementation with P80 in strains DSM 20600^T, FFH, and FFL 1 grown at 6 °C, respectively. In contrast to cultures grown at 6 °C, an increase of growth rates could be demonstrated for all strains at 37 °C after supplementation with P60 and with P80. Growth rates increased from 0.72 to 0.95 and 0.93 for strain DSM 20600^T, from 0.61 to 0.97 and 0.94 for strain FFH, and from 0.63 to 0.96 and 1.0 for strain FFL 1, grown at 37 °C after supplementation with P60 or P80, respectively. Thus, the exogenous fatty acid with high T_m ($C_{18:0}$) inhibits growth at 6 °C for all strains, whereas a fatty acid with low T_m ($C_{18:1}$ *cis* 9) positively affected growth rates. In contrast, both types of fatty acids positively affected growth rates at 37 °C. These growth rates are in accord with our observation that all three strains showed faster colony formation at 6 °C growth temperature on tryptic soy agar-yeast extract medium (TSA-YE) if supplemented with ME, MME, or SSE, reflecting the positive influence of exogenous fatty acids from foods.

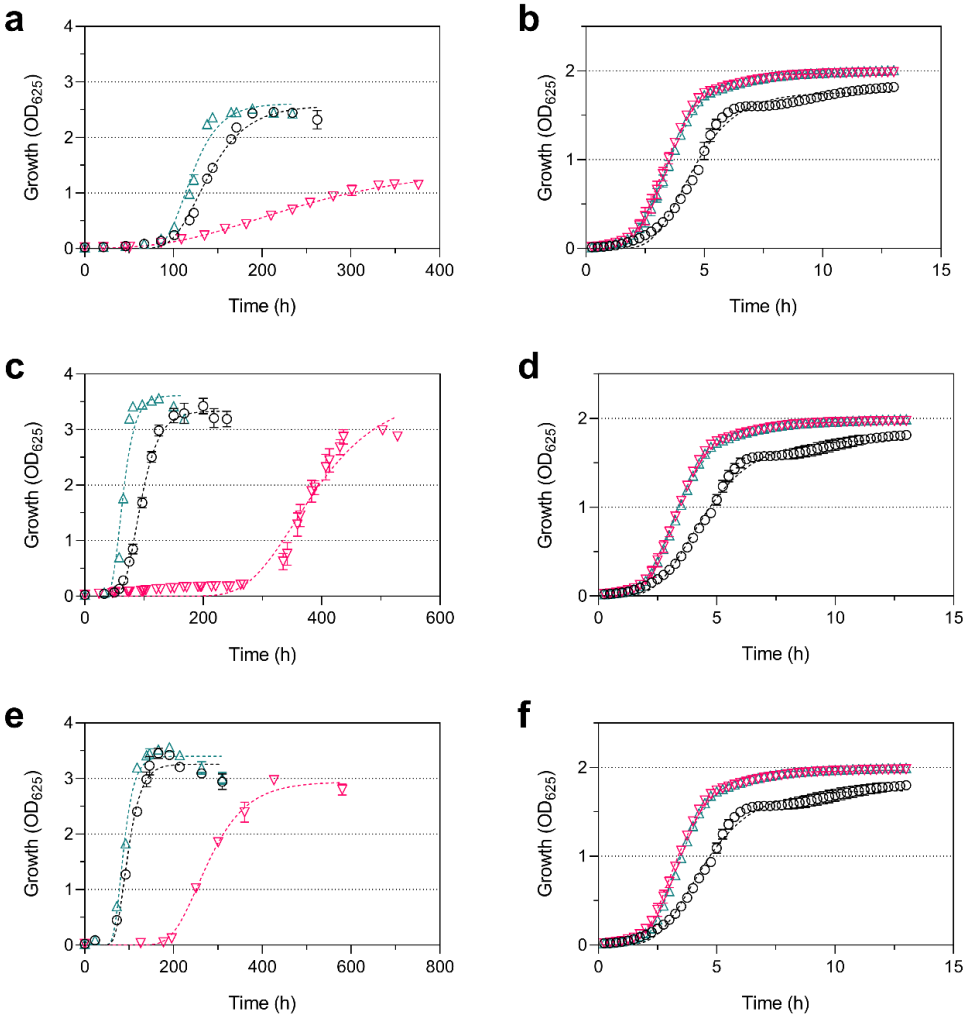

Figure 2.5 Growth kinetics. *Listeria monocytogenes* strains DSM 20600^T (a, b), FFH (c, d) and FFL 1 (e, f) grown at 6 °C (a, c, e) and 37 °C (b, d, f) in tryptic soy broth-yeast extract medium without supplementation (○), with 0.1% (wt/vol) of polysorbate 60 (▽), and with 0.1% (wt/vol) of polysorbate 80 (△) Values are means ± standard deviation (n = 3 at 6 °C; n = 8 at 37 °C).

3 Discussion

Some foods are known to have an increased risk for contamination with *L. monocytogenes* even under low-temperature storage conditions (Lopez-Valladares *et al.* 2018; Ryser & Marth 2007). We used P60 with a high T_m fatty acid ($C_{18:0}$, T_m 69.2 °C) and P80 with a low T_m fatty acid ($C_{18:1}$ *cis* 9, T_m 12.8 °C) as supplements. Straight chain fatty acids, saturated and unsaturated, were not synthesized by *L. monocytogenes*. Therefore the incorporated $C_{18:0}$ and $C_{18:1}$ *cis* 9 must be exogenous in origin (Giotis *et al.* 2007; Singh *et al.* 2008; Zhu *et al.* 2005a; Zhu *et al.* 2005b). The same is true for other unsaturated fatty acids supplemented with the food extracts such as $C_{18:2}$ *cis* 9,12 with a T_m of – 7.2 °C and $C_{18:1}$ *cis* 11 with a T_m of 15.4 °C. The three *L. monocytogenes* strains studied showed a temperature-dependent change of their fatty acid profiles (Table 2.1, 2.2) which were in accord with the previous reports (Annous *et al.* 1997; Flegler *et al.* 2021; Mastronicolis *et al.* 1998; Mastronicolis *et al.* 2006; Seel *et al.* 2018). The adaptation mechanism shifted the $Ri_{ai\text{-}15/ai\text{-}17}$ from *anteiso*-$C_{17:0}$ (T_m 37.1 °C) to *anteiso*-$C_{15:0}$ (T_m 24.1 °C). *L. monocytogenes* strain DSM 20600^T and FFH showed a less pronounced fatty acid shift at lower growth temperatures than strain FFL 1 (Table 2.1, 2.2). As described before, MK-7 is an additional modulator of membrane fluidity for these strains and is crucial for bacterial cell fitness (Flegler *et al.* 2021; Seel *et al.* 2018). However, all strains showed an expansion of their fatty acid profiles after supplementation with exogenous fatty acids as these were assimilated by all *L. monocytogenes* strains (Table 2.1–2.3). All strains were even able to incorporate polyunsaturated fatty acids such as $C_{20:5}$ with a T_m of – 53 °C and $C_{22:6}$ with a T_m of – 44 °C derived from the supplemented SSE. The bactericidal effects of polyunsaturated fatty acids (Knapp and Melly 1986), as previously described, did not occur in *L. monocytogenes*. As expected, exogenous fatty acids with lower T_m and those with higher T_m such as $C_{14:0}$ with a T_m of 53.5 °C and $C_{16:0}$ with a T_m of 62.2 °C were incorporated. We found no indication for selective incorporation of particular fatty acids. The supplementation with an equimolar mixture of P60 and P80 showed no favored incorporation of the lower melting point fatty acid in all strains at low-temperature growth conditions. All strains did not selectively incorporate the supplemented fatty acids according to their T_m, but their percentage availability in the medium (Table 2.1–2.3). This finding is also in accord with the increasing appearance of exogenous fatty acids in the fatty acid profiles of the strains during cultivation (data not shown).

Exogenous fatty acids replaced endogenously synthesized fatty acids and affected the fatty acid synthesis of *L. monocytogenes*. We found a decrease of the $Ri_{ai\text{-}15/ai\text{-}17}$ in the presence of exogenous fatty acids, which indicated the stimulation of chain elongation during the synthesis of branched-chain fatty acids. The reduction of the $Ri_{ai\text{-}15/ai\text{-}17}$ was related to the presence of exogenous fatty acids but not to the nature of these fatty acids. Although the shift to longer branched-chain

fatty acids should increase the membrane melting temperature, we found WAMT values primarily affected by the melting temperatures of exogenously supplied fatty acids. WAMT values increased in all strains after supplementation with P60 due to the presence of $C_{16:0}$ and $C_{18:0}$ (Table 2.1). In addition, we detected significant differences for WAMT and MK-7 content between tested strains supplemented with P60 and P80. For *L. monocytogenes* strains DSM 20600^T and FFH, a reduced MK-7 content was detected when $C_{18:1}$ *cis* 9 was incorporated and WAMT decreased. In contrast, strain FFL 1, which was previously reported not to have an MK-mediated temperature adaptation, increased MK-7 content in the presence of $C_{16:0}$ and $C_{18:0}$. These results support the previous evidence that fatty acids are not selectively incorporated as WAMT increased after supplementation with P60 compared to the non-supplemented cultures. Furthermore, our data demonstrate that the previously described MK-mediated adaptation of membrane fluidity (Seel *et al.* 2018) and (Flegler *et al.* 2021) in *L. monocytogenes* is affected by low growth temperatures and the presence of exogenous fatty acids. Thus, the interlocking of MK-mediated adaptation and FA-dependent cold adaptation is more complex as expected, as exogenous fatty acids can impact the MK content and, therefore, are also involved in the cold adaptation of *L. monocytogenes*.

A critical feature of this study was to confirm the incorporation of exogenous fatty acids into membrane lipids. *L. monocytogenes* cannot synthesize unsaturated fatty acids (Giotis *et al.* 2007; Singh *et al.* 2008; Zhu *et al.* 2005a; Zhu *et al.* 2005b). Therefore, $C_{18:1}$ covalently linked to phospholipids PG and LPG as revealed by total Q-TOF MS must be exogenous in origin (Fig. 2.1a, b). All phospholipids analyzed contained one $C_{15:0}$ acyl chain combined with a second acyl chain ($C_{15:0}$, $C_{18:1}$, $C_{16:0,}$ or $C_{17:0}$). PG and LPG species containing $C_{15:0}/C_{15:0}$ or $C_{15:0}/C_{18:1}$ were the dominating molecular species (Fig. 2.1c–f). Two different acyltransferases are involved in the synthesis of phospholipids in bacteria. A glycerolphosphate acyltransferase synthesizes lysophosphatidic acid, and a lysophosphatidic acid acyltransferase produces phosphatidic acid, the precursor of all phospholipids (Yao *et al.* 2016). Due to the presence of $C_{15:0}$ in all phospholipids of *L. monocytogenes,* one of the two acyltransferases may be characterized by a high substrate specificity for $C_{15:0}$. In contrast, the other acyltransferase may show a broader substrate specificity for different fatty acids. Furthermore, a high similarity between the molecular species distribution regarding PG and LPG could be observed. Besides, we could detect neither $C_{18:1}$ nor $C_{18:0}$ in glycolipids, which are present in *L. monocytogenes* in addition to phospholipids (Fischer & Leopold 1999). Therefore, all these observations favor the enzymatic and probably selective (concerning the *sn*-position of the glycerol) incorporation of high amounts of $C_{18:1}$ and conclusively of other exogenous fatty acids into phospholipids. These results suggest that other detected exogenous fatty acids of the fatty acid profile are also covalently bound to the polar lipids of *L. monocytogenes*, contrasting a previous report, which found no integration

of $C_{18:1}$ into phospholipids only the intercalation of this lipid in the bacterial membrane (DeMars *et al.* 2020). This discrepancy may be attributed to the use of ester-bound fatty acids (P60, P80, food extracts) in our study, in contrast to free fatty acids as a supplement in previous studies. We did not study the polar lipids in more detail, as the polar head groups of the membrane lipids have only minor effects on the thermal membrane properties and show no changes in their composition in *L. monocytogenes* at low growth temperatures (Russel 1984; Verheul *et al.* 1997; Zhang & Rock 2008).

Fatty acids with a high T_m (saturated, straight-chain fatty acids) decrease membrane fluidity, whereas fatty acids with a low T_m (unsaturated and branched-chain fatty acids) increase membrane fluidity (Heinrich 1976). TMA-DPH-dependent anisotropy measurements confirmed the influence of exogenous fatty acids on the membrane fluidity of whole living cells with a complex lipid composition (Fig. 2.2). None of the strains showed the two typical plateaus that indicate the two temperature-dependent ultimate states of biomembranes: the gel-like solid-state (high TMA-DPH anisotropy) and the liquid-crystalline liquid-state (low TMA-DPH anisotropy). A linear curve progression rather than a sigmoidal curve described the relation between anisotropy and measuring temperature for all strains tested, which generally describes the phase transition of the membrane (Harris *et al.* 2002). The cultures grown in TSB-YE supplemented with P80 or SSE showed a higher membrane fluidity in all strains than those without supplementation. These results indicated significantly more fluid membrane below 20 °C and unchanged fluidity above 20 °C. The change in TMA DPH anisotropy with a value of 0.03 was approximately the same for all three strains. After supplementation with P80 and SSE (Table 2.1, 2.3), the altered fatty acid profile suggests that the exogenous unsaturated fatty acids with low T_m cause this effect, resulting in more beneficial membrane fluidity and more pronounced adaptation of the membrane to low temperatures. Because washed cells incubated in Ringer's solution and supplemented with P80 and SSE did neither show the implementation of supplemented fatty acids nor any change in TMA DPH anisotropy, we concluded that active incorporation of exogenous fatty acids in growing cells is a prerequisite for impacting cell membrane fluidity by these exogenous lipids (Fig. 2.3).

We also demonstrated that cell membranes complemented with exogenous and low T_m fatty acids, such as $C_{18:1}$ *cis* 9, are protective against freeze-thaw stress. Resistance against freeze-thaw stress is used to indicate a resilient and robust membrane structure (Carlquist *et al.* 2012). Significantly higher resistance was detected as $\log_{10}$-reduction of CFU mL^{-1} for all strains grown at 6 °C with incorporated $C_{18:1}$ *cis* 9. In contrast, only strain DSM 20600^T showed lower $\log_{10}$-reduction of CFU mL^{-1} after $C_{16:0}$ and $C_{18:0}$ incorporation. The strains FFH and FFL 1 showed no significant changes in the $\log_{10}$-reduction of CFU mL^{-1} when $C_{16:0}$ was incorporated. Furthermore, bacterial cell growth was reduced after incorporation of $C_{16:0}$ and $C_{18:0}$ and increased after the incorporation of $C_{18:1}$ in all

strains grown at 6 °C. On the other hand, if cells were grown at 37 °C, both fatty acids increased the growth rate for all strains (Fig. 2.5).

Yao *et al.* (2016) stated that *L. monocytogenes* do not actively incorporate exogenous fatty acids into their membrane phospholipids. Nevertheless, the genome encodes the gene loci *lmo1814*, *lmo1863,* and *lmo2514*, representing homologs of the two-component fatty acid kinase system FakA/FakB of *S. aureus*. For *S. aureus,* this system catalyzes the first steps in exogenous fatty acid incorporation, which is the binding and phosphorylation of exogenous fatty acids. The acyl-phosphates formed can then enter the phospholipid synthesis (Yao & Rock 2013, 2015). A standard nucleotide Basic Local Alignment Search Tool (BLAST) check revealed that homologs of the FakA/FakB genes are present in at least 100 deposited genomes of *L. monocytogenes*, highlighting the conservation of these genes and the crucial importance of this mechanism.

In this study, we could demonstrate that the fatty acid profile of *L. monocytogenes* was modified by exogenous fatty acids at low and high growth temperatures, changing membrane fluidity and growth properties. The present exogenous fatty acid improves membrane fluidity and cell viability at low growth temperatures. The influence of external fatty acids from the food matrix significantly affects the contamination dynamics of chilled foods. We demonstrated that the acyl chain composition plays a crucial role in the survival of *L. monocytogenes*, and an increase in straight-chain fatty acids reduces the organism's growth rate.

4 Materials and Methods

Materials

All chemical reagents and solvents were purchased from Alfa Aesar, Carl Roth, MilliporeSigma, Sigma-Aldrich, Thermo Fisher Scientific, or VWR. All solvents and water for analytics were HPLC grade and used as received. Ultra-high temperature processed milk (3.5% fat), modified atmosphere packaged minced meat, and pre-cut vacuum-packed smoked salmon were purchased at a local supermarket chain store.

Strains, culture media, and cultivation

In this research, three different strains of *L. monocytogenes* were examined. Strain FFH (= DSM 112142; serovar group 4b, 4d, or 4e) was isolated from minced meat in 2011 and strain FFL 1 (= DSM 112143; serovar group 1/2a or 3a) from smoked salmon in 2012. In addition, the strain *L. monocytogenes* DSM 20600^{T} (serovar group 1/2a) was obtained from the Leibniz Institute DSMZ-German Collection of Microorganisms and Cell Cultures GmbH. The adaptive response of strain FFL 1 to low

temperature is primarily an FA-dependent mechanism, while strains DSM 20600^T and FFH also expressed an MK-based response (Seel *et al.* 2018).

All strains were aerobically cultured in 200 µL or 100 mL TSB-YE. The medium is composed of tryptic soy broth containing 17 g peptone from casein L^{-1}, 3 g peptone from soy meal L^{-1}, 2.5 g D-glucose L^{-1}, 5 g sodium chloride L^{-1}, and 2.5 g dipotassium hydrogen phosphate L^{-1} supplemented with 6 g yeast extract L^{-1} or in BHI broth composed of 12.5 g brain infusion solids L^{-1}, 5 g beef heart infusion solids L^{-1}, 10 g protease peptone L^{-1}, 2 g glucose L^{-1}, 5 g sodium chloride L^{-1} and 2.5 g disodium phosphate L^{-1} using 96-well microplates or 300 mL Erlenmeyer flasks, respectively. The TSB-YE was supplemented with 0.1% (wt/vol) polysorbate 60 (P60), with 0.1% (wt/vol) polysorbate 80 (P80), with each of 0.05% (wt/vol) P60 and P80 (P60P80), with 0.1% (wt/vol) ME, with 0.1% (wt/vol) MME, or with 0.1% (wt/vol) SSE, respectively. 0.078% (wt/vol) D-sorbitol was used as control. We measured the medium's a_w with a LabMaster-aw instrument (Novasina, Switzerland). OD_{625} documented growth in TSB-YE with or without supplementation by a GENESYS 30 visible spectrophotometer (Thermo Fisher Scientific, USA) or a Synergy H1 modular multimode microplate reader (BioTek Instruments, Inc., USA). Growth was fitted by the Gompertz growth model as previously described (López *et al.* 2004). Cultures were prepared in multiple independent replicates, inoculated with 1% (vol/vol) of an overnight culture at 30 °C and incubated on an orbital shaker at 6 or 37 °C and 150 rpm until late exponential phase (OD_{625} = 0.8–1.0) or stationary phase for growth rate determination. Cultures were harvested by centrifugation (10 min at 10000 × *g*) at growth temperature and washed thrice with sterile phosphate-buffered saline (PBS) pH 7.4. Subsequently, bacterial cells were used for temperature stress tests, fatty acid analysis, determination of MK content, polar lipid analysis, and membrane fluidity analysis. Colonies were cultivated on TSA-YE at 30 °C. Additionally, each strain was incubated on TSA-YE supplemented with 0.1% (wt/vol) ME, with 0.1% (wt/vol) MME, or with 0.1% (wt/vol) SSE for fatty acid analysis.

To determine colony forming units (CFU) for the freeze-thaw stress test, 50 µL of serial dilutions were plated on TSA-YE (90 mm Petri dish) using the exponential mode (ISO 4833-2, ISO 7218, and AOAC 977.27) of the easySpiral automatic plater (Interscience, France). After a one-day incubation at 37 °C, the CFU were counted for the corresponding dilution steps, and the weighted average of enumerated *L. monocytogenes* was given in CFU mL^{-1}. The results for the temperature stress test were presented as decadic logarithm (log_{10}) reduction relative to the initial CFU mL^{-1}, respectively.

Lipid extraction from food

Total lipids from commercially available milk (3.5% fat), minced meat, and smoked salmon were extracted using the method by Bligh and Dyer as previously described (Manirakiza *et al.* 2001). Minced meat and smoked salmon were used directly without any pretreatments. Milk was freeze-dried before extraction. One hundred grams of food were incubated for 2 h at room temperature under shaking with 150 mL of chloroform/methanol (1:2, vol/vol) in a 500 mL Erlenmeyer flask. Then we added 50 mL of chloroform and let the mixture shake for another 1 h. The extract was filtered using cellulose filter paper. For phase separation, 90 mL of PBS (pH 7.4) were added, mixed vigorously, and incubated at – 20 °C. The lower layer was evaporated to dryness with nitrogen and stored at – 20 °C.

Freeze-thaw stress tests

The freeze-thaw stress test was performed by subjecting each strain to three freeze-thaw cycles. First, three aliquots of 2 mL bacterial cell suspension for each strain were frozen at – 20 °C. Then, after 24, 48, and 72 h, aliquots were thawed for 20 min at room temperature, and the number of CFU mL^{-1} was determined. Finally, the remaining aliquots were refrozen for subsequent freeze-thaw cycles.

Fatty acid extraction and analysis

Approximately 40 mg of washed bacterial cells per sample were used for fatty acid analysis. Fatty acids were extracted and analyzed as methyl esters (FAMEs) as previously described (Seel *et al.* 2018). First, cells were resuspended in 1 mL of 15% (wt/vol) sodium hydroxide (NaOH) in methanol/water (1:1, vol/vol) using 10 mL hydrolysis tubes and saponified for 30 min at 100 °C. Next, fatty acids were methylated with 2 mL (6 N) hydrochloric acid/methanol (1:1.2, vol/vol) for 10 min at 80 °C and immediately cooled on ice. Next, fatty acid methyl esters were extracted with 1.25 mL hexane/methyl *tert*-butyl ether (1:1, vol/vol) for 10 min in an overhead mixer. Phases were separated by centrifugation (5 min at 3000 × *g*), and the lower phase was discarded. Subsequently, a base wash of the upper phase was performed with 3 mL of 1.2% (wt/vol) NaOH in water. The fatty acid methyl esters were identified by gas chromatography-mass spectrometry (GC-MS) with a 7890A gas chromatograph (Agilent Technologies, USA) equipped with a 5% phenylmethyl silicone capillary column coupled with a 5975C mass spectrometer (Agilent Technologies, USA), as previously described (Lipski & Altendorf 1997). Fatty acid analysis was performed with MSD ChemStation software (version E.02.00.493, Agilent Technologies, USA), and their retention times and mass spectra were identified. In addition, dimethyl disulfide (DMDS) derivatization and analyses of unsaturated FAMEs were performed as described by Nichols *et al.* (1986).

The effect of alterations in fatty acid profiles associated with the supplemented lipids on membrane fluidity was determined by calculating the weighted average melting temperature (WAMT) as described previously (Seel *et al.* 2018). Considering the individual melting temperatures of each FA, this parameter allows integrating the quantitative changes of all membrane-associated fatty acids. However, the WAMT value does not represent the actual melting temperature of the cytoplasmic membrane, which also depends on the total polar lipid structure. Therefore, the melting temperatures for fatty acids were taken from previously described research

$$\mathrm{WAMT} = \mathrm{FA_1}(\%) \times \mathrm{T_m}(\mathrm{FA_1}) + \mathrm{FA_2}(\%) \times \mathrm{T_m}(\mathrm{FA_2}) + \ \ldots \ + \ \mathrm{FA_n}(\%) \times \mathrm{T_m}(\mathrm{FA_n})$$

Equation 2.1 The bacterial membrane's weighted average melting temperature (WAMT). All fatty acids (FA_1 to FA_n) that are present in the fatty acid profile, FA_1 (%) is the percentage of fatty acid no. 1 and melting temperature (T_m) of the corresponding fatty acid. The difference in WAMT (ΔWAMT) indicates the extent of adaptation through the fatty acid shift.

Polar lipid extraction and analysis

The mass spectra of polar lipids were analyzed to verify whether the fatty acids from the supplemented culture media were covalently linked to polar lipids of the bacterial membrane. Total lipids from bacterial cells were extracted according to Bligh & Dyer(1959). Approximately 50 mg bacterial cells were resuspended in 3 mL H_2O and boiled for 10 min using 10 mL hydrolysis tubes. Ruptured cells were centrifuged (15 min at 3000 × *g*), and the supernatant was discarded. The extraction was performed in two steps using 3 mL chloroform/methanol (1:2, vol/vol) and 3 mL chloroform/methanol (2:1 vol/vol) under shaking for 30 min. Extracts were pooled, and phases were separated by adding 3 mL chloroform and 0.75 ml water (with a final ratio of chloroform/methanol/water of 2:1:0.75, vol/vol/vol) followed by centrifugation (15 min at 3000 × *g*). The organic phase was evaporated to dryness with nitrogen and stored at – 80 °C until analysis. For analysis, the evaporated extracts were dissolved in 0.1 mL with chloroform/methanol (2:1 vol/vol) and filtered through 0.2 µm polytetrafluoroethylene (PTFE) filters (VWR International, Germany).

Membrane lipids were analyzed using a 6530 Q-TOF MS (Agilent Technologies, United States) by direct infusion of total lipid extracts in the positive ion mode (Devers *et al.* 2011). PG and LPG were additionally measured in the negative ion mode with 50 V collision energy. Lipids were selected in a non-targeted approach in the "auto-MS/MS" mode, which means that the most intense precursor ions are selected automatically. Glycolipids were separated by solid-phase extraction of total lipid extracts with Isolute SI Columns (Biotage AB, Sweden) before analyzing with Q-TOF MS. The data acquisition was performed with MassHunter software (version B.02.00; Agilent Technologies, USA).

Isoprenoid quinone extraction and analysis

About 30–50 mg cells were extracted with methanol/chloroform (9:5, vol/vol) as previously described (Hu *et al.* 1999; Seel *et al.* 2018). Evaporated extracts were made up to 1 mL with methanol and analyzed using a 1260 Infinity Quaternary LC system (Agilent Technologies, USA) equipped with a quaternary pump, an autosampler, a thermo-controlled column compartment, and a diode array detector. Compounds were separated isocratically at 30 °C on a Hypersil™ ODS C18 column (Thermo Fisher Scientific, USA) using methanol/diisopropyl ether (9:2, vol/vol) as eluent (flow rate of 1 mL min^{-1}). Isoprenoid quinones were detected at 270 and 275 nm and were identified by their absorption spectrum and retention time. The quinones were quantified as vitamin K_1 equivalents using an external calibration curve and an internal vitamin K_1 standard. Data acquisition was performed with OpenLAB CDS ChemStation software (version C.01.07, Agilent Technologies, USA).

Membrane fluidity analyses by anisotropy

Whole bacterial cells were prepared and stained with the fluorescent probe TMA-DPH to determine anisotropy, as Seel *et al.* (2018) described. TMA-DPH anisotropy is particularly suitable for measuring membrane fluidity measuring the direct mobility of the probe and adjacent lipids (Harris *et al.* 2002). High TMA-DPH anisotropy values correspond to low fluidity and low values to high membrane fluidity. Steady-state fluorescence was measured in an LS 55 fluorescence spectrometer combined with a PTP-1 Peltier system (PerkinElmer, United States) for sample temperature regulation. Cells were washed and resuspended in Tris-EDTA (TE) buffer solution (pH 7.4) and diluted to OD_{625} 0.2. TMA-DPH stock solution was prepared in dimethyl sulfoxide (DMSO) at a concentration of 0.4 mM. Cells were stained with 0.5 µM TMA-DPH for 10 min at 30 °C in the dark and washed twice. Measurements were performed with a 2 mL sample volume in 3.5 mL quartz glass cuvettes (Hellma, Germany). For TMA-DPH anisotropy measurements, samples were excited at 355 nm, and emission intensities were recorded at 425 nm. Anisotropy (*r*) values were calculated from polarized intensities using Eq. 2.

$$r = \frac{I_{\mathrm{VV}} - GI_{\mathrm{VH}}}{I_{\mathrm{VV}} + 2GI_{\mathrm{VH}}}$$

Equation 2.2 Anisotropy (*r*) of trimethylammonium diphenylhexatriene (TMA-DPH). The fluorescence intensity (*I*) from which blank values of non-dyed cells were subtracted. Grating factor (*G*), calculated by the ratio of horizontal (H) and vertical (V) polarizer positions for the excited and the emitted light. Each data point was calculated from 10–20 single measurements.

The abiotic effect of P80 on biomembranes was tested with non-growing *L. monocytogenes* cells. For this purpose, bacterial cells were grown in TSB, washed thrice (10 min at 3000 × *g*) with Tris-EDTA (TE) buffer (Alfa Aesar, USA) solution (pH 7.4). The bacterial cell pellet was then dissolved in

100 mL TE buffer to OD_{625nm} 0.8 without or with 0.1% (wt/vol) P80 and incubated at 6 °C for 24, 48, and 78 h. After each time point, the membrane fluidity, $OD_{625,}$ and fatty acid profile were determined as described previously.

Statistical analysis

Statistical analysis was performed using Prism (version 9.2.0; GraphPad Software, USA). Mean values (M) and standard deviations (SD) of *n* (see legends) biological replicates were calculated for all experiments. Two-way ANOVA was performed with recommended post hoc test ($\alpha = 0.001$). Data are presented as M ± SD; *$p < 0.001$, **$p < 0.0001$, ***$p < 0.00001$, ****$p < 0.000001$.

References

Angelidis AS, Smith LT, Hoffman LM, Smith GM (2002) Identification of *opuC* as a chill-activated and osmotically activated carnitine transporter in *Listeria monocytogenes*. *Appl Environ Microbiol* 68:2644–2650

Angelo KM, Conrad AR, Saupe A, Dragoo H, West N *et al.* (2017) Multistate outbreak of *Listeria monocytogenes* infections linked to whole apples used in commercially produced, prepackaged caramel apples: United States, 2014–2015. *Epidemiol Infect* 145:848–856

Annous BA, La Becker, Bayles DO, Labeda DP, Wilkinson BJ (1997) Critical role of *anteiso*-$C_{15:0}$ fatty acid in the growth of *Listeria monocytogenes* at low temperatures. *Appl Environ Microbiol* 63:3887–3894

Atila M, Luo Y (2016) Profiling and tandem mass spectrometry analysis of aminoacylated phospholipids in *Bacillus subtilis*. *F1000Research* 5:121

Balemans W, Lounis N, Gilissen R, Guillemont J, Simmen K *et al.* (2010) Essentiality of FASII pathway for *Staphylococcus aureus*. *Nature* 463:E3

Bligh EG, Dyer WJ (1959) A rapid method of total lipid extraction and purification. *Can J Biochem Physiol* 37:911–917

Brinster S, Lamberet G, Staels B, Trieu-Cuot P, Gruss A, Poyart C (2009) Type II fatty acid synthesis is not a suitable antibiotic target for Gram-positive pathogens. *Nature* 458:83–86

Buchanan RL, Gorris LG, Hayman MM, Jackson TC, Whiting RC (2017) A review of *Listeria monocytogenes*: An update on outbreaks, virulence, dose-response, ecology, and risk assessments. *Food Control* 75:1–13

Carlquist M, Fernandes RL, Helmark S, Heins A-L, Lundin L *et al.* (2012) Physiological heterogeneities in microbial populations and implications for physical stress tolerance. *Microbial Cell Factories* 11:94

De Sarrau B, Clavel T, Zwickel N, Despres J, Dupont S *et al.* (2013) Unsaturated fatty acids from food and in the growth medium improve growth of *Bacillus cereus* under cold and anaerobic conditions. *Food Microbiol* 36:113–122

DeMars Z, Singh VK, Bose JL (2020) Exogenous fatty acids remodel *Staphylococcus aureus* lipid composition through fatty acid kinase. *J Bacteriol* 202:e00128–20

Devers EA, Wewer V, Dombrink I, Dörmann P, Hölzl G (2011) A processive glycosyltransferase involved in glycolipid synthesis during phosphate deprivation in *Mesorhizobium loti*. *J Bacteriol* 193:1377–1384

European Food Safety Authority and European Centre for Disease Prevention and Control (2021) The European Union One Health 2019 Zoonoses Report. *EFSA J* 19:e06406

Farber JM, Peterkin PI (1991) *Listeria monocytogenes*, a food-borne pathogen. *Microbiol Rev* 55:476–511

Fischer W, Leopold K (1999) Polar lipids of four *Listeria* species containing L-lysylcardiolipin, a novel lipid structure, and other unique phospholipids. *Int J Syst Bacteriol* 2:653–662

Flegler A, Kombeitz V, Lipski A (2021) Menaquinone-mediated regulation of membrane fluidity is relevant for fitness of *Listeria monocytogenes*. *Arch Microbiol* 203:3353–3360

Giotis ES, McDowell DA, Blair IS, Wilkinson BJ (2007) Role of branched-chain fatty acids in pH stress tolerance in *Listeria monocytogenes*. *Appl Environ Microbiol* 73:997–1001

Hamon M, Bierne H, Cossart P (2006) *Listeria monocytogenes*: a multifaceted model. *Nat Rev Microbiol* 4:423–434

Harris FM, Best KB, Bell JD (2002) Use of laurdan fluorescence intensity and polarization to distinguish between changes in membrane fluidity and phospholipid order. *BBA Biomembr* 1565:123–128

Heinrich MR (1976) *Extreme Environments: Mechanisms of Microbial Adaptation*. Elsevier Science, Burlington

Hernandez-Milian A, Payeras-Cifre A (2014) What is new in listeriosis? *Biomed Res Int* 2014:358051

Hu H-Y, Fujie K, Urano K (1999) Development of a novel solid phase extraction method for the analysis of bacterial quinones in activated sludge with a higher reliability. *J Biosci Bioeng* 87:378–382

Juneja VK, Foglia TA, Marmer BS (1998) Heat resistance and fatty acid composition of *Listeria monocytogenes*: effect of pH, acidulant, and growth temperature. *J Food Prot* 61:683–687

Knapp HR, Melly MA (1986) Bactericidal effects of polyunsaturated fatty acids. *J Infect Dis* 154:84–94

Knothe G, Dunn RO (2009) A comprehensive evaluation of the melting points of fatty acids and esters determined by differential scanning calorimetry. *J Am Oil Chem Soc* 86:843–856

Lipski A, Altendorf K (1997) Identification of heterotrophic bacteria isolated from ammonia-supplied experimental biofilters. *Syst Appl Microbiol* 20:448–457

López S, Prieto M, Dijkstra J, Dhanoa MS, France J (2004) Statistical evaluation of mathematical models for microbial growth. *Int J Food Microbiol* 96:289–300

Lopez-Valladares G, Danielsson-Tham M-L, Tham W (2018) Implicated food products for listeriosis and changes in serovars of *Listeria monocytogenes* affecting humans in recent decades. *Foodborne Pathog Dis* 15:387–397

Manirakiza P, Covaci A, Schepens P (2001) Comparative study on total lipid determination using Soxhlet, Roese-Gottlieb, Bligh & Dyer, and Modified Bligh & Dyer extraction methods. *J Food Compos Anal* 14:93–100

Mastronicolis S, German J, Megoulas N, Petrou E, Foka P, Smith G (1998) Influence of cold shock on the fatty-acid composition of different lipid classes of the food-borne pathogen *Listeria monocytogenes*. *Food Microbiol* 15:299–306

Mastronicolis SK, Boura A, Karaliota A, Magiatis P, Arvanitis N et al.(2006) Effect of cold temperature on the composition of different lipid classes of the foodborne pathogen *Listeria monocytogenes*: focus on neutral lipids. *Food Microbiol* 23:184–194

Mead PS, Slutsker L, Dietz V, McCaig LF, Bresee JS *et al.* (1999) Food-related illness and death in the United States. *Emerging Infect Dis* 5:607–625

Nichols PD, Guckert JB, White DC (1986) Determination of monosaturated fatty acid double-bond position and geometry for microbial monocultures and complex consortia by capillary GC-MS of their dimethyl disulphide adducts. *J Microbiol Met* 5:49–55

Parsons JB, Frank MW, Subramanian C, Saenkham P, Rock CO (2011) Metabolic basis for the differential susceptibility of Gram-positive pathogens to fatty acid synthesis inhibitors. *Proc Natl Acad Sci USA* 108:15378–15383

Russel N (1984) Mechanisms of thermal adaptation in bacteria: blueprints for survival. Trends Biochem Sci 9:108–112

Ryser ET, Marth EH (2007) *Listeria, listeriosis, and food safety*. Taylor & Francis, Boca Raton

Saldivar JC, Davis ML, Johnson MG, Ricke SC (2017) *Chapter13–Listeria monocytogenes adaptation and growth at low temperatures: mechanisms and implications for foodborne disease*. In: Ricke SC, Atungulu GG, Rainwater C, Park SH (eds) *Food and Feed Safety Systems and Analysis*. Elsevier Science, Saint Louis

Seel W, Flegler A, Zunabovic-Pichler M, Lipski A (2018) Increased isoprenoid quinone concentration modulates membrane fluidity in *Listeria monocytogenes* at low growth temperatures. *J Bacteriol* 200:00148–18

Singh VK, Hattangady DS, Giotis ES, Singh AK, Chamberlain NR *et al.* (2008) Insertional inactivation of branched-chain alpha-keto acid dehydrogenase in *Staphylococcus aureus* leads to decreased branched-chain membrane fatty acid content and increased susceptibility to certain stresses. *Appl Environ Microbiol* 74:5882–5890

Tatituri RVV, Wolf BJ, Brenner MB, Turk J, Hsu F-F (2015) Characterization of polar lipids of *Listeria monocytogenes* by HCD and low-energy CAD linear ion-trap mass spectrometry with electrospray ionization. *Anal Bioanal Chem* 407:2519–2528

Verheul A, Russell NJ, Van't Hof R, Rombouts FM, Abee T (1997) Modifications of membrane phospholipid composition in nisin-resistant *Listeria monocytogenes* Scott A. *Appl Environ Microbiol* 63:3451–3457

Walker SJ, Archer P, Banks JG (1990) Growth of *Listeria monocytogenes* at refrigeration temperatures. *J Appl Bacteriol* 68:157–162

Weitkamp AW (1945) The acidic constituents of degras. A new method of structure elucidation. *J Am Chem Soc* 1:447–454

Yao J, Rock CO (2013) Phosphatidic acid synthesis in bacteria. *BBA* 1831:495–502

Yao J, Rock CO (2015) How bacterial pathogens eat host lipids: implications for the development of fatty acid synthesis therapeutics. *J Biol Chem* 290:5940–5946

Yao J, Rock CO (2017) Exogenous fatty acid metabolism in bacteria. *Biochimie* 141:30–39

Yao J, Ericson ME, Frank MW, Rock CO (2016) Enoyl-acyl carrier protein reductase I (FabI) is essential for the intracellular growth of *Listeria monocytogenes*. *Infect Immun* 84:3597–3607

Zhang Y-M, Rock CO (2008) Membrane lipid homeostasis in bacteria. *Nat Rev Microbiol* 6:222–233

Zhang X, Wang S, Chen X, Qu C (2021) Review controlling *Listeria monocytogenes* in ready-to-eat meat and poultry products: An overview of outbreaks, current legislations, challenges, and future prospects. *Trends Food Sci Technol* 116:24–35

Zhou Y, Peisker H, Dörmann P (2016) Molecular species composition of plant cardiolipin determined by liquid chromatography mass spectrometry. *J Lipid Res* 57:1308–1321

Zhu K, Ding X, Julotok M, Wilkinson BJ (2005a) Exogenous isoleucine and fatty acid shortening ensure the high content of *anteiso*-$C_{15:0}$ fatty acid required for low-temperature growth of *Listeria monocytogenes*. *Appl Environ Microbiol* 71:8002–8007

Zhu K, Bayles DO, Xiong A, Jayaswal RK, Wilkinson BJ (2005b) Precursor and temperature modulation of fatty acid composition and growth of *Listeria monocytogenes* cold-sensitive mutants with transposon-interrupted branched-chain alpha-keto acid dehydrogenase. *Microbiology* 151:615–623

Chapter 3

Menaquinone-mediated regulation of membrane fluidity is relevant for fitness of *Listeria monocytogenes*

Listeria monocytogenes is a food-borne pathogen with the ability to grow at low temperatures down to -0.4 °C. Maintaining cytoplasmic membrane fluidity by changing the lipid membrane composition is important during growth at low temperatures. In *Listeria monocytogenes*, the dominant adaptation effect is the fluidization of the membrane by shortening of fatty acid chain length. In some strains, however, an additional response is the increase in menaquinone content during growth at low temperatures. The increase of this neutral lipid leads to fluidization of the membrane and thus represents a mechanism that is complementary to the fatty acid-mediated modification of membrane fluidity. This study demonstrated that the reduction of menaquinone content for *Listeria monocytogenes* strains resulted in significantly lower resistance to temperature stress and lower growth rates compared to unaffected control cultures after growth at 6 °C. Menaquinone content was reduced by supplementation with aromatic amino acids, which led to a feedback inhibition of the menaquinone synthesis. Menaquinone-reduced *Listeria monocytogenes* strains showed reduced bacterial cell fitness. This confirmed the adaptive function of menaquinones for growth at low temperatures of this pathogen.

Keywords: *Listeria monocytogenes*; Cold adaptation; Fatty acids; Menaquinone; Membrane fluidity; Bacterial cell fitness

Flegler A, Kombeitz V, Lipski A (2021) Menaquinone-mediated regulation of membrane fluidity is relevant for fitness of *Listeria monocytogenes*. *Arch Microbiol* 203:3353–3360. DOI: 10.1007/s00203-021-02322-6

Author contributions: AF designed research and wrote the manuscript. AF and VK performed research and analysed data. AL reviewed and edited the manuscript.

1 Introduction

Listeria monocytogenes (*L. monocytogenes*) is a Gram-positive, facultative anaerobic bacterium that is responsible for the foodborne disease listeriosis. In 2018, the European Food Safety Authority (EFSA) identified listeriosis as one of the most severe zoonoses with the highest case fatality rate of 15.6% based on severity data (EFSA-ECDC 2019). The ability of *L. monocytogenes* to grow at low temperatures allows this bacterium to persist in food processing plants, which can lead to the contamination of food and thus to the spread of listeriosis (Lopez-Valladares *et al.* 2018). *L. monocytogenes* can grow in a temperature range from -0.4 to 50 °C (Farber & Peterkin 1991; Walker *et al.* 1990). For that reason, the capacity of *L. monocytogenes* to grow at low temperatures is crucial for its ability to colonize, reproduce and persist in the food-processing environment and on food-processing equipment (Ryser & Marth 2007).

One of the most important adaptations to low growth temperatures is the regulation of membrane fluidity (Gounot & Russell 1999; Mykytczuk *et al.* 2007; Suutari & Laakso 1994; Zhang & Rock 2008). The function of the cell membrane depends on the physical state of the lipid bilayer. To provide an ideal setting for membrane-associated cell functions, a lipid bilayer must be in a liquid-crystalline state (De Mendoza & Cronan 1983). A decrease in membrane fluidity and the associated phase transition to a solid, gel-like state leads to an impairment of growth (Annous *et al.* 1997; Chihib *et al.* 2003; Jones *et al.* 2002). Therefore, the regulation of the membrane fluidity ensures the biologically active state of the membrane and enables the bacterial cells to adapt to varying environmental temperatures. Generally, a decrease in the temperature slows down the reaction rates of various cellular processes and also reduces the fluidity of the bacterial cell membrane (Tasara & Stephan 2006). The decrease of the membrane fluidity could disrupt membrane-associated processes such as electron transport in the respiratory chain, membrane permeability and substrate transport (Zhang & Rock 2008). Moreover, lower reaction rates also result in lower growth rates. To avoid those disruptions, bacteria modulate membrane fluidity by modifying their fatty acid composition. To prevent liquid-gel transition at low temperatures, fatty acids with lower melting temperatures are incorporated into the membrane. The fluidity of biological membranes is mainly determined by the lipid-acyl chains of polar lipids (Russel 1984). The cytoplasmic membrane of *L. monocytogenes* consists mainly of the branched fatty acids *anteiso*-$C_{15:0}$ and *anteiso*-$C_{17:0}$. When growing under cold conditions, the proportion of *anteiso*-$C_{17:0}$ decreases and the proportion of *anteiso*-$C_{15:0}$ increases until the latter accounts for up to 80% of the total fatty acid profile (Annous *et al.* 1997; Mastronicolis *et al.* 1998, 2006; Tatituri *et al.* 2015). This causes the membrane fluidity to be maintained since the fatty acid *anteiso*-$C_{15:0}$ has a lower melting point (Knothe & Dunn

2009). Several strains of *L. monocytogenes* show an additional mechanism for the regulation of membrane fluidity. In a previous study, it was shown that besides fatty acid modification, the menaquinone-7 (MK-7) content also contributes to the regulation of membrane fluidity in *Listeria* by broadening the phase transition (Seel *et al.* 2018). Similar effects were previously shown for various artificial systems in lipid vesicles mixed with ubiquinone-3, vitamin K_1, and cholesterol (Asai 2000; Asai & Watanabe 1999; Harris *et al.* 2002; Ortiz & Aranda 1999; Seel *et al.* 2018). Quinones are ubiquitous lipid-soluble molecules that are mainly known for their involvement in membrane-bound electron transport in the respiratory chain and part of the cytoplasmic membrane (Søballe & Poole 1999). Low temperatures of 6 °C induce an increased production of MK-7 in some *L. monocytogenes* strains, thus expanding the phase transition to a gel-like membrane state to maintain the membrane fluidity under low- temperature growth conditions. The synthesis of MK-7 could be a second important cold adaptation mechanism due to the less energy requirement compared to the required energy for the fatty acid synthesis (Seel *et al.* 2018; Zhang & Rock 2008). However, it is still unknown how the suppression of the thermotropic phase transition by higher amounts of menaquinones (MKs) has an impact on membrane integrity and finally on bacterial cell fitness under low-temperature conditions. Using the term fitness as a quantitative attribute for the survival of an external stressor, this study tested the fitness of bacterial cells by subjecting them to freeze-thaw stress. Resistance to freeze-thaw stress is an accepted indicator for cell membrane integrity and bacterial cell fitness (Carlquist *et al.* 2012; Sleight *et al.* 2006). It was hypothesised that supplementation with inhibitors for MK synthesis will cause negative effects on membrane integrity and finally on resistance to temperature stress and growth rates of *L. monocytogenes* strains under low-temperature conditions. In this project, aromatic amino acids (AAA) were used as inhibitors for MK synthesis. Tsukamoto *et al.* (2001) demonstrated for a *Bacillus subtilis* (*B*. *subtilis*) strain the inhibitory effect of AAA on MK synthesis. Because MKs, as well as AAA, are synthesised via the shikimate pathway, the supplementation with AAA results in a lower MK content due to feedback inhibition. In accordance with this observation, a previous study also showed for *L. monocytogenes* strains the inhibitory effect of AAA on MK-7 synthesis and moreover an effect on the phase transition performance of the membrane-associated with the lowered MK content (Seel *et al.* 2018). The present study demonstrated the relationship between MK content and bacterial cold adaptation and revealed the regulation of MK synthesis as additional adaptive response to growth under low temperature conditions.

2 Materials and methods

Materials

All chemical reagents and solvents were purchased from Alfa Aesar, Carl Roth, MilliporeSigma, Sigma-Aldrich, Thermo Fisher Scientific, and VWR. Solvents and water for analytics were of HPLC grade and used as received.

Strains, culture media, and cultivation

In this research, three different strains of *L. monocytogenes* were examined. The strain FFH (= DSM 112142; serovar group 4b, 4d, or 4e) was isolated from minced meat in 2011 and the strain FFL 1 (= DSM 112143; serovar group 1/2a or 3a) from Irish smoked organic salmon in 2012. The type strain DSM 20600^T (serovar group 1/2a) was included as the reference strain in this study. The type strain was obtained from the Leibniz Institute DSMZ-German Collection of Microorganisms and Cell Cultures. The two strains FFH and FFL 1 were deposited at the DSMZ open collection. These strains were assigned to serovar groups by multiplex polymerase chain reaction (PCR) according to the method of Doumith *et al.* (2004). The adaptive response of strain FFL 1 to low temperature is primarily a fatty acid-dependent mechanism while strains DSM 20600^T and FFH expressed, in addition, MK-mediated response (Seel *et al.* 2018).

All strains were aerobically cultured in 100 ml tryptic soy broth-yeast extract (TSB-YE) medium composed of tryptic soy broth containing 17.0 g peptone from casein l^{-1}, 3.0 g peptone from soy l^{-1}, 2.5 g D-glucose l^{-1}, 5.0 g sodium chloride l^{-1}, and 2.5 g dipotassium hydrogen phosphate l^{-1} supplemented with 6.0 g yeast extract l^{-1} or in 100 ml ultra-high temperature processed milk (UHT-milk, 3.5% fat) using 300 ml Erlenmeyer flasks. The TSB-YE medium or the UHT-milk, respectively, was supplemented with a mixture of the AAA L-phenylalanine, L-tryptophan and L-tyrosine (each of 200, 400, 600, or 800 mg l^{-1}). Non-AAA L-alanine, L-cysteine, and L-serine were used as controls. Water activity (a_w) of the medium was measured with a LabMaster-aw instrument (Novasina, Switzerland). Growth in TSB-YE medium was documented by optical density (OD) at 625 nm with a GENESYS 30 visible spectrophotometer (Thermo Fisher Scientific, USA) and fitted by the Gompertz growth model as described by López *et al.* (2004). Cultures were prepared in two to six independent replicates, inoculated with 1% (vol/vol) of an overnight culture for growth in TSB-YE medium or 0.02% (vol/vol) for cultivation in milk, and incubated on an orbital shaker at 6 °C and 150 rpm until late exponential phase (OD_{625nm} = 0.8–1.0). Cultures were harvested by centrifugation (10000 × *g* for 10 min) at growth temperature and washed thrice with sterile phosphate-buffered saline (PBS) which was adjusted to growth temperature, pH 7.4. Subsequently, this biomass was used for fatty

acid analysis, determination of MK-7 content, and temperature stress test. Colonies were cultivated on tryptic soy agar-yeast extract (TSA-YE) medium at 30 °C.

To determine colony forming units (CFU) for the temperature stress test and the growth inhibition test in milk, 50 µl of serial dilutions were plated on TSA-YE medium (90 mm Petri dish) using the exponential mode (ISO 4833-2, ISO 7218 and AOAC 977.27) of the easySpiral automatic plater (Interscience, France). After a 1-day incubation at 37 °C, the CFU were counted for the corresponding dilution steps and the weighted average of enumerated *L. monocytogenes* was given in CFU ml^{-1}. The results for the temperature stress test and the growth inhibition test in milk were presented as decadic logarithm (log_{10}) decrease or increase relative to the initial CFU ml^{-1}, respectively.

Temperature stress tests

Each strain was subjected to three freeze-thaw cycles. Three aliquots of 2 ml cell suspension for each strain were frozen at -20 °C. After 24, 48 and 72 h cells were thawed for 20 min at room temperature and the number of CFU was determined. The remaining sample volume was refrozen for subsequent freeze-thaw cycles.

Fatty acid analysis

About 40 mg cells per sample were used for the fatty acid analysis. Fatty acids were extracted and analysed as methyl-esters as described by Sasser (1990) in biological triplicates from independent cultures. Fatty acid methyl esters were identified by gas chromatography-mass spectrometry (GC-MS) with a 7890A gas chromatograph (Agilent Technologies, USA) equipped with a 5% phenyl methyl silicone capillary column coupled with a 5975C mass spectrometer (Agilent Technologies, USA), as previously described by Lipski & Altendorf (1997). Fatty acids analysis was performed with MSD ChemStation software (version E.02.00.493, Agilent Technologies, USA) and identified by their retention times and mass spectra. The effect of alterations in fatty acid profiles associated with the amino acid supplementation on membrane fluidity was determined by calculation of the weighted average melting temperature (WAMT) according to Seel *et al.* (2018). The melting temperatures for fatty acids were taken from Knothe & Dunn (2009).

Isoprenoid quinone analysis

About 30–50 mg cells were extracted with methanol-chloroform (9:5, v/v) as described before by Hu *et al.* (1999) and Seel *et al.* (2018) in biological triplicates from independent cultures. Extracts were analysed using a 1260 Infinity Quaternary LC system (Agilent Technologies, USA) equipped with a quaternary pump, an autosampler, a thermo-controlled column compartment, and a diode array detector. Compounds were separated isocratically at 30 °C on a Hypersil™ ODS C_{18} column (Thermo Fisher, United States) using methanol/diisopropyl ether (9:2, vol/vol) as eluent (flow rate

of 1 ml min^{-1}). Isoprenoid quinones were detected at 270 and 275 nm and were identified by their absorption spectrum and retention time. The quinones were quantified as vitamin K_1 equivalents using an external calibration curve and an internal vitamin K_1 standard. Data acquisition was performed with OpenLAB CDS ChemStation software (version C.01.07, Agilent Technologies, USA).

Statistical evaluation

Statistical analysis was performed using Prism (version 8.4.3; GraphPad Software, United States). Mean values and standard deviations of *n* (see legends) biological replicates were calculated for all experiments. All datasets were tested for normal distribution by Shapiro–Wilk normality test using the method of Royston (1995) before two-way ANOVA with Tukey-Kramer post hoc test ($\alpha = 0.001$) was performed. Potential outlier values were determined using Grubbs outlier tests (Grubbs 1950). Data are presented as means ± standard deviation; $*P < 0.001$, $**P < 0.0001$, $***P < 0.00001$, $****P < 0.000001$.

3 Results and discussion

Menaquinone content affects growth rates and resistance to temperature stress

Several strains of *L. monocytogenes* have been described previously, which showed a less significant adaptation of the fatty acid profiles at 4 and 6 °C growth temperature than the majority of *L. monocytogenes* strains (Neunlist *et al.* 2005; Seel *et al.* 2018).

Table 3.1 Fatty acid (FA) composition, weighted-average melting temperature (WAMT) and menaquinone-7 (MK-7) content of *Listeria monocytogenes* strains DSM 20600^T, FFH and FFL 1 grown at 6 °C in tryptic soy broth-yeast extract medium supplemented with 800 mg each of L-phenylalanine, L-tryptophan, and L-tyrosine l^{-1} (AAA), and supplemented with 800 mg each of L-alanine, L-cysteine, and L-serine l^{-1} (non-AAA).

Parameter	DSM 20600^T		FFH		FFL 1	
	AAA	Non-AAA	AAA	Non-AAA	AAA	Non-AAA
FA composition (%)						
iso-$C_{14:0}$	2.2 ± 0.6	2.0 ± 0.1	1.3 ± 0.2	1.7 ± 0.8	1.7 ± 0.9	1.5 ± 0.1
$C_{14:0}$	1.0 ± 0.2	0.7 ± 0.2	0.8 ± 0.4	1.1 ± 0.7	1.2 ± 0.1	0.6 ± 0.1
iso-$C_{15:0}$	10.7 ± 1.0	11.5 ± 0.3	8.7 ± 1.0	9.7 ± 1.2	8.3 ± 1.7	8.0 ± 0.0
anteiso-$C_{15:0}$	74.8 ± 2.5	74.1 ± 2.1	79.8 ± 1.7	79.2 ± 2.2	84.2 ± 3.6	85.7 ± 0.8
iso-$C_{16:0}$	1.4 ± 0.1	1.5 ± 0.1	1.8 ± 1.0	1.6 ± 0.4	1.5 ± 0.3	2.0 ± 0.5
$C_{16:0}$	0.6 ± 0.4	1.6 ± 1.2	1.3 ± 0.7	1.3 ± 0.4	0.5 ± 0.2	0.6 ± 0.3
iso-$C_{17:0}$	0.5 ± 0.1	0.4 ± 0.1	0.5 ± 0.1	0.5 ± 0.1	0.3 ± 0.1	0.3 ± 0.0
anteiso-$C_{17:0}$	8.7 ± 1.2	8.3 ± 0.1	5.9 ± 0.6	5.0 ± 0.2	2.3 ± 0.9	1.3 ± 0.1
WAMT (°C)	30.0 ± 1.6	30.4 ± 1.2	29.1 ± 1.8	29.4 ± 1.8	28.3 ± 2.1	28.1 ± 0.6
MK-7 (nmol $g^{-1}_{cell\ wet\ wt}$)	125 ± 14****	204 ± 5	94 ± 18****	165 ± 12	77 ± 7	85 ± 15

Values are means ± standard deviation (*n* = 3). Asterisks represent *P* values, (****$P < 0.000001$) between cultures supplemented with AAA and with non-AAA

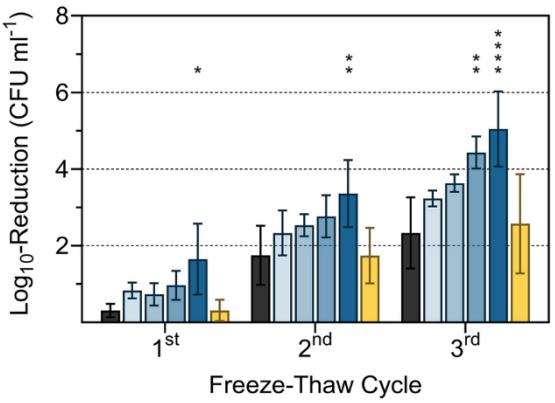

Figure 3.1 Logarithmic reduction of viable cell counts of *Listeria monocytogenes* strain FFH grown at 6 °C in tryptic soy broth-yeast extract medium without supplementation (black), with 200, 400, 600, and 800 mg each of L-phenylalanine, L-tryptophan, and L-tyrosine l^{-1} (AAA; very light blue, light blue, blue, dark blue), and with 800 mg each of L-alanine, L-cysteine, and L-serine l^{-1} (non-AAA; yellow) after one, two and three freeze-thaw cycles (each 24 h) relative to the initial cell count. Values are means ± standard deviation (very light blue, light blue, and blue $n = 3$; black, dark blue, and yellow $n = 6$). Asterisks represent P values (*$P < 0.001$, **$P < 0.0001$, ***$P < 0.00001$, ****$P < 0.000001$) between cultures supplemented with AAA and with non-AAA as well as without supplementation.

In accordance with previous findings by Seel et al. (2018), *L. monocytogenes* strains DSM 20600^T and FFH showed less adaptation in their fatty acid profiles to 6 °C growth temperature based on the ΔWAMT values but had significantly higher MK-7 contents than strain FFL 1 (Table 3.1). This indicated the involvement of this neutral lipid in the adaptation of membrane fluidity. Although an impact of MK-7 content on the membrane transition phase was reported before, a direct influence of MK-7 on the cold resistance of *L. monocytogenes* strains was not analysed so far. To determine whether the suppression of the MK-7 content in *L. monocytogenes* affects resistance to temperature stress and growth, studies were conducted by supplementation with AAA, which caused product inhibition of the 3-deoxy-D-arabino-heptulosonic acid 7-phosphate synthase in the shikimate pathway. This approach has been used by Tsukamoto *et al.* (2001) to reduce the MK content in *B. subtilis*. Supplementation with AAA and non-AAA did not affect the a_w of the medium (data not shown). The non-AAA L-alanine, L-cysteine and L-serine were used as controls. These non-AAA have similar polarities as L-phenylalanine, L-tryptophan, and L-tyrosine, and were used to exclude cryo-protective properties of amino acids.

To confirm the correlation between MK-7 content and resistance to freeze-thaw stress, MK-7 synthesis in strain FFH was inhibited by adding different concentrations of AAA, ranging from 200 to 800 mg l^{-1} (Fig. 3.1). After supplementation with AAA, concentration-dependent $\log_{10}$-reduction rates were observed, but this was significant only at 800 mg of each AAA l^{-1} after each freeze-thaw cycle. Supplementation with 600 mg of each AAA l^{-1} showed significance only in the third freeze-thaw cycle in strain FFH. This indicates that the feedback inhibition increases with increasing AAA concentrations but is already effective at lower concentrations of AAA. A reduction of the MK-7 content was already achieved with 180 mg of each AAA l^{-1} by Seel *et al.* (2018). The high concentration with 800 mg of each AAA l^{-1} was used to achieve a more pronounced reduction of the MK-7 content.

The freeze-thaw test confirmed the positive influence of MK-7 on bacterial cell resistance to freeze-thaw stress (Fig. 3.2). After growth at 6 °C and subjected to freeze-thaw stress, *L. monocytogenes* strains DSM 20600^T and FFH showed a significant reduction of viable cells, quantified as CFU ml^{-1}, if supplemented with AAA but were unaffected if supplemented with non-AAA or without amino acid supplementation (Fig. 3.2). The number of viable cells was significantly reduced after freeze-thaw stress by 2.8 ± 0.6, 5.2 ± 0.4, and 7.0 ± 0.2 $\log_{10}$ CFU ml^{-1} for strain DSM 20600T and 1.7 ± 0.9, 3.4 ± 0.9, and 5.1 ± 1.0 $\log_{10}$ CFU ml^{-1} for strain FFH after each of the three freeze-thaw steps. This corresponded to a percentage increase in the $\log_{10}$-reduction of CFU ml^{-1} from freeze-thaw cycle to cycle compared to the cultures without supplementation of about 41, 25 and 25% and 433, 92 and 116% for strains DSM 20600^T and FFH, respectively. No significant increase in the reduction of CFU ml^{-1} could be detected for strain FFL 1 after supplementation with AAA in comparison to non-AAA supplementation and without supplementation, respectively. This is in accord with the absence of any MK accumulation at 6 °C for this strain (Table 3.1). Moreover, this confirmed the beneficial effect of MK-7 on cell membrane integrity at 6 °C in strains DSM 20600^T and FFH. Both strains increase MK-7 content at low growth temperatures. The reduction of MK-7 by supplementation with AAA resulted in a steeper phase transition of the membrane as described earlier by Seel *et al.* (2018), which resulted in increased susceptibility to freeze-thaw stress as demonstrated in this study. Furthermore, the influence of MK-7 content on the growth characteristics of *L. monocytogenes* strains was analysed to detect growth inhibitory effects provoked by AAA supplementation. In addition to TSB-

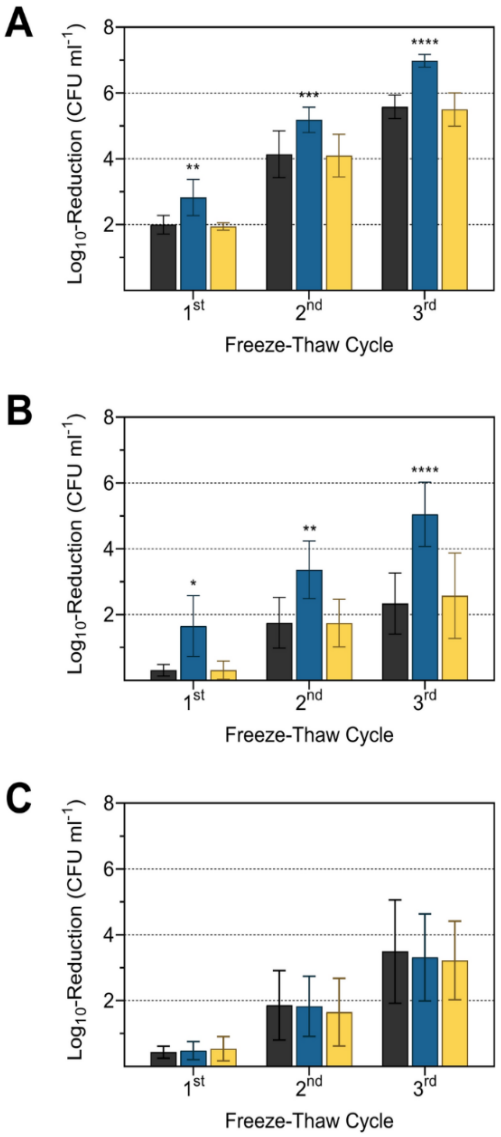

Figure 3.2 Logarithmic reduction of viable cell counts of *Listeria monocytogenes* strains DSM 20600^T (a), FFH (b) and FFL 1 (c) grown at 6 °C in tryptic soy broth-yeast extract medium without supplementation (black), with 800 mg each of L-phenylalanine, L-tryptophan, and L-tyrosine l^{-1} (AAA; dark blue) and with 800 mg each of L-alanine, L-cysteine, and L-serine l^{-1} (non-AAA; yellow) after one, two and three freeze-thaw cycles (each 24 h) relative to the initial cell count. Values are means ± standard deviation (n = 6). Asterisks represent P values (*P < 0.001, **P < 0.0001, ***P < 0.00001, ****P < 0.000001) between cultures supplemented with AAA and with non-AAA as well as without supplementation

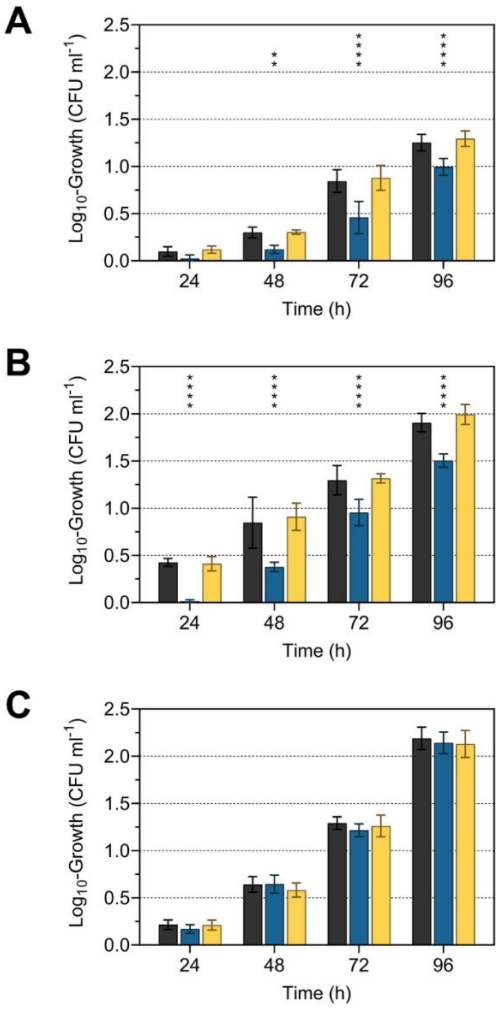

Figure 3.3 Logarithmic growth of *Listeria monocytogenes* strains DSM 20600^T (a), FFH (b) and FFL 1 (**c**) at 6 °C in ultra-high temperature processed milk without supplementation (black), with 800 mg each of L-phenylalanine, L-tryptophan, and L-tyrosine l^{-1} (AAA; dark blue) and with 800 mg each of L-alanine, L-cysteine, and L-serine l^{-1} (non-AAA; yellow) after 24, 48, 72, and 96 h relative to the initial cell count. Values are means ± standard deviation (n = 6). Asterisks represent P values (*P < 0.001, **P < 0.0001, ***P < 0.00001, ****P < 0.000001) between cultures supplemented with AAA and with non-AAA as well as without supplementation.

YE medium, milk was used as a growth medium to demonstrate AAA-associated effects also in a food matrix typical for *L. monocytogenes* (De Buyser *et al.* 2001; Fleming *et al.* 1985). Bacterial cell growth in AAA-supplemented milk was reduced for strains DSM 20600^T and FFH after 96 h (Fig. 3.3). Significant growth inhibition in milk occurred after 24 h in strain DSM 20600^T and after 48 h in strain FFH. No growth inhibition was observed for strain FFL 1. Cultures with non-AAA supplementation and without amino acid supplementation showed similar cell growth in milk (Fig. 3.3). Moreover, growth experiments in TSB-YE medium showed the same significant effects as in milk when AAA were added (Fig. 3.4). The growth rate was reduced in strains DSM 20600^T and FFH after supplementation with AAA compared to the supplementation with non-AAA. The growth rate decreased from 0.036 to 0.026 and 0.050 to 0.041 after supplementation with AAA in strain DSM 20600^T and FFH, respectively.

Membrane adaptation by isoprenoid quinone content substitutes fatty acid profile modification

For all three *L. monocytogenes* strains, fatty acid profiles were determined after growth in TSB-YE medium with or without supplementation at 6 °C growth temperature to exclude effects of AAA on them. All three strains showed an *iso*/*anteiso* fatty acid profile with dominating fatty acids *iso*-$C_{15:0}$, *anteiso*-$C_{15:0}$, and *anteiso*-$C_{17:0}$ (Table 3.1). These three branched-chain fatty acids represented at least 90% of the total fatty acids at 6 °C growth temperature. According to previous findings by Seel *et al.* (2018), the two strains, DSM 20600^T and FFH differed from strain FFL 1 in terms of adaptation of the fatty acid profile to low growth temperatures. Strain FFL 1 showed the highest ratio of *anteiso*-$C_{15:0}$/*anteiso*-$C_{17:0}$, the lowest WAMT value and the lowest MK-7 content at 6 °C growth temperature compared

to strains DSM 20600^T and FFH. The two strains DSM 20600^T and FFH showed two to three times higher content of MK-7 at the growth temperature of 6 °C compared to 37 °C. AAA and non-AAA supplementation did not alter the fatty acid profile in all three strains. Feedback inhibition of MK-7 synthesis was successfully induced by supplementation with AAA in strains DSM 20600^T and FFH (Table 3.1). While both strains showed a significant decrease in MK-7 content after supplementation with AAA at 6 °C growth temperature, strain FFL 1 showed no significant decrease in MK-7 content after AAA supplementation. As expected, no decrease in MK-7 content was detected if cultures were supplemented with non-AAA, which is consistent with the described mechanism for feedback inhibition by Tsukamoto *et al.* (2001). For all tested *L. monocytogenes* strains, only MK-7 was detected. Others, such as MK-5 and MK-6, which had been described for *L. monocytogenes* before, were not detected (Collins *et al.* 1979). The *L. monocytogenes* strains DSM 20600^T and FFH showed a content of about 204.4 ± 5.4 and 164.7 ± 11.6 nmol MK-7 g^{-1}, respectively. Supplementation with AAA reduced MK-7 content by 38.7% in strain DSM 20600^T and 42.8% in strain FFH. Strain FFL 1 had a content of about 85.5 ± 14.9 and 76.6 ± 7.3 nmol MK-7 g^{-1} after supplementation with AAA and non-AAA, respectively. The controls with non-AAA of the tested strains are in accord with the MK-7 contents described previously by Seel *et al.* (2018).

4 Conclusion

The disruption of the menaquinone-dependent membrane fluidization under low-temperature conditions resulted in a reduced bacterial cell fitness. This shows that this fatty acid-independent mechanism for regulation of membrane fluidity represents an additional adaptive response to low growth temperatures with a beneficial impact on membrane integrity, growth rate and bacterial cell resistance to temperature stress. The findings suggest that food components such as aromatic amino acids and menaquinone (vitamin K), respectively, may affect growth rates and fitness of certain *Listeria monocytogenes* strains at low temperatures and should be considered for future modelling of food stability against *Listeria monocytogenes* colonization.

References

Annous BA, Becker La, Bayles DO, Labeda DP, Wilkinson BJ (1997) Critical role of anteiso-C15:0 fatty acid in the growth of *Listeria monocytogenes* at low temperatures. Appl Environ Microbiol 63:3887–3894

Asai Y (2000) The interaction of vitamin K1 with phospholipid membranes. Colloid Surf A Physicochem Eng Asp 163:265–270

Asai Y, Watanabe S (1999) The interaction of ubiquinone-3 with phospholipid membranes. *FEBS Lett* 446:169–172

Carlquist M, Fernandes RL, Helmark S, Heins A-L, Lundin L, Sørensen SJ, Gernaey KV, Lantz AE (2012) Physiological heterogeneities in microbial populations and implications for physical stress tolerance. *Microb Cell Fact* 11:94

Chihib N-E, Ribeiro da Silva M, Delattre G, Laroche M, Federighi M (2003) Different cellular fatty acid pattern behaviours of two strains of *Listeria monocytogenes* Scott A and CNL 895807 under different temperature and salinity conditions. *FEMS Microbiol Lett* 218:155–160

Collins MD, Jones D, Goodfellow M, Minnikin DE (1979) Isoprenoid quinone composition as a guide to the classification of *Listeria*, *Brochothrix*, *Erysipelothrix* and *Caryophanon*. *J Gen Microbiol* 111:453–457

De Buyser M-L, Dufour B, Maire M, Lafarge V (2001) Implication of milk and milk products in food-borne diseases in France and in different industrialised countries. *Int J Food Microbiol* 67:1–17

De Mendoza D, Cronan JE (1983) Thermal regulation of membrane lipid fluidity in bacteria. *Trends Biochem Sci* 8:49–52

Doumith M, Buchrieser C, Glaser P, Jacquet C, Martin P (2004) Differentiation of the major *Listeria monocytogenes* serovars by multiplex PCR. *J Clin Microbiol* 42:3819–3822

EFSA-ECDC (2019) The European Union One Health 2018 Zoonoses Report. *EFSA J* 17:e05926

Farber JM, Peterkin PI (1991) *Listeria monocytogenes*, a food-borne pathogen. *Microbiol Rev* 55:476–511

Fleming DW, Cochi SL, MacDonald KL, Brondum J, Hayes PS, Plikaytis BD, Holmes MB, Audurier A, Broome CV, Reingold AL (1985) Pasteurized milk as a vehicle of infection in an outbreak of listeriosis. *N Engl J Med* 312:404–407

Gounot AM, Russell NJ (1999) Physiology of cold-adapted microorganisms. In: Margesin R, Schinner F (eds) *Cold-adapted organisms*. Springer, Berlin

Grubbs FE (1950) Sample criteria for testing outlying observations. *Ann Math Statist* 21:27–58

Harris FM, Best KB, Bell JD (2002) Use of laurdan fluorescence intensity and polarization to distinguish between changes in membrane fluidity and phospholipid order. *Biochim Biophys Acta Biomembr* 1565:123–128

Hu H-Y, Fujie K, Urano K (1999) Development of a novel solid phase extraction method for the analysis of bacterial quinones in activated sludge with a higher reliability. *J Biosci Bioeng* 87:378–382

Jones SL, Drouin P, Wilkinson BJ, Morse PD (2002) Correlation of long-range membrane order with temperature-dependent growth characteristics of parent and a cold-sensitive, branched-chain-fatty-acid-deficient mutant of *Listeria monocytogenes*. *Arch Microbiol* 177:217–222

Knothe G, Dunn RO (2009) A comprehensive evaluation of the melting points of fatty acids and esters determined by differential scanning calorimetry. *J Am Oil Chem Soc* 86:843–856

Lipski A, Altendorf K (1997) Identification of heterotrophic bacteria isolated from ammonia-supplied experimental biofilters. *Syst Appl Microbiol* 20:448–457

López S, Prieto M, Dijkstra J, Dhanoa MS, France J (2004) Statistical evaluation of mathematical models for microbial growth. *Int J Food Microbiol* 96:289–300

Lopez-Valladares G, Danielsson-Tham M-L, Tham W (2018) Implicated food products for listeriosis and changes in serovars of *Listeria monocytogenes* affecting humans in recent decades. *Foodborne Pathog Dis* 15:387–397

Mastronicolis SK, Boura A, Karaliota A, Magiatis P, Arvanitis N *et al.* (2006) Effect of cold temperature on the composition of different lipid classes of the foodborne pathogen *Listeria monocytogenes*: focus on neutral lipids. *Food Microbiol* 23:184–194

Mastronicolis SK, German JB, Megoulas N, Petrou E, Foka P, Smith GM (1998) Influence of cold shock on the fatty-acid composition of different lipid classes of the food-borne pathogen *Listeria monocytogenes*. *Food Microbiol* 15:299–306

Mykytczuk NCS, Trevors JT, Leduc LG, Ferroni GD (2007) Fluorescence polarization in studies of bacterial cytoplasmic membrane fluidity under environmental stress. *Prog Biophys Mol Biol* 95:60–82

Neunlist MR, Federighi M, Laroche M, Sohier D, Delattre G *et al.* (2005) Cellular lipid fatty acid pattern heterogeneity between reference and recent food isolates of *Listeria monocytogenes* as a response to cold stress. *Antonie Van Leeuwenhoek* 88:199–206

Ortiz A, Aranda FJ (1999) The influence of vitamin K_1 on the structure and phase behaviour of model membrane systems. *Biochim Biophys Acta Biomembr* 1418:206–220

Royston P (1995) Remark AS R94: A remark on algorithm AS 181: the W-test for normality. *J Appl Stat* 44:547

Russel N (1984) Mechanisms of thermal adaptation in bacteria: blueprints for survival. *Trends Biochem Sci* 9:108–112

Ryser ET, Marth EH (2007) *Listeria, listeriosis, and food safety*. Taylor & Francis, Boca Raton

Sasser M (1990) Identification of bacteria through fatty acid analysis. In: Klement Z, Rudolph K, Sands DC (eds) *Methods in Phytobacteriology*. Akadémiai Kiadó, Budapest

Seel W, Flegler A, Zunabovic-Pichler M, Lipski A (2018) Increased isoprenoid quinone concentration modulates membrane fluidity in *Listeria monocytogenes* at low growth temperatures. *J Bacteriol* 200:e00148-18

Sleight SC, Wigginton NS, Lenski RE (2006) Increased susceptibility to repeated freeze-thaw cycles in *Escherichia coli* following long-term evolution in a benign environment. *BMC Evol Biol* 6:104

Søballe B, Poole RK (1999) Microbial ubiquinones: multiple roles in respiration, gene regulation and oxidative stress management. *Microbiol* 145:1817–1830

Suutari M, Laakso S (1994) Microbial fatty acids and thermal adaptation. *Crit Rev Microbiol* 20:285–328.

Tasara T, Stephan R (2006) Cold stress tolerance of *Listeria monocytogenes*: a review of molecular adaptive mechanisms and food safety implications. *J Food Prot* 69:1473–1484

Tatituri RVV, Wolf BJ, Brenner MB, Turk J, Hsu F-F (2015) Characterization of polar lipids of *Listeria monocytogenes* by HCD and low-energy CAD linear ion-trap mass spectrometry with electrospray ionization. *Anal Bioanal Chem* 407:2519–2528

Tsukamoto Y, Kasai M, Kakuda H (2001) Construction of a *Bacillus subtilis* (natto) with high productivity of vitamin K_2 (menaquinone-7) by analog resistance. *Biosci Biotechnol Biochem* 65:2007–2015

Walker SJ, Archer P, Banks JG (1990) Growth of *Listeria monocytogenes* at refrigeration temperatures. *J Appl Bacteriol* 68:157–162

Zhang Y-M, Rock CO (2008) Membrane lipid homeostasis in bacteria. *Nat Rev Microbiol* 6:222–233.

Chapter 4

Arthrobacter bussei sp. nov., a pink-coloured organism isolated from cheese made of cow's milk

A pink-coloured bacterium (strain KR32^T) was isolated from cheese and assigned to the '*Arthrobacter agilis* group'. Members of the 'pink *Arthrobacter agilis* group' form a stable clade (100% bootstrap value) and contain the species *Arthrobacter agilis*, *Arthrobacter ruber* and *Arthrobacter echini*, which share ≥ 99.0% 16S rRNA gene sequence similarity. Isolate KR32^T showed highest 16S rRNA gene sequence similarity (99.9%) to *A. agilis* DSM 20550^T. Additional multilocus sequence comparison confirmed the assignment of strain KR32^T to the clade 'pink *A. agilis* group'. Average nucleotide identity and digital DNA–DNA hybridization values between isolate KR32^T and *A. agilis* DSM 20550^T were 82.85 and 26.30%, respectively. The G+C content of the genomic DNA of isolate KR32^T was 69.14 mol%. Chemotaxonomic analysis determined anteiso-$C_{15:0}$ as the predominant fatty acid and MK-9(H_2) as the predominant menaquinone. Polar lipids were diphosphatidylglycerol, phosphatidylglycerol, phosphatidylinositol and monoacyldimannosyl-monoacylglycerol. The peptidoglycan type of the isolate was A3α. The carotenoid bacterioruberin was detected as the major pigment. At 10 °C, strain KR32^T grew with increased concentrations of bacterioruberin and production of unsaturated fatty acids. Strain KR32^T was a Gram-stain-positive, catalase-positive, oxidase-positive and coccus-shaped bacterium with optimal growth at 27–30 °C and pH 8. The results of phylogenetic and phenotypic analyses enabled the differentiation of the isolate from other closely related species of the 'pink *A. agilis* group'. Therefore, strain KR32^T represents a novel species for which the name *Arthrobacter bussei* sp. nov. is proposed. The type strain is KR32^T (= DSM 109896^T = LMG 31480^T = NCCB 100733^T).

Keywords: *Micrococcaceae*; *Arthrobacter*; cheese; novel species; bacterioruberin; cold-adapted

This chapter has been published:

Flegler A, Runzheimer K, Kombeitz V, Mänz AT, Heidler von Heilborn D, Etzbach L, Schieber A, Hölzl G, Hüttel B, Woehle C, Lipski A. (2020) *Arthrobacter bussei* sp. nov., a pink-coloured organism isolated from cheese made of cow's milk. *Int J Syst Evol Microbiol* 70:3027–3036. DOI: 10.1099/ijsem.0.004125

1 Introduction

The colonization of food with pigmented micro-organisms represents a well-known source of food spoilage documented by famous historical reports describing the discovery of *Serratia marcescens* and *Halobacterium salinarum* as spoiling organisms of polenta and codfish (Harrison & Kennedy 1922, Merlino 1924). Some of these pigmented and food-related micro-organisms show a more intense pigmentation under low temperature conditions, which impairs the properties of food products under low temperature storage conditions (Seel *et al.* 2020). In the course of analyses of pigmented bacterial strains from cold stored food samples, we found a pink-pigmented bacterial strain which shows a temperature-dependent intensity of pigmentation. The strain was assigned to the '*Arthrobacter agilis* group' of the genus *Arthrobacter*. The known species of this group have been associated with environmental habitats like biofilms on building walls, glacier ice or cyano-bacterial mats but not with food samples. An in-depth analysis of this strain revealed differences in its genome sequence to other species of this group, which justifies the proposal of a new species for this strain.

The genus *Arthrobacter* was first described by Conn & Dimmick (1947) as a member of the family *Micrococcaceae*, which has been subjected to several taxonomic revisions during the last few years (Busse 2012). In particular, a considerable number of species of the genus *Arthrobacter* was assigned to new genera closely related to the genus *Arthrobacter* (Busse 2016). Therefore, at present this genus appears as a paraphyletic taxon, which was also confirmed by recent phylogenomic studies (Nouioui *et al.* 2018). Members of this genus are distributed ubiquitously and are also associated with milk and dairy products (Bockelmann & Hoppe-Seyler 2001, Delbès *et al.* 2007). Some *Arthrobacter* species have already been isolated from smear-ripened cheeses and contribute to the typical colour, flavour and texture properties of the final product (Irlinger *et al.* 2005, Monnet *et al.* 2010). Their rapid growth also reduces the risk of contamination with pathogens such as *Listeria monocytogenes* (Valdes-Stauber et al 1991). Pink or red-pigmented species of the genus *Arthrobacter* were previously isolated from cold environmental samples, such as glacier ice (Liu et al 2018), Antarctic lakes (Dieser *et al.* 2010) or Antarctic sea ice (Bowman et al 1997), and most of them were assigned to the '*A. agilis* group'. To date, no pink-coloured *Arthrobacter* species has been isolated from food.

At the present time, 99 species of this genus are described with validated names and 50 of them were assigned to other genera during the last years (Parte 2018). Bacteria belonging to the genus *Arthrobacter* producing pigments may represent value-adding food ingredients including colourants of a broad range of hues (Sutthiwong *et al.* 2014) or may act as antioxidants (Mandelli

et al 2012). The characterization of new food-related organisms of the genus *Arthrobacter* is an important step toward the assessment of food-associated micro-organisms concerning spoilage potential or even desired metabolic activities like flavour improvement or production of food-grade pigments.

2 Isolation and ecology

The novel strain producing pink colonies was isolated from cheese slices (45% fat in dry matter) packaged under modified atmosphere, described and designated KR32^T. The cheese contained 1.0% (w/w) NaCl and was produced and packed in the Allgäu region, Germany (47° 35’ N; 9° 53’ E). Homogenised cheese sample (100 µl; 10 g cheese mixed with 90 ml Ringer’s solution) was plated on tryptic soy agar (TSA; Merck). The isolate was recovered from TSA plates after incubation at 10 °C for 7 days. The isolate was subcultivated on TSA and tryptic soy broth (TSB; Merck) at 10 and 30 °C for further analyses. Remarkably, isolate KR32^T showed a more intense pigmentation at 10 °C than at 30 °C. This reaction to low temperature incubation was already reported for a red-pigmented *A*. *agilis* and a *Micrococcus roseus* (now *Kocuria rosea*) strain both isolated from Antarctic soil and ice samples (Fong *et al.* 2001, Chattopadhyay *et al.* 1997). We could show this response also for the type strain of the species *A*. *agilis* but less pronounced than for isolate KR32^T (Fig. 4.1).

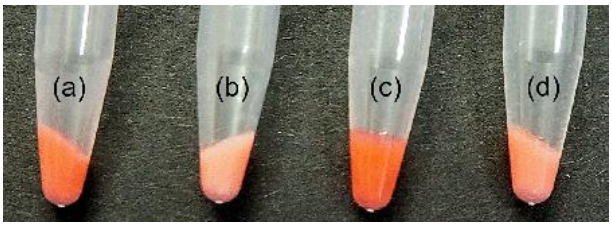

Figure 4.1 Pigmentation of strain KR32^T (a) and *Arthrobacter agilis* DSM 20550^T (c) at 10 °C growth temperature after 7 days and of strain KR32^T (b) and *Arthrobacter agilis* DSM 20550^T (d) at 30 °C growth temperature after 72 h in TSB.

3 Phylogeny

Extraction of genomic DNA and amplification and sequencing of 16S rRNA genes were performed as described previously (Wiertz *et al.* 2013) The 16S rRNA gene sequence of KR32^T (MN080869) was compared with those of type strains of species with validly published names using EzBioCloud (Yoon *et al.* 2017). The phylogenetic tree of 16S rRNA gene was reconstructed as described by Zimmermann *et al.* (2016). Mega X (Kumar *et al.* 2018) was used to perform a multiple sequence alignment by muscle (Edgar 2004) and to reconstruct maximum-likelihood, neighbour-joining and maximum-parsimony trees supported by bootstrap test with 1000 replications. The genetic distances for the maximum-likelihood analysis were calculated using the model of Tamura & Nei (1993) and the generalized time-reversible model of Tavaré (1986). In addition, a proportion of

invariable sites (+I) (Shoemaker & Fitch 1989) and/or rate of variation across sites (+G) (Reddy *et al.* 2000) was incorporated into both models. The maximum-likelihood tree is given in Fig. 4.2.

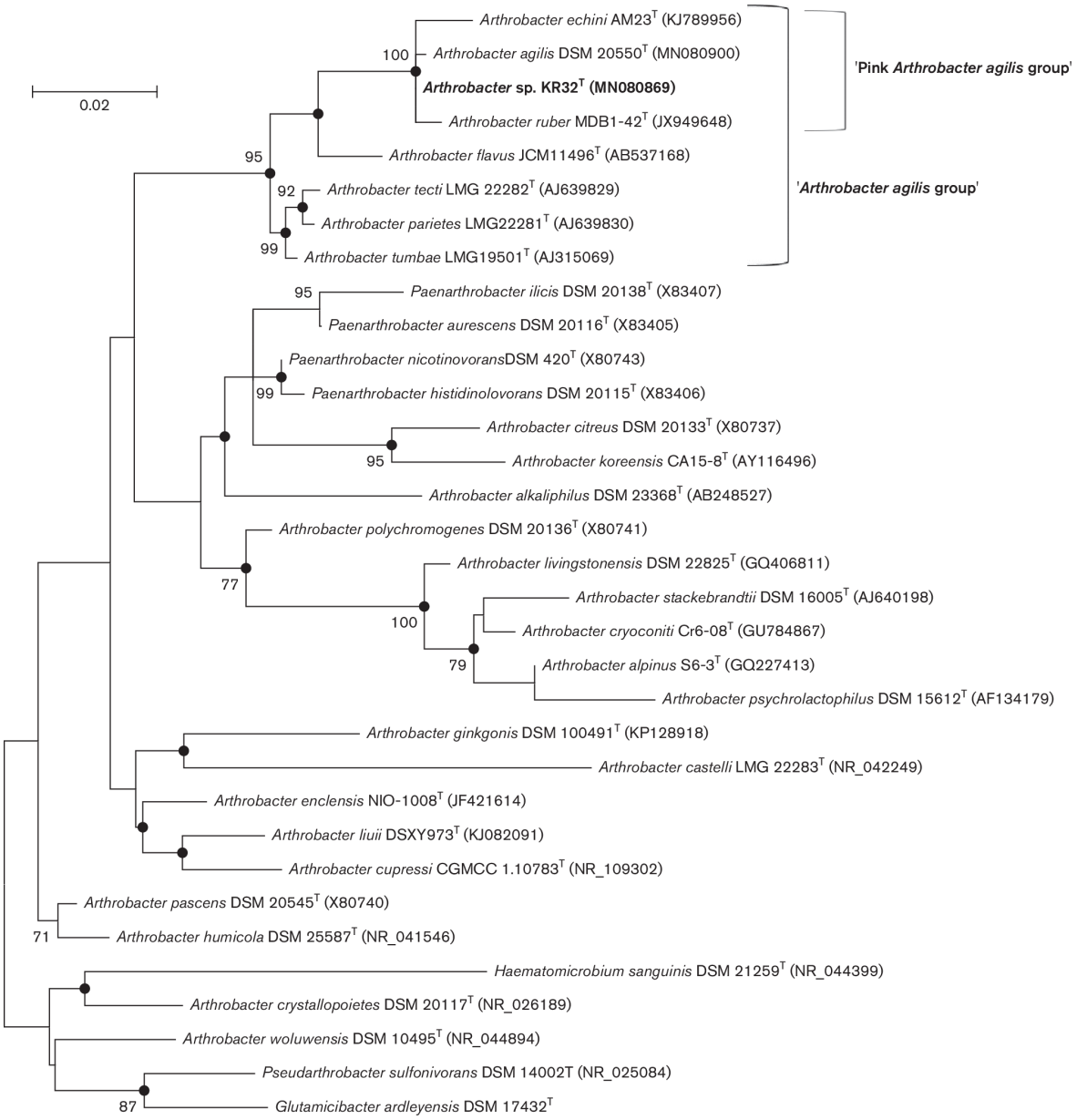

Figure 4.2 The phylogenetic reconstruction based on 16S rRNA gene sequences was inferred by using the maximum-likelihood method and the Tamura-Nei model (1993). Filled circles indicate that the corresponding branches were recovered in the maximum-likelihood, neighbour-joining and maximum-parsimony trees. The tree with the highest log likelihood (-5267.72) is shown. Bootstrap values >70 are shown next to the branches. Initial tree(s) for the heuristic search were obtained automatically by applying Neighbor-Join and BioNJ algorithms to a matrix of pairwise distances estimated using the maximum composite likelihood (MCL) approach, and then selecting the topology with superior log likelihood value. A discrete Gamma distribution was used to model evolutionary rate differences among sites [5 categories (+G; parameter, 0.4162)]. The rate variation model allowed for some sites to be evolutionarily invariable ([+I], 70.78% sites). The tree is drawn to scale, with branch lengths measured in the number of substitutions per site. There were a total of 1368 positions in the final dataset. Evolutionary analyses were conducted in Mega X (Kumar *et al.* 2018). The rooted outgroups were *Glutamicibacter ardleyensis* DSM 17432^T and *Paeniglutamicibacter sulfureus* DSM 20167^T.

The almost-complete 16S rRNA gene sequence (1466 bp) of KR32^T was determined and revealed that the novel strain represented a member of the '*A. agilis* group' (Fig. 4.2). The 16S rRNA gene sequence shows almost identical similarity of 99.9% to *A. agilis* DSM 20550^T (MN080900), followed by 99.8% to *Arthrobacter ruber* MDB1-42^T (JX949648), 99.0% to *Arthrobacter echini* AM23^T (KJ789956), 97.9% to *Arthrobacter subterraneus* CH7^T (DQ097525), 97.8% to *Arthrobacter tumbae* LMG 19501^T (AJ315069), 97.8% to *Arthrobacter parietis* LMG 22281^T (AJ639830), 97.5% to *Arthrobacter flavus* JCM 11496^T (AB537168) and 97.1% to *Arthrobacter tecti* LMG 22282^T (AJ639829). These species form the '*A. agilis* group', which is a stable clade, as indicated by a high bootstrap value (95%) (Fig. 4.2). The group contains the species *A. agilis*, *A. echini*, *A. pityocampae*, *A. flavus*, *A. parietis*, *A. subterraneus*, *A. tecti* and *A. tumbae*, which share 97.3–99.6% 16S rRNA gene sequence similarities, a peptidoglycan Lys-Thr-Ala_{2-3} corresponding to peptidoglycan structures A11.27/A11.28 and a quinone system with the predominant menaquinone MK-9(H_2) (Busse 2016). A subgroup including the strain KR32^T and the species *A. agilis*, *A. ruber*, *A. pityocampae* and *A. echini* showed all pink pigmentation and can be designated as the 'pink *A. agilis* group'. Other species of the '*A. agilis* group', *A. flavus*, *A. tecti*, *A. parietis* and *A. tumbae* are yellow or yellow-orange pigmented (Reddy *et al.* 2000, Heyrman *et al.* 2005).

4 Genome features

Illumina genome sequencing and data processing was performed as described by Weber *et al.* (2018) for isolate KR32^T and *A. agilis* DSM 20550^T. Extracted DNA was treated with RNase before genome sequencing. Genome assemblies were generated using SPAdes (Bankevich *et al.* 2012) with modified settings (k: 21, 33, 55, 77, 99, 127, -careful). Vector contaminations were identified and removed by using ContEst16S (Lee *et al.* 2017) plus VecScreen and quality of the assemblies (Table S4.2, available in the online version of this article) were assessed with Quast (Gurevich *et al.* 2013). Genome sequences of other strains of the 'pink *A. agilis* group' were taken from GenBank.

The genome size of KR32^T (VJXX00000000), *A. agilis* DSM 20550^T (VHIM00000000), *A. ruber* MDB1-42^T (PPTH00000000) and *A. echini* AM23^T (SSWH00000000) were 3.63, 3.24, 3.66 and 3.18 Mb, respectively. Average nucleotide identity (ANI) values were calculated using the web-service software ANI Calculator from EzBioCloud (Yoon *et al.* 2017). The digital DNA-DNA hybridization (dDDH) values were computed using the Genome-to Genome Distance Calculator (GGDC) version 2.1 (Meier-Kolthoff *et al.* 2013). The ANI values between KR32^T and reference strains *A. agilis* DSM 20550^T, *A. ruber* MDB1-42^T and *A. echini* AM23^T were 82.85, 82.22, and 79.54%, respectively. The dDDH values between KR32^T and the reference strains *A. agilis* DSM 20550^T, *A. ruber* MDB1-42^T and *A. echini* AM23^T were 26.3, 25.4 and 22.8%, respectively. These values fall

below the accepted species limits of 95-96% ANI and 70% dDDH for species delineation (Chun *et al.* 2018). Therefore, based on the genomic data, KR32^T represents a novel species of the genus *Arthrobacter*. A comparison with genome sequences of other strains of the 'pink *A*. *agilis* group' indicated no similarity above species threshold with any other sequenced strain of this cluster (Table 4.1). However, this analysis also indicated that several strains (4041, UMCV2, P9) temporarily identified as *A*. *agilis* or *A*. *echini* were future candidates for separate species within this taxon because of low ANI and dDDH values in comparison with type strain sequences.

Table 4.1 Comparative average nucleotide identity (ANI) and digital DNA–DNA hybridization (dDDH) values between KR32^T and other *Arthrobacter* strains of the 'pink *A*. *agilis* group' Strains: 1, *A. agilis* DSM 20550^T (VHIM00000000); 2, *A*. *agilis* CGMCC 1.15723^T (PRKX00000000); 3, *A*. *agilis* 4042 (NFSD00000000); 4, KR32^T (VJXX00000000); 5, *A*. *agilis* 4041 (NFSC00000000); 6, *A*. *agilis* UMCV2 (CP024915); 7, *A*. *ruber* MDB1-42^T (PPTH00000000); 8, *A*. *echini* AM23^T (SSWH00000000); 9, *A*. *echini* P9 (VSLD00000000). Data for strain KR32^T are presented in bold.

		ANI								
		1	**2**	**3**	**4**	**5**	**6**	**7**	**8**	**9**
dDDH	**1**		99.97	99.99	**82.85**	81.33	81.94	81.66	79.39	79.65
	2	99.4		99.97	**82.84**	81.20	81.79	81.51	79.11	79.77
	3	99.8	99.7		**82.89**	81.36	81.91	81.62	79.23	79.68
	4	**26.3**	**26.3**	**26.3**		**81.92**	**82.6**	**82.22**	**79.54**	**79.88**
	5	24.5	24.5	24.5	**25.2**		85.17	83.69	79.79	80.22
	6	24.9	24.9	24.9	**26.0**	29.7		83.94	80.57	81.04
	7	24.6	24.5	24.6	**25.4**	27.3	27.6		80.23	80.56
	8	22.4	22.3	22.3	**22.8**	23.0	23.4	23.0		84.49
	9	22.4	22.4	22.4	**23.0**	23.2	23.8	23.3	27.8	

In addition, multilocus sequence analysis (MLSA) of *Arthrobacter sensu lato* groups based on *tuf*, *secY*, *rpoB*, *recA*, *fusA* and *atpD* genes (Liu *et al.* 2018b) was conducted by using data of Liu *et al.* (2018a) (Fig. 4.3). All data were extracted from GenBank (Table S4.1). The MLSA phylogenetic tree confirmed the assignment of isolate KR32^T to the 'pink *A*. *agilis* group' but also showed the separation from the species described so far. For comparison of the concatenated sequences (*tuf*, *secY*, *rpoB*, *recA*, *fusA* and *atpD*), we selected sequences from type strains with a 16S rRNA gene sequences similarity ≥98.7% (Liu *et al.* 2018b). Isolate KR32^T clustered together with *A*. *agilis* DSM 20550^T (100% bootstrap value) in the phylogenetic tree based on 16S rRNA gene sequence and MLSA data (Figs 4.2 and 4.3). The similarity between strain KR32^T and *A*. *agilis* DSM 20550^T was 99.9% for 16S rRNA gene sequence similarity or 93.5% for MLSA, respectively. The novel isolate could not be assigned to any recognised species due to the similarities of the concatenated sequences between the species with validly published names present in the MLSA tree ranging from 93.47 to 77.93% (Liu et al 2018a).

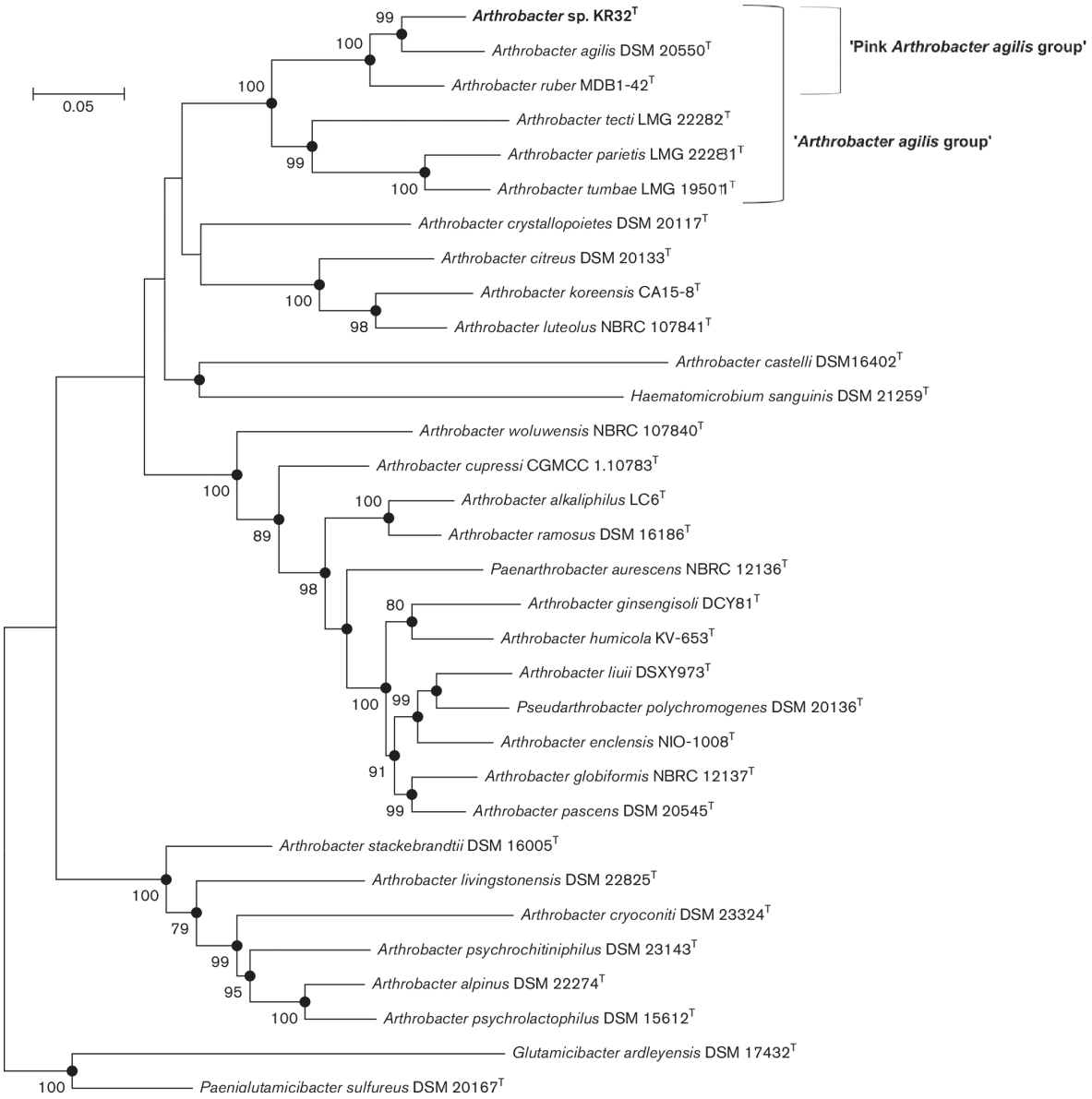

Figure 4.3 The phylogenetic reconstruction was inferred by using the maximum-likelihood method and the general time reversible model (Nei & Kumar 2000) from MLSA data (*tuf–secY–rpoB–recA–fusA–atpD*). Filled circles indicate that the corresponding branches were recovered in the maximum-ikelihood, neighbour-joining and maximum-parsimony trees. Bootstrap values >70 are shown next to the branches. Initial tree(s) for the heuristic search were obtained automatically by applying Neighbor-Join and BioNJ algorithms to a matrix of pairwise distances estimated using the maximum composite likelihood (MCL) approach, and then selecting the topology with superior log likelihood value. A discrete Gamma distribution was used to model evolutionary rate differences among sites [5 categories (+G; parameter, 0.3458)]. The rate variation model allowed for some sites to be evolutionarily invariable ([+I], 27.81% sites). The tree is drawn to scale, with branch lengths measured in the number of substitutions per site. There were a total of 3801 positions in the final dataset. Evolutionary analyses were conducted in Mega X (Kumar *et al.* 2018). Rooted outgroups were *Glutamicibacter ardleyensis* DSM 17432^T and *Paeniglutamicibacter sulfureus* DSM 20167^T.

5 Physiology and chemotaxonomy

The reference strains *A. agilis* DSM 20550^T and *Arthrobacter globiformis* DSM 20124^T were obtained from Leibniz-Institut–Deutsche Sammlung von Mikroorganismen und Zellkulturen GmbH (DSMZ) for comparative studies. In addition to phylogenetic analysis of 16S rRNA gene sequence and MLSA, chemotaxonomic analyses were conducted and phenotypic characteristics were determined to confirm the taxonomic position of the isolate.

Colony morphology was observed on TSA plates after incubation at 30 °C for 4 days. Cell morphology, cell dimensions, motility and the presence of endospores were determined using phase-contrast microscopy at magnification of × 1000 with a Zeiss Axio Observer microscope. The average cell size was determined by measuring of at least 100 cells by Zen 2012 software. Gram-staining and catalase activity was determined according to Gerhardt (1984). Oxidase activity was tested with Bactident Oxidase test stripes (Merck, Darmstadt, Germany)

Table 4.2 Differentiating characteristics of KR32^T and the reference strain. Strains: 1, KR32^T; 2, *Arthrobacter agilis* DSM 20550^T. +, Positive; –, negative; w, weakly positive. All data were obtained in this study.

	1	2
Pigmentation	Pink	Rose Red
Optimum NaCl for growth (%)	2.5	0.5
Optimum temperature for growth (°C)	30	25
Temperature range for growth (°C)	1–45	1–35*
pH range for growth	7–8	7–8
Maximum tolerable NaCl (%) concentration	7.5	4.5*
Assimilation of:		
N-Acetylglucosamine	+	–
L-Arabinose	+	–
Arbutin	+	w†
Lactose	–	w
Melibiose	+	–
Melezitose	–	+
Potassium gluconate	+	–
Raffinose	+	–
Salicin	w	–
Starch	+	w
Trehalose	w	+
Methyl α-d-xylopyranoside	–	+
Enzyme activity:		
Trypsin	+	–
Acid phosphatase	–	+

*Data differs from Liu *et al.* (2018a).
†Data differs from Lee *et al.* (2016).

Strain KR32^T produced pink-pigmented, circular, raised and smooth colonies with 1.0 mm diameter on TSA. Older colonies showed a bleached-out centre after some weeks. The colony morphology clearly separated isolate KR32^T from *A. agilis* DSM 20550^T. This reference strain formed smaller colonies, had a stronger pigmentation and did not show bleaching after a longer time. The cells of the isolate KR32^T showed a coccus-shaped morphology after 24 h on TSA. The cell morphology of the isolate did not change over time and a rod–coccus life cycle as described for species of the genus *Arthrobacter* (Busse 2016) was not observed within 3 months. The cells of the

isolate were not motile and endospores were not detected. Dimensions of strain KR32^T and *A. agilis* DSM 20550^T were 1.1–1.5 µm and 0.9–1.3 µm of 4 days old cells in diameter, respectively, and 0.9–1.3 and 1.1–1.5 µm of 3 months old cells in diameter, respectively. The isolate was Gram-stain-positive, oxidase-positive and catalase-positive.

Growth of the isolate and reference strain was tested at different temperatures (1, 2, 4, 10, 15, 25, 30, 35, 37, 40, 42 and 45 °C), different NaCl concentrations [0.5–15% (w/v), in intervals of 0.5%] and different pH values (pH 4–10, in intervals of 1 pH unit) in TSB. For adjusting the pH we used acetate buffer (pH 4.0 and 5.0), phosphate buffer (pH 6.0–8.0) and glycine buffer (pH 9.0 and 10.0). Growth optima for temperature, NaCl concentration and pH value were determined by optical density at 600 nm (OD_{600}) after 72 h in TSB or 24 h for optimum temperature, respectively. Lipolytic activity was detected on tributyrin agar (TSA supplemented with 1% tributyrin) and proteolytic activity was determined on skim milk agar (Harrigan 1998). Biofilm-forming capacity was analysed in polystyrene microtiter plates as described previously (Kolari *et al.* 2001). Lipolytic activity, proteolytic activity and biofilm-forming capacity were examined at the temperatures mentioned above.

The growth temperature and the tolerance for NaCl allowed a differentiation between the isolate and the reference strain. Strains KR32^T and *A. agilis* DSM 20550^T were both able to grow at 1 °C but *A. agilis* DSM 20550^T was not able to grow above 35 °C. Growth above 37 °C was an exclusive property of strain KR32^T in comparison to all other species of the 'pink *A. agilis* group' (Liu *et al.* 2018, Lee *et al.* 2016). The optimum temperature was 27–30 °C for KR32^T and 25 °C for *A. agilis* DSM 20550^T. The maximum tolerable NaCl concentration for KR32^T and *A. agilis* DSM 20550^T were 7.5 and 4.5%, respectively. The optimum NaCl concentration for KR32^T was 2.5 and 0.5% for *A. agilis* DSM 20550^T. Both strains grew at pH 7.0–8.0. The optimum pH value for the isolate and reference strain was pH 8.0. Strain KR32^T and reference strain *A. agilis* DSM 20550^T showed no proteolytic or lipolytic activity and did not produce biofilms at any tested temperature. A summary of the differentiating characteristics is shown in Table 4.2.

Biochemical characteristics were analysed using API Coryne, API ZYM and API 50 CH (with AUX medium) test systems (bioMérieux) amended to the manufacturer's specifications at 30 °C for at least 48 h. Strain KR32^T and the reference strain were positive for leucine arylamidase and naphthol-AS-BI-phosphohydrolase. Full reaction profiles of the isolate and the reference strain are given as supplemental tables (Tables S4.3 and S4.4). Strain KR32^T could be differentiated from *A. agilis* DSM 20550^T based on a positive reaction for trypsin and on a negative reaction for acid phosphatase. Moreover, isolate KR32^T was positive for assimilation of L-arabinose, *N*-

acetylglucosamine, arbutin, salicin, melibiose, raffinose, starch and potassium gluconate in contrast to *A. agilis* DSM 20550^T, which was negative for these tests.

Fatty acid methyl esters (FAMEs), isoprenoid quinones, polar lipid profiles and acyl type of peptidoglycan of strain KR32^T and the reference strain were analysed as described by Wiertz *et al.* (2018). Cells were grown in TSB at 10 and 30 °C until an OD_{600} of about 1 ± 0.2 was reached for comparative temperature-dependent studies. Cells were harvested by centrifugation at 10 000 *g* for 5 min and washed with Ringer's solution prior to chemotaxonomic analyses. Dimethyl disulfide (DMDS) derivatization and analyses of unsaturated FAMEs were performed as described by Nichols *et al.* (1986). To visualize polar lipids on thin-layer chromatography (TLC) plates, they were stained with a 0.05% solution of primuline dye (50 mg primuline in 100 ml acetone/water, 8:2, v/v) (White *et al.* 1998). Primuline was used as a nondestructive lipophilic dye which allows subsequent extraction and further analyses of single lipid spots. Unidentified lipid spots were scratched off from the TLC plates, extracted and analysed by quadrupole time-of-flight (Q-TOF) mass spectrometry as described by Hölzl *et al.* (2018). Carotenoids were extracted from lyophilised biomass and analysed as described by Kaiser *et al.* (2007) and Etzbach *et al.* (2018).

Isolate KR32^T showed the main fatty acids described for the genera of the family *Micrococcaceae* (Busse 2012). Table 4.3 shows the fatty acid profiles of the isolate and reference strain. The cellular fatty acids of KR32^T were *anteiso*-$C_{15:0}$ (69.1%), *iso*-$C_{15:0}$ (20.4%), and $C_{14:0}$ (1.0%) after cultivation for 48 h at 30 °C. The cellular fatty acid composition was similar but had minor differences from those of *A. agilis* DSM 20550^T. Results of FAME analyses of cultures grown at 10 °C revealed adaptation of the membranes by synthesis of monounsaturated fatty acids, particularly $C_{16:1}$ *cis* 9. Genome analysis of strain KR32^T confirmed the presence of two putative acyl-CoA desaturases (WP_152817044, WP_152813168) as a prerequisite for the production of unsaturated fatty acids. Most likely,

Table 4.3 Fatty acid profiles of KR32^T and reference strain. Strain: 1, KR32^T; 2, *Arthrobacter agilis* DSM 20550^T. All data were obtained in this study. Percentages are means of three analyses. –, Not detected.

Fatty acid (%)	**1**		**2**	
Temperature (°C)	10	30	10	30
iso-$C_{14:0}$	1.0	0.4	0.2	0.2
$C_{14:1}$ *cis* 9	0.2	–	–	–
$C_{14:0}$	1.4	1.0	0.9	1.4
iso-$C_{15:1}$ *cis* 9	0.4	–	0.2	–
iso-$C_{15:1}$ *cis* 4	0.6	–	0.3	–
iso-$C_{15:0}$	6.9	20.4	13.7	12.0
anteiso-$C_{15:0}$	76.2	69.1	64.6	75.6
iso-$C_{16:1}$ *cis* 9	1.7	–	0.3	–
iso-$C_{16:0}$	0.8	0.9	1.1	0.7
$C_{16:1}$ *cis* 9	7.6	1.1	9.6	1.4
$C_{16:0}$	0.6	2.0	1.7	4.1
$C_{17:1}$ *cis* 10/11	–	0.4	–	–
$C_{17:1}$ *cis* 9	1.8	0.2	3.0	0.2
iso-$C_{17:0}$	–	0.4	0.2	0.2
anteiso-$C_{17:0}$	0.8	4.1	4.2	–

the cold adaptation in strain KR32^T is not realized by changing the ratio of *iso*/*anteiso* fatty acids as it is demonstrated for other bacteria (Annous *et al.* 1997).

The predominant menaquinone of KR32^T was MK-9(H_2) (90.5%), which is the major quinone of the genus *Arthrobacter*, with MK-8(H_2) (4.3%) and MK-9 (2.7%) as minor compounds (Busse 2016). The menaquinone composition of the isolate KR32^T is similar to that of *A*. *agilis* DSM 20550^T. *A*. *agilis* DSM 20550^T showed MK-9(H_2) (94.6%) as the predominant menaquinone, and MK-8(H_2) (3.6%) and MK-9 (1.8%) as minor compounds, respectively.

Thin-layer chromatography of the polar lipid profile of strains KR32^T and *A*. *agilis* DSM 20550^T revealed the presence of diphosphatidylglycerol (DPG), phosphatidylglycerol (PG), phosphatidylinositol (PI), and a glycolipid (GL1) (Fig. S4.1). In addition, *A*. *agilis* DSM 20550^T contained an unidentified lipid (L1). The glycolipid was subsequently identified as monoacyldimannosyl-monoacylglycerol (MDMMG) by Q-TOF-MS/MS analysis. The fragmentation pattern of this polar lipid revealed a characteristic monoacylmannosyl fragment which is in accord with the structure proposed by Paściak *et al.* (2010) for the major glycolipid of *A*. *globiformis*. A comparative analysis of the major glycolipid of *A*. *globiformis* DSM 20124^T and the glycolipid of strain KR32^T revealed an identical fragmentation pattern between these two glycolipids, which supports identification as MDMMG. The main molecular MDMMG species of strain KR32^T was detected with *m/z* 882.61 with a fragmentation pattern indicating the presence of two C_{15} fatty acids in the molecule. Three minor molecular species were detected in *A*. *globiformis* DSM 20124^T, but were below the detection limit in strain KR32^T. These three minor molecular species of MDMMG were detected with *m/z* 868.60 (C_{14} and C_{15}), *m/z* 896.63 (C_{15} and C_{16}) and *m/z* 910.65 (C_{15} and C_{17}). This coincides with the results of the fatty acid analysis, in which mainly the *anteiso*-$C_{15:0}$ fatty acid was present. The polar lipids of the isolate and the reference strain were not significantly different. Both strains contained DPG, PG, PI and GL1. This was in accord with the description for the family *Micrococcaceae*, where a core polar lipid profile was described, consisting of DPG, PG and at least one glycolipid (Busse 2016). Strain KR32^T and *A*. *agilis* DSM 20550^T showed the acetyl type of peptidoglycan.

The pink pigment of strain KR32^T and *A*. *agilis* DSM 20550^T was identified by HPLC-DAD-APCI-MS^n as the C_{50} carotenoid bacterioruberin and a range of mono-, di- and tetra-glycosylated derivatives. The colonies of strain KR32^T had a less intense colouration and differed in the hue from *A*. *agilis* DSM 20550^T at 30 °C growth temperature on TSA and TSB (Fig. 4.1). HPLC analysis showed that strain KR32^T had a lower content and a slightly different composition of carotenoids, lacking the first eluting carotenoid peak in comparison to *A*. *agilis* DSM 20550^T at 30 °C growth temperature

(Figs S4.2 and S4.3). Carotenoid compounds were partially identified by mass spectrometric analysis (Table S4.5) using data of Fong *et al.* (2001). The C_{50} carotenoid bacterioruberin and its glycosylated derivatives are the main carotenoids of halophilic archaea and of several bacterial species of the phylum Actinobacteria (Fong *et al.* 2001; Chattopadhyay et al; 1997, Dummer *et al.* 2011; Saito *et al.* 1994).

Cell-wall amino acid composition was determined for KR32^T and *A. agilis* DSM 20550^T. Isolates were grown at 30 °C for 24 h in TSB, harvested by centrifugation, washed and lyophilised. Cell-wall amino acids were purified and derivatized to their heptafluorobutyryl isobutyl esters as described by O'Donnell *et al.* (1982). Samples were analysed on an Agilent 7890A/5975C GC-MSD system equipped with an HP5-MS column. For strain KR32^T the dominating cell-wall amino acids were alanine, threonine, glycine and lysine with a ratio of 1.0:0.2:0.2:0.2 and for *A. agilis* DSM 20550^T alanine, threonine, glycine, lysine and glutamate with a ratio of 1.0:0.2:0.2:0.2:0.5. Accordingly, the peptidoglycan of both strains were classified as A3α (A11.28) type according to Schleifer and Kandler (1972) but showed differences in the amount of glutamate. These results are in agreement with the peptidoglycan structure Lys-Thr-Ala_{2-3} of the '*A. agilis* group' (Busse 2016).

Isolate KR32^T is the first representative of a pink-coloured bacterium isolated from food that clustered in the '*A. agilis* group'. The stimulation of pigment production under low temperature conditions may be a so far underrated factor for food spoilage. On the other hand, the characterization of pigments from non-pathogenic, food-related micro-organisms may represent a new source of food colourants.

6 Description of *Arthrobacter bussei* sp. nov.

Arthrobacter bussei (bus'se.i. N.L. gen. n. *bussei*, of Busse; named after the German microbiologist Hans-Jürgen Busse).

Cells are Gram-stain-positive, oxidase-positive, catalase-positive, aerobic, coccus-shaped and non-motile. Cells are 1.1–1.5 µm in diameter. Rod-coccus life cycle is not observed. Colonies are pink-pigmented, convex, round and 1.0 mm in diameter after 5 days of incubation on TSA at 30 °C. Growth occurs at 1–45 °C and pH 7.0–8.0. Tolerates a maximum of 7.5% NaCl. Growth on Columbia blood agar but not on violet red bile dextrose agar. No proteolytic or lipolytic activity on skimmed milk and tributyrin agar in a temperature range from 1 to 45 °C. Optimal temperature for growth is 27–30 °C. Growth at pH 7.0–8.0, optimum at pH 8.0. Hydrolyses aesculin but not gelatin. Positive for alkaline phosphatase, esterase (C_4), esterase lipase (C_8), lipase (C_{14}), leucine arylamidase, valine arylamidase, cystine arylamidase, trypsin, naphthol-AS-BI-phosphohydrolase, α-galactosidase, β-

galactosidase, α-glucosidase, β-glucosidase and α-mannosidase. Negative for nitrate reduction, α-chymotrypsin, acid phosphatase, β-glucuronidase, *N*-acetyl-β-glucosaminidase, α-fucosidase, arginine dihydrolase and urease. Assimilates L-arabinose, *N*-acetylglucosamine, arbutin, salicin, melibiose, trehalose, raffinose, starch and potassium gluconate. The main fatty acids are *anteiso*-$C_{15:0}$ and *iso*-$C_{15:0}$ at 30 °C. The fatty acid $C_{16:1}$ *cis* 9 is produced at 10 °C growth temperature. MK-9(H_2), MK-8(H_2), MK-9, and MK-9 (H_6) are present. The polar lipids are diphosphatidylglycerol, phosphatidylglycerol, phosphatidylinositol and monoacyldimannosyl-monoacylglycerol.

The type strain KR32^T (= DSM 109896^T = LMG 31480^T = NCCB 100733^T), was isolated from refrigerated sliced cheese made of cow's milk. The Whole Genome Shotgun project has been deposited at DDBJ/ENA/GenBank under the accession VJXX00000000. The genomic DNA G+C content of the type strain is 69.14 mol%, based on the whole genome sequence. The accession number of the 16S rRNA gene sequence is MN080869.

Supporting information

Table S4.1 Used multilocus sequence analysis (MLSA) data with accession numbers of genome sequences, *tuf*, *secY*, *rpoB*, *recA*, *fusA*, and *atpD*.

Organism	Genome	*tuf*	*secY*	*rpoB*	*recA*	*fusA*	*atpD*
Arthrobacter sp. KR32^T	VJXX00000000						
Arthrobacter agilis DSM 20550^T	VHIM00000000						
Arthrobacter ruber MDB1-42^T	PPTH00000000						
Arthrobacter tecti LMG 22282^T		KY827764	KY827696	KY827628	KY827560	KY827492	KY827424
Arthrobacter parietis LMG 22281^T		KY827758	KY827690	KY827622	KY827554	KY827486	KY827418
Arthrobacter tumbae LMG 19501^T		KY827765	KY827697	KY827629	KY827561	KY827493	KY827425
Arthrobacter crystallopoietes DSM 20117^T		KY827750	KY827682	KY827614	KY827546	KY827478	KY827410
Arthrobacter citreus DSM 20133^T		KY827748	KY827680	KY827612	KY827544	KY827476	KY827408
Arthrobacter koreensis CA15-8^T		KY827755	KY827687	KY827619	KY827551	KY827483	KY827415
Arthrobacter luteolus NBRC 107841^T	BCQM01000000						
Arthrobacter castelli DSM 16402^T	AUMN00000000						
Haematomicrobium sanguinis DSM 21259^T	JIAG00000000						
Arthrobacter woluwensis NBRC 107840^T	FNSN00000000						
Arthrobacter cupressi CGMCC 1.10783^T		KY827751	KY827683	KY827615	KY827547	KY827479	KY827411
Arthrobacter alkaliphilus LC6^T		KY827746	KY827678	KY827610	KY827542	KY827474	KY827406
Arthrobacter ramosus DSM 16186^T		KY827762	KY827694	KY827626	KY827558	KY827490	KY827422
Paenarthrobacter aurescens NBRC 12136^T		KY827769	KY827701	KY827633	KY827565	KY827497	KY827429
Arthrobacter ginsengisoli DCY81^T		KY827752	KY827684	KY827616	KY827548	KY827480	KY827412
Arthrobacter humicola KV-653^T		KY827754	KY827686	KY827618	KY827550	KY827482	KY827414
Arthrobacter liuii DSXY973^T		KY827756	KY827688	KY827620	KY827552	KY827484	KY827416
Pseudarthrobacter polychromogenes DSM 20136^T		KY827779	KY827711	KY827643	KY827575	KY827507	KY827439
Arthrobacter enclensis NIO-1008^T	LNQM00000000						
Arthrobacter globiformis NBRC 12137^T		KY827753	KY82768	KY827617	KY827549	KY827481	KY827413
Arthrobacter pascens DSM 20545^T		KY827759	KY827691	KY827623	KY827555	KY827487	KY827419
Arthrobacter stackebrandtii DSM 16005^T		KY827763	KY827695	KY827627	KY827559	KY827491	KY827423
Arthrobacter livingstonensis DSM 22825^T		KY827757	KY827689	KY827621	KY827553	KY827485	KY827417
Arthrobacter cryoconiti DSM 23324^T		KY827749	KY827681	KY827613	KY827545	KY827477	KY827409
Arthrobacter psychrochitiniphilus DSM 23143^T		KY827760	KY827692	KY827624	KY827556	KY827488	KY827420
Arthrobacter alpinus DSM 22274^T		KY827747	KY827679	KY827611	KY827543	KY827475	KY827407
Arthrobacter psychrolactophilus DSM 15612^T		KY827761	KY827693	KY827625	KY827557	KY827489	KY827421
Glutamicibacter ardleyensis DSM 17432^T		KY827766	KY827698	KY827630	KY827562	KY827494	KY827426
Paeniglutamicibacter sulfureus DSM 20167^T		KY827775	KY827707	KY827639	KY827571	KY827503	KY827435

Table S4.2 Results of assemblies assessed with Quast of strain KR32^T and type strain of the most closely related species. 1, strain KR32^T; 2, *Arthrobacter agilis* DSM 20550^T. All data were obtained in this study.

	1	2
Contigs	15	28
Largest contig	1728676	617265
Total length	3620993	3234685
GC (%)	69.14	68.84
N50	550094	391922
N75	300400	255075
L50	2	4
L75	4	6
N's per 100 kbp	0.00	0.00

Table S4.3 Profiles obtained by the API® ZYM test system for strain KR32^T and type strain of the most closely related species. 1, Strain KR32^T; 2, *Arthrobacter agilis* DSM 20550^T. +, positive; -, negative; w, weakly positive. All data were obtained in this study.

	1	2
Alkaline Phosphatase	+	+
Esterase (C4)	+	+
Esterase Lipase (C8)	+	+
Lipase (C14)	+	+*
Leucine arylamidase	+	+
Valine arylamidase	+	+
Cysteine arylamidase	+	+*
Trypsin	+	-
α-Chymotrypsin	-	-
Acid Phosphatase	-	+
Naphthol-AS-BI-phosphohydrolase	+	+*
α-Galactosidase	+	+
β-Galactosidase	+	+
β-Glucuronidase	-	-
α-Glucosidase	+	-*
β-Glucosidase	+	-
N-Acetyl-β-Glucosaminidase	-	-
α-Mannosidase	+	-
β-Fucosidase	-	-

*Data differs from Lee *et al.* (2016)

Table S4.4. Profiles obtained by the API® 50CH test system for strain KR32T and type strain of the most closely related species. 1, Strain KR32^T; 2. *A. agilis* DSM 20550^T. +, positive; -, negative; w, weakly positive. All data were obtained in this study.

	1	2
Glycerol	+	+
Erythritol	-	-
D-Arabinose	-	-
L-Arabinose	+	-
D-Ribose	-	-
D-Xylose	+	+
L-Xylose	-	-
D-Adonitol	-	-
Methyl-βD-Xylopyranoside	-	+
D-Galactose	+	+*
D-Glucose	+	+
D-Fructose	+	+
D-Mannose	+	+
L-Sorbose	-	-
L-Rhamnose	+	+
Dulcitol	-	-
Inositol	-	-
D-Mannitol	+	+
D-Sorbitol	-	-†
Methyl-αD-Mannopyranoside	-	-
Methyl-αD-Glucopyranoside	-	-
N-Acetylglucosamine	+	-
Amygdalin	-	-
Arbutin	+	w†
Esculin ferric citrate	+	+
Salicin	w	-
D-Cellobiose	+	+
D-Maltose	+	+
D-Lactose (bovine origin)	-	w
D-Melibiose	+	-
D-Saccharose (sucrose)	+	+
D-Trehalose	w	+
Inulin	-	-
D-Melezitose	-	+
D-Raffinose	+	-
Amidon (starch)	+	w
Glycogen	+	+
Xylitol	-	-
Gentiobiose	-	-*
D-Turanose	+	+
D-Lyxose	-	-

(Continued) Table S4.4. Profiles obtained by the API® 50CH test system for strain KR32T and type strain of the most closely related species. 1, Strain KR32^T; 2. *A. agilis* DSM 20550^T. +, positive; -, negative; w, weakly positive. All data were obtained in this study.

	1	2
D-Tagatose	-	-
D-Fucose	-	-
L-Fucose	-	-
D-Arabitol	-	-
L-Arabitol	-	-
Potassium gluconate	+	-
Potassium 2-Ketogluconate	-	-
Potassium 5-Ketogluconate	+	+

†Data differs from Lee *et al.* (2016)
*Data differs from Liu *et al.* (2018)

Table S4.5 Chromatographic, UV/Vis, and mass spectrometric characteristics of carotenoids from strain KR 32^T and *Arthrobacter agilis* DSM 20550^T, obtained by HPLC-DSD-APCI-MS^n.

Fraction	t_R (min)	Compound identification	λ_{max} (nm)	Mass (*m/z*)
a*	2.318	Potential bacterioruberin glucoside	470, 494, 527	903
b	3.031	Bacterioruberin diglucoside	370, 386, 470, 494, 527	1066, 903
c	3.655	Bacterioruberin monoglucoside	370, 386, 469, 494, 527	903, 845, 811, 797, 723, 705, 687
d	4.501	3',4'-Dihydromonoanhydrobacterioruberin	370, 386, 470, 494, 526	725, 723, 707
e	5.304	Bacterioruberin	369, 385, 470, 488, 521	741, 723, 647
f	5.616	unidentified	369, 385, 470, 494, 522	-
g	6.819	Bisanhydrobacterioruberin	470, 494, 522	705

*Not present in strain KR32^T

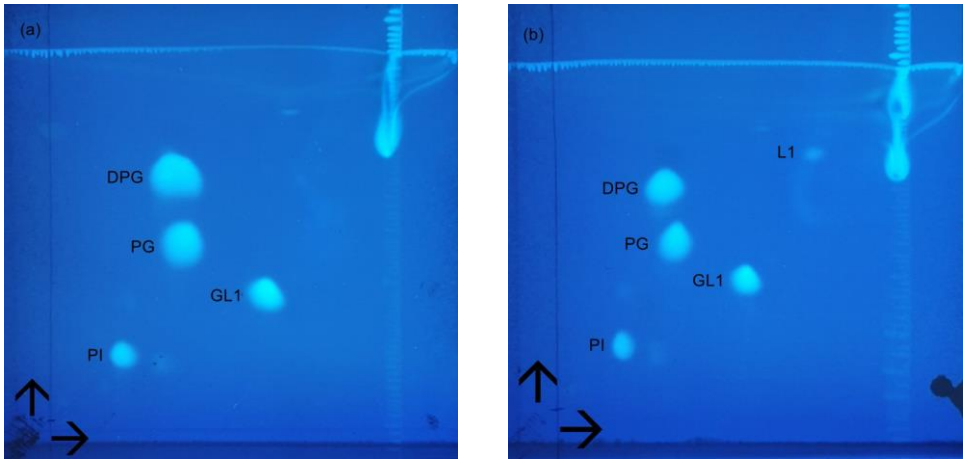

Fig. S4.1 Two-dimensional TLC with polar lipid patterns of strain KR32^T (a) and *Arthrobacter agilis* DSM 20550^T (b) after detection with primuline. DPG, diphosphatidylglycerol; PG, phosphatidylglycerol; PI, phosphatidylinositol; GL1, dimannosyldiglyceride; L1, unidentified lipid; →,first dimension; ↑, second dimension.

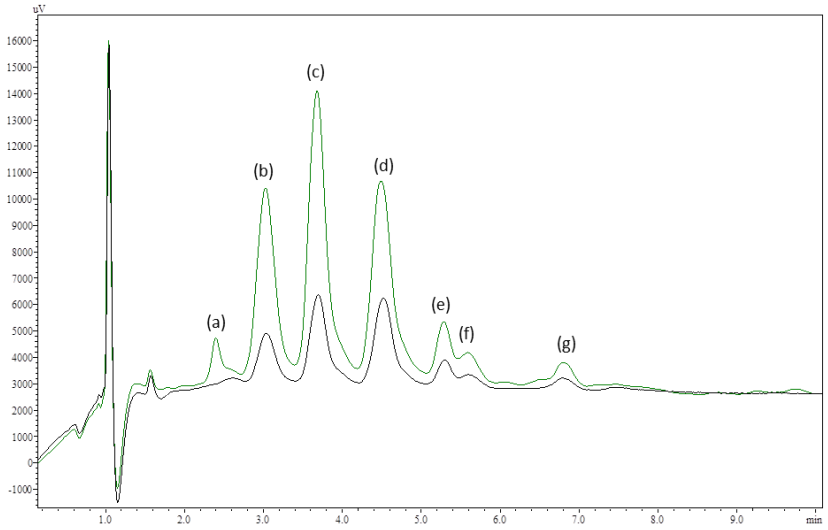

Fig. S4.2 Separation of carotenoids from strain KR32^T (black line) and *Arthrobacter agilis* DSM 20550^T (green line) by HPLC-DAD (450 nm) on a C30 column.

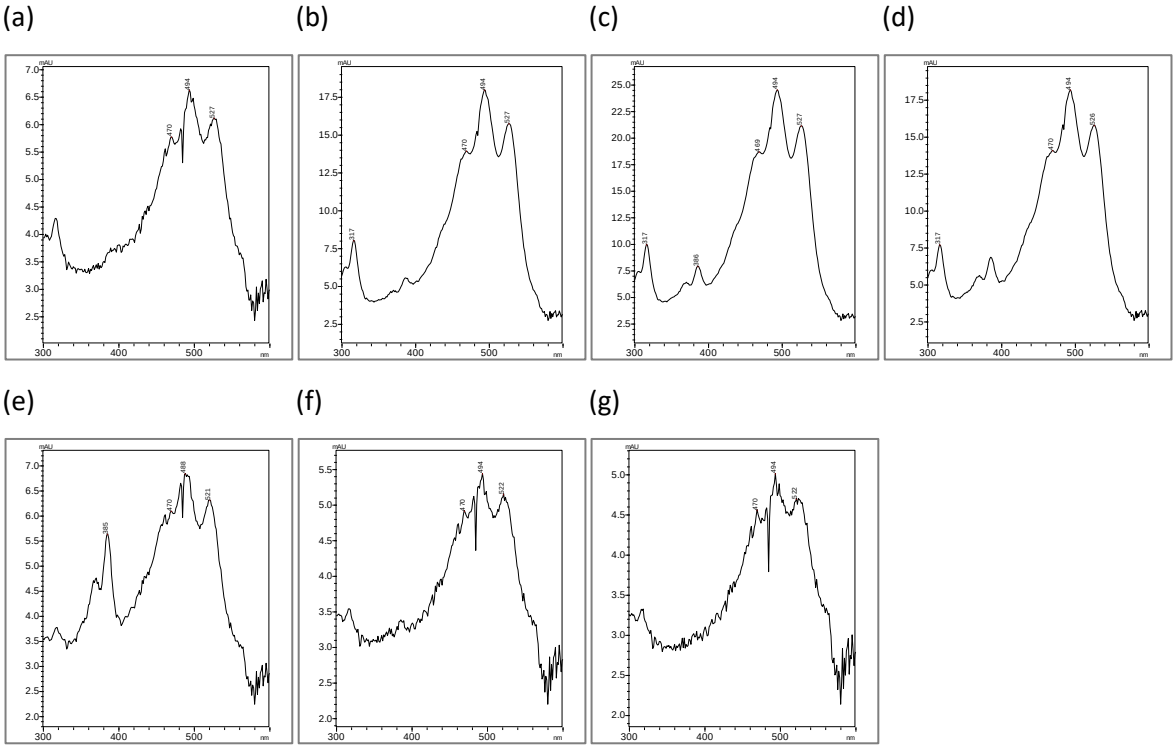

Fig. S4.3 UV/Vis characteristics of carotenoids from *Arthrobacter agilis* DSM 20550^T obtained by HPLC-DAD on a C30 column. Peaks (a): 470, 494, 527 nm; Peaks (b): 317, 470, 494, 527 nm; Peaks (c): 317, 386, 469, 494, 527 nm; Peaks (d): 317, 470, 494, 526 nm; Peaks (e): 385, 470, 488, 521 nm; Peaks (f): 470, 494, 522 nm; Peaks (g): 470, 494, 522 nm.

References

Annous BA, Becker LA, Bayles DO, Labeda DP, Wilkinson BJ. (1997) Critical role of *anteiso*-$C_{15:0}$ fatty acid in the growth of *Listeria monocytogenes* at low temperatures. *Appl Environ Microbiol* 63:3887–3894

Bankevich A, Nurk S, Antipov D, Gurevich AA, Dvorkin M *et al.* (2012) SPAdes: a new genome assembly algorithm and its applications to single-cell sequencing. *J Comput Biol* 19:455–477

Bockelmann W, Hoppe-Seyler T (2001). The surface flora of bacterial smear-ripened cheeses from cow's and goat's milk. *Int Dairy J* 2001 11:307–314

Bowman JP, McCammon SA, Brown MV, Nichols DS, McMeekin TA (1997). Diversity and association of psychrophilic bacteria in Antarctic sea ice. *Appl Environ Microbiol* 63:3068–3078

Busse H-J (2012) Family I *et al. Micrococcaceae* Pribram 1929, 361^{AL} emend. In: Goodfellow M, Kämpfer P, BusseH-J, Trujillo ME, Suzuki K-I, Ludwig W, William B. Whitman P (eds) *Bergey's Manual of Systematic Bacteriology.* Springer, New York

Busse H-J (2016). Review of the taxonomy of the genus *Arthrobacter*, emendation of the genus *Arthrobacter sensu lato*, proposal to reclassify selected species of the genus *Arthrobacter* in the novel genera *Glutamicibacter* gen. nov., *Paeniglutamicibacter* gen. nov., *Pseudoglutamicibacter* gen. nov., *Paenarthrobacter* gen. nov. and *Pseudarthrobacter* gen. nov., and emended description of *Arthrobacter roseus*. *Int J Syst Evol Microbiol* 66:9–37

Chattopadhyay MK, Jagannadham MV, Vairamani M, Shivaji S (1997). Carotenoid pigments of an antarctic psychrotrophic bacterium *Micrococcus roseus*: temperature dependent biosynthesis, structure, and interaction with synthetic membranes. *Biochem Biophys Res Commun* 239:85–90

Chun J, Oren A, Ventosa A, Christensen H, Arahal DR *et al.* (2018) Proposed minimal standards for the use of genome data for the taxonomy of prokaryotes. *Int J Syst Evol Microbiol* 68:461–466

Conn HJ, Dimmick I. (1947) Soil bacteria similar in morphology to *Mycobacterium* and *Corynebacterium*. *J Bacteriol* 54:291–303

Delbès C, Ali-Mandjee L, Montel M-C (2007). Monitoring bacterial communities in raw milk and cheese by culture-dependent and -independent 16S rRNA gene-based analyses. *Appl Environ Microbiol* 73:1882–1891

Dieser M, Greenwood M, Foreman CM (2010). Carotenoid pigmentation in Antarctic heterotrophic bacteria as a strategy to withstand environmental stresses. *Arct Antarct Alp Res* 42:396–405

Dummer AM, Bonsall JC, Cihla JB, Lawry SM, Johnson GC *et al.* (2011) Bacterioopsin-mediated regulation of bacterioruberin biosynthesis in *Halobacterium salinarum*. *J Bacteriol* 193:5658–5667

Edgar RC (2004). Muscle: multiple sequence alignment with high accuracy and high throughput. *Nucleic Acids Res* 32:1792–1797

Etzbach L, Pfeiffer A, Weber F, Schieber A (2018). Characterization of carotenoid profiles in goldenberry (*Physalis peruviana* L.) fruits at various ripening stages and in different plant tissues by HPLC-DAD-APCI-MS^n. *Food Chem* 245:508–517

Fong NJ, Burgess ML, Barrow KD, Glenn DR (2001). Carotenoid accumulation in the psychrotrophic bacterium *Arthrobacter agilis* in response to thermal and salt stress. *Appl Microbiol Biotechnol*, 56:750–756

Gerhardt P (1981). Manual of methods for general bacteriology. *Am Soc Microbiol*

Gurevich A, Saveliev V, Vyahhi N, Tesler G (2013). QUAST: quality assessment tool for genome assemblies. *Bioinformatics* 29:1072–1075

Harrigan WF (1998). *Laboratory methods in food microbiology.* Academic Press, Sam Diego

Harrison FC, Kennedy ME (1922). The red discoloration of cured codfish. *Trans R Soc Can* 16:101–152

Heyrman J, Verbeeren J, Schumann P, Swings J, De Vos P (2005). Six novel *Arthrobacter* species isolated from deteriorated mural paintings. *Int J Syst Evol Microbiol* 55:1457–1464

Hölzl G, Sohlenkamp C, Vences-Guzmán MA, Gisch N (2018). Headgroup hydroxylation by OlsE occurs at the C_4 position of ornithine lipid and is widespread in proteobacteria and bacteroidetes. *Chem Phys Lipids* 213:32–38

Irlinger F, Bimet F, Delettre J, Lefèvre M, Grimont PAD (2005). *Arthrobacter bergerei* sp. nov. and *Arthrobacter arilaitensis* sp. nov., novel coryneform species isolated from the surfaces of cheeses. *Int J Syst Evol Microbiol* 55:457–462

Kaiser P, Surmann P, Vallentin G, Fuhrmann H (2007). A small-scale method for quantitation of carotenoids in bacteria and yeasts. *J Microbiol Methods*, 70:142–149

Kolari M, Nuutinen J, Salkinoja-Salonen MS (2001). Mechanisms of biofilm formation in paper machine by Bacillus species: the role of *Deinococcus geothermalis*. *J Ind Microbiol Biotechnol* 27:343–351

Kumar S, Stecher G, Li M, Knyaz C, Tamura K (2018). MEGA X: molecular evolutionary genetics analysis across computing platforms. *Mol Biol Evol* 35:1547–1549

Lee I, Chalita M, Ha S-M, Na S-I, Yoon S-H *et al.* (2017). ContEst16S: an algorithm that identifies contaminated prokaryotic genomes using 16S RNA gene sequences. *Int J Syst Evol Microbiol* 67:2053–2057

Lee J-Y, Hyun D-W, Soo Kim P, Sik Kim H, Shin N-R *et al.* (2016). *Arthrobacter echini* sp. nov., isolated from the gut of a purple sea urchin, *Heliocidaris crassispina*. *Int J Syst Evol Microbiol* 66:1887–1893

Liu Q, Xin Y-H, Chen X-L, Liu H-C, Zhou Y-G *et al.* (2018a) *Arthrobacter ruber* sp. nov., isolated from glacier ice. *Int J Syst Evol Microbiol* 68:1616–1621

Liu Q, Xin Y-H, Zhou Y-G, Chen W-X (2018b). Multilocus sequence analysis of homologous recombination and diversity in *Arthrobacter sensu lato* named species and glacier-inhabiting strains. *Syst Appl Microbiol* 41:23–29

Mandelli F, Miranda VS, Rodrigues E, Mercadante AZ (2012). Identification of carotenoids with high antioxidant capacity produced by extremophile microorganisms. *World J Microbiol Biotechnol* 28:1781–1790

Meier-Kolthoff JP, Auch AF, Klenk H-P, Göker M (2013). Genome sequence-based species delimitation with confidence intervals and improved distance functions. *BMC Bioinformatics* 14:60

Merlino CP (1924). Bartolomeo Bizio's letter to the most Eminent Priest, Angelo Bellani, concerning the phenomenon of the red colored polenta. *J Bacteriol* 9:527–543

Monnet C, Loux V, Gibrat J-F, Spinnler E, Barbe V *et al.* (2010) The *Arthrobacter arilaitensis* Re117 genome sequence reveals its genetic adaptation to the surface of cheese. *PLoS One* 5:e15489

Nei M, Kumar S (2000). *Molecular evolution and phylogenetics*. Oxford University Press, New York

Nichols PD, Guckert JB, White DC (1986). Determination of monosaturated fatty acid double-bond position and geometry for microbial monocultures and complex consortia by capillary GC-MS of their dimethyl disulphide adducts. *J Microbiol Methods* 5:49–55

Nouioui I, Carro L, García-López M, Meier-Kolthoff JP, Woyke T *et al.* (2018) Genome-based taxonomic classification of the phylum *Actinobacteria*. *Front Microbiol* 9:2007

O'Donnell AG, Minnikin DE, Goodfellow M, Parlett JH (1982). The analysis of actinomycete wall amino acids by gas chromatography. FEMS Microbiol Lett, 15:75–78

Parte AC (2018). LPSN - List of prokaryotic names with standing in nomenclature (bacterio.net), 20 years on. *Int J Syst Evol Microbiol* 68:1825–1829

Paściak M, Sanchez-Carballo P, Duda-Madej A, Lindner B, Gamian A *et al.* (2010) Structural characterization of the major glycolipids from *Arthrobacter globiformis* and *Arthrobacter scleromae*. *Carbohydr Res* 345:1497–1503

Reddy GS, Aggarwal RK, Matsumoto GI, Shivaji S (2000). *Arthrobacter flavus* sp. nov., a psychrophilic bacterium isolated from a pond in McMurdo Dry Valley, Antarctica. *Int J Syst Evol Microbiol* 50:1553–1561

Saito T, Terato H, Yamamoto O (1994). Pigments of *Rubrobacter radiotolerans*. *Arch Microbiol* 162:414–421

Schleifer KH, Kandler O (1972). Peptidoglycan types of bacterial cell walls and their taxonomic implications. *Bacteriol Rev* 36:407–477

Seel W, Baust D, Sons D, Albers M, Etzbach L *et al.* (2020) Carotenoids are used as regulators for membrane fluidity by *Staphylococcus xylosus*. *Sci Rep* 10:330

Shoemaker JS, Fitch WM (1989). Evidence from nuclear sequences that invariable sites should be considered when sequence divergence is calculated. *Mol Biol Evol* 6:270–289

Sutthiwong N, Fouillaud M, Valla A, Caro Y, Dufossé L (2014). Bacteria belonging to the extremely versatile genus *Arthrobacter* as novel source of natural pigments with extended hue range. *Food Res Int* 65:156–162

Tamura K, Nei M (1993). Estimation of the number of nucleotide substitutions in the control region of mitochondrial DNA in humans and chimpanzees. *Mol Biol Evol* 10:512–526

Tavaré S (1986). Some probabilistic and statistical problems in the analysis of DNA sequences. In: Miura RM (ed) *Lectures on mathematics in the life science*s. AMS, Providence.

Valdes-Stauber N, Götz H, Busse M (1991). Antagonistic effect of coryneform bacteria from red smear cheese against *Listeria* species. *Int J Food Microbiol* 13:119–130

Weber M, Schünemann W, Fuß J, Kämpfer P, Lipski A (2018). *Stenotrophomonas lactitubi* sp. nov. and *Stenotrophomonas indicatrix* sp. nov., isolated from surfaces with food contact. *Int J Syst Evol Microbiol* 68:1830–1838

White T, Bursten S, Federighi D, Lewis RA, Nudelman E (1998). High-resolution separation and quantification of neutral lipid and phospholipid species in mammalian cells and sera by multi-one-dimensional thin-layer chromatography. *Anal Biochem* 258:109–117

Wiertz R, Schulz SC, Müller U, Kämpfer P, Lipski A (2013). *Corynebacterium frankenforstense* sp. nov. and *Corynebacterium lactis* sp. nov., isolated from raw cow milk. *Int J Syst Evol Microbiol* 63:4495–4501

Yang Z (1994). Maximum likelihood phylogenetic estimation from DNA sequences with variable rates over sites: approximate methods. *J Mol Evol* 39:306–314

Yoon S-H, Ha S-M, Kwon S, Lim J, Kim Y *et al.* (2017) Introducing EzBioCloud: a taxonomically United database of 16S rRNA gene sequences and whole-genome assemblies. *Int J Syst Evol Microbiol* 67:1613–1617

Zimmermann J, Rückert C, Kalinowski J, Lipski A (2016). *Corynebacterium crudilactis* sp. nov., isolated from raw cow's milk. *Int J Syst Evol Microbiol* 66:5288–5293

Chapter 5

The C_{50} carotenoid bacterioruberin regulates membrane fluidity in pink-pigmented *Arthrobacter* species

Carotenoids have several crucial biological functions and are part of the cold adaptation mechanism of some bacteria. Some pink-pigmented *Arthrobacter* species produce the rare C_{50} carotenoid bacterioruberin, whose function in these bacteria is unclear and is found mainly in halophilic archaea. Strains *Arthrobacter agilis* DSM 20550^T and *Arthrobacter bussei* DSM 109896^T show an increased bacterioruberin content if growth temperature is reduced from 30 down to 10 °C. In vivo anisotropy measurements with trimethylammonium-diphenylhexatriene showed increased membrane fluidity and a broadening phase transition with increased bacterioruberin content in the membrane at low-temperature growth. Suppression of bacterioruberin synthesis at 10 °C using sodium chloride confirmed the function of bacterioruberin in modulating membrane fluidity. Increased bacterioruberin content also correlated with increased cell resistance to freeze-thaw stress. These findings confirmed the adaptive function of bacterioruberin for growth at low temperatures for pink-pigmented *Arthrobacter* species.

Keywords: *Arthrobacter*; Bacterioruberin; Carotenoid; Membrane fluidity; Cold adaptation

Flegler A, Lipski A (2022) The C_{50} carotenoid bacterioruberin regulates membrane fluidity in pink-pigmented *Arthrobacter* species. *Arch Microbiol* 204**:**70. DOI: 10.1007/s00203-021-02719-3

Author contributions: AF and AL designed the study. AF performed research, analyzed data, prepared figures, and wrote the manuscript. AL reviewed and edited the manuscript.

1 Main

To date, 1204 carotenoids of 722 source organisms have been identified and classified as C_{30}, $C_{40,}$ and C_{50} carotenoids depending on the number of carbons in their carotene backbones (Yabuzaki 2017, 2020). They are involved as accessory pigments in photosynthesis (Holt *et al.* 2005), act as antioxidants (Mandelli *et al.* 2012; Miller *et al.* 1996), light protection pigments (Shahmohammadi *et al.* 1998), oxidative stress protection (Giani & Martínez-Espinosa 2020), and membrane stabilizers (Lazrak *et al.* 1987). As lipophilic compounds, carotenoids are located in the cellular membrane, but their orientation within the membrane can vary depending on their chemical structure and the thickness of the membrane (Gruszecki 2004; Milon *et al.* 1986). More than 95% of all natural carotenoids are based on the symmetric C_{40} phytoene backbone, and only a small number of C_{30} and even fewer C_{50} carotenoids have been discovered (Tobias and Arnold 2006). Previous studies showed that carotenoids were able to lower the phase transition temperature of synthetic lipids (Subczynski *et al.* 1992, 1993), and this effect was dependent on the concentration of the pigment (Chaturvedi & Ramakrishna Kurup 1986; Strzałka & Gruszecki 1994; Subczynski *et al.* 1992). In accord with these observations, several authors argued that carotenoids might have a similar function in regulating membrane fluidity as sterols such as cholesterol or ergosterol in eukaryotic cells (Rohmer *et al.* 1979; Subczynski *et al.* 1992). Concerning the functions mentioned above, the involvement of carotenoids in bacterial cold adaptation was suspected especially for *Arthrobacter agilis*, *Micrococcus roseus*, and confirmed for *Staphylococcus xylosus* (Chattopadhyay *et al.* 1997; Fong *et al.* 2001; Seel *et al.* 2020; Strand *et al.* 1997).

The genus *Arthrobacter*, described by Conn & Dimmick (1947) and with an amendment by Busse (2016), is a predominant group of bacteria isolated from various sources such as soil, air, food, water, and plants, which has been found to produce a great variety of pigment hues, e.g., yellow, red, green, and blue (Sutthiwong *et al.* 2014). The species *A. agilis* and *Arthrobacter bussei* are known for the temperature-dependent pigmentation of the rare C_{50} carotenoid bacterioruberin and its glycosylated derivatives (Flegler *et al.* 2020; Fong *et al.* 2001). Fong *et al.* (2001) suspected that bacterioruberin is involved in adapting *A. agilis* strain MB813 to low-temperature growth conditions, which was isolated from Antarctic sea ice by Bowman *et al.* (1997). Therefore, we assumed that bacterioruberin in pink-pigmented *Arthrobacter* species has a similar function in regulating membrane fluidity as the carotenoid staphyloxanthin in *S. xylosus*, a species that also shows intense pigmentation at 10 °C growth temperature but no pigmentation at 30 °C (Seel *et al.* 2020). This assumption is strengthened by the fact that, to date, all pink-pigmented *Arthrobacter* species have

been isolated from low-temperature environments. Therefore, we hypothesized that bacterioruberin improves membrane properties under low-temperature conditions in *A*. *agilis* and *A*. *bussei* as model organisms. Using the methods employed in this work, we were able to relate changes in bacterioruberin content to changes in membrane fluidity by measuring the anisotropy of entire cells. Moreover, freeze-thaw stress tests demonstrate that the carotenoids also stabilize the cell membrane.

Comparative fatty acid profiles have already been established for strains *A*. *agilis* DSM 20550^T and *A*. *bussei* DSM 109896^T at 10 and 30 °C growth temperature (Flegler *et al.* 2020). Both *Arthrobacter* species showed an adaptive response to low growth temperature, mainly based on the increase of unsaturated FAs for *A*. *agilis* and a shift from *iso*-branched to *anteiso*-branched fatty acid for *A*. *bussei*, respectively. The difference of the weighted average melting temperature (ΔWAMT) between cultures grown at 10 and 30 °C was calculated using the available percentage fatty acid abundance to derive the extent of FA-dependent temperature adaptation as described by Seel *et al.* (2020). In addition, we calculated ΔWAMT values from the fatty acid profiles published previously, based on the melting temperatures of free fatty acid given by Knothe & Dunn (2009). Both organisms showed a similar but moderate alteration in fatty acid composition resulting in a ΔWAMT of about 3 °C for *A*. *agilis* and 6.7 °C for *A*. *bussei*. Thus, FA-dependent cold adaptation was lower in *A*. *agilis* compared to *A*. *bussei*.

Increased bacterioruberin content alter membrane fluidity and support cold adaptation

According to previous observations, the colonies of both *Arthrobacter* strains showed more pronounced pigmentation at low-temperature growth. The total carotenoid content of bacterioruberin and its glycosylated derivates was extracted with high-performance liquid chromatography (HPLC) as described by Kaiser *et al.* (2007) and Seel *et al.* (2020) and quantified as β-carotene equivalents using an external calibration curve. The quantitative HPLC analysis confirmed a significant increase in bacterioruberin at a growth temperature of 10 °C by about 60.4% in *A*. *agilis* and 264.1% in *A*. *bussei*. The total bacterioruberin content was higher in *A*. *agilis* compared to *A*. *bussei* if both strains were grown at 30 °C (Fig. 5.1a). Anisotropy was measured to determine a correlation between the membrane fluidity and the bacterioruberin content. Sample preparation and membrane fluidity determination by trimethylammonium-diphenylhexatriene (TMA-DPH) anisotropy measurement were performed as Seel *et al.* (2018) described. The results showed a similar behavior of the two strains with an evident influence of the higher bacterioruberin content at low growth temperatures (Fig. 5.1b). Growth at 30 °C significantly reduced the bacterioruberin content of both *Arthrobacter*

species, which showed an approximating phase transition, indicated by the changed curve of measured anisotropy in a temperature range of 5–50 °C. Characteristically, constant anisotropy values at the measurement range limits indicate the membranes' complete phase transition from the gel-like solid-state (high anisotropy) to the liquid-crystalline fluid state (low anisotropy). Cultures grown at 10 °C with high bacterioruberin content showed no pronounced phase transitions in both species, evident from the slight increase of anisotropy with a decrease in temperature. However, *A. bussei* DSM 109896^T with the lower bacterioruberin content at 10 °C exhibited higher average anisotropy values than *A. agilis* strain DSM 20550^T. Nevertheless, the membrane fluidity in both species was almost constant over the entire measured temperature range indicating a membrane fluidizing effect of the *Arthrobacter* carotenoids at low temperatures.

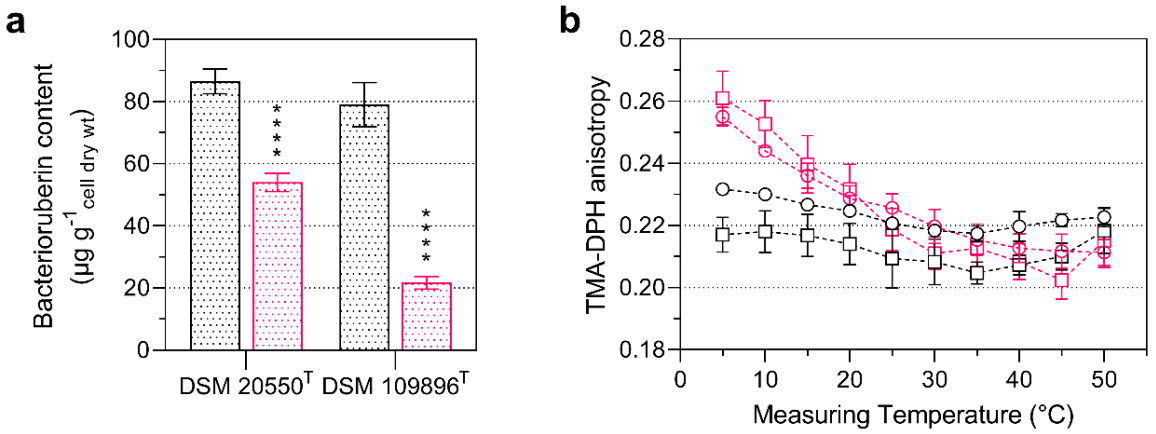

Figure 5.1 Temperature-dependent bacterioruberin content and membrane fluidity. a Total bacterioruberin content of strains *Arthrobacter agilis* DSM 20550^T and *Arthrobacter bussei* DSM 109896^T grown at 10 °C (black) or 30 °C (red). b Membrane fluidity analyzed by TMA-DPH anisotropy of strains *Arthrobacter agilis* DSM 20550^T (squares) and *Arthrobacter bussei* DSM 109896^T (circles) grown at 10 °C (black) and 30 °C (red). Values are means ± standard deviation (a: $n = 6$, b: $n = 3$). Asterisks represent p values (*$p < 0.001$, **$p < 0.0001$, ***$p < 0.00001$, ****$p < 0.000001$) compared to cultures grown at 10 °C (colour figure online)

To confirm the effects of bacterioruberin content on membrane fluidity, we suppressed its synthesis for both *Arthrobacter* species by diphenylamine supplementation, according to Hammond & White (1970). Diphenylamine concentrations of 25, 50, and 75 µM significantly reduced the bacterioruberin content in both tested species grown at 10 °C (data not shown). This approach, however, proved to be unsuitable because diphenylamine itself significantly alters membrane properties due to its lipophilic character, as already mentioned by Seel *et al.* (2020). Alternatively, to verify the effect of bacterioruberin on membrane fluidity, we suppressed bacterioruberin synthesis by adding sodium chloride (NaCl), as achieved previously by Fong *et al.* (2001). A correlation between NaCl concentration and bacterioruberin synthesis was already reported for *A. agilis* and *S. xylosus*. We detected a similar correlation for *A. agilis* DSM 20550^T but not for *A. bussei* DSM

109896^T (Fig. 5.2a). Supplementation of 2, 3, or 4% (wt/vol) NaCl significantly reduced the bacterioruberin content of *A. agilis* by about 64.2, 70.9, or 72.4%, respectively. This allows verifying the effect of bacterioruberin on the biophysical parameters of the cell membrane without changing the cultivation temperature. The decreased bacterioruberin content of *A. agilis* showed a clear impact on membrane fluidity (Fig. 5.2b). The anisotropy values showed a similar progression of the phase transition pattern between *A. agilis* cells grown at 30 °C and cells supplemented with 4% NaCl at 10 °C. This resulted in a loss of membrane fluidity at low temperatures. On the other hand, *A. bussei* retained a higher membrane fluidity, which is related to the almost unchanged bacterioruberin content. These results confirmed that the measured effect on membrane fluidity was due to the cells' bacterioruberin content.

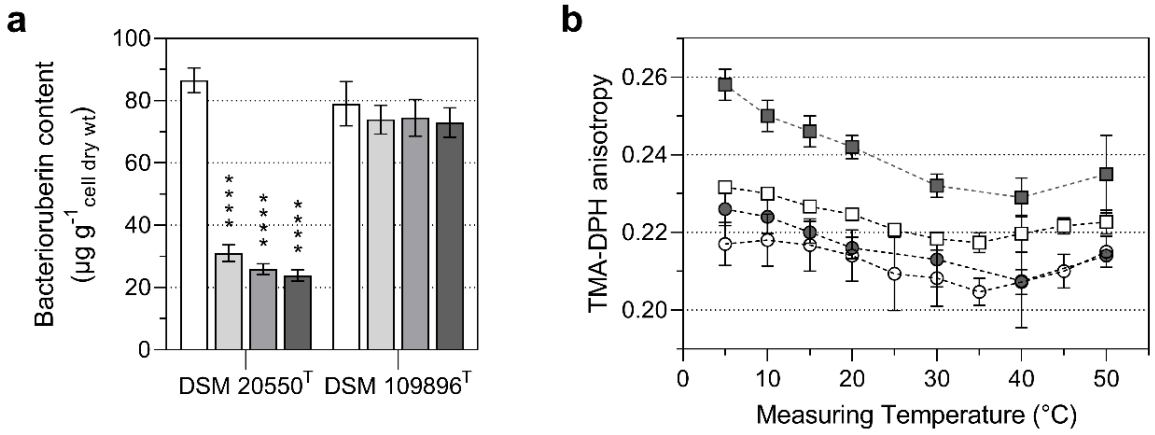

Figure 5.2 Sodium chloride (NaCl)-dependent bacterioruberin content and membrane fluidity. (a) Total bacterioruberin content of strains *Arthrobacter agilis* DSM 20550^T and *Arthrobacter bussei* DSM 109896^T grown at 10 °C in tryptic soy broth supplemented with 0% (white), 2% (light grey), 3% (grey) or 4% (dark grey) (wt/vol) NaCl. (b) Membrane fluidity analyzed by TMA-DPH anisotropy of strains *Arthrobacter agilis* DSM 20550^T (squares) and *Arthrobacter bussei* DSM 109896^T (circles) grown at 10 °C in tryptic soy broth without NaCl (white) or with 4% (wt/vol) NaCl (dark grey). Values are means ± standard deviation (n = 3). Asterisks represent p values (*p < 0.001, **p < 0.0001, ***p < 0.00001, ****p < 0.000001) compared to cultures grown at 10 °C

Bacterioruberin content affects resistance to temperature stress

It is unknown if the thermotropic phase transition by higher amounts of bacterioruberin finally impacts bacterial cell fitness under low-temperature conditions. In this study, using the term fitness as a quantitative attribute for the survival of an external stressor, the fitness of bacterial cells was tested by exposing them to freeze-thaw stress. Freeze-thaw stress resistance is a recognized indicator of cell membrane integrity and bacterial cell fitness (Carlquist *et al.* 2012; Flegler *et al.* 2021; Sleight *et al.* 2006). To confirm the correlation between bacterioruberin content and cell fitness, we achieved a reduced bacterioruberin content in both strains by cultivation at 30 °C. The freeze-thaw stress test was performed according to Flegler *et al.* (2021). Indeed, freeze-thaw stress tests

showed the positive effect of bacterioruberin on membrane integrity. *A. agilis* and *A. bussei* significantly reduced the number of viable cells grown at 30 °C compared to cultures grown at 10 °C (Fig.5.3). Cells grown at 30 °C gradually decreased in the number of viable cells after each freeze-thaw cycle to a minimum of about 6.7×10^6 and 3.2×10^6 CFU mL^{-1} for *A. agilis* and *A. bussei*, respectively, after the third freeze-thaw step. Almost no reduction in viable cells was measured for *A. bussei* grown at 10 °C. In contrast, *A. agilis* grown at 10 °C showed a slight decrease of viable cells after the second freeze-thaw step. These results confirmed the beneficial effect of an elevated bacterioruberin content on cell membrane integrity at 10 °C in both species.

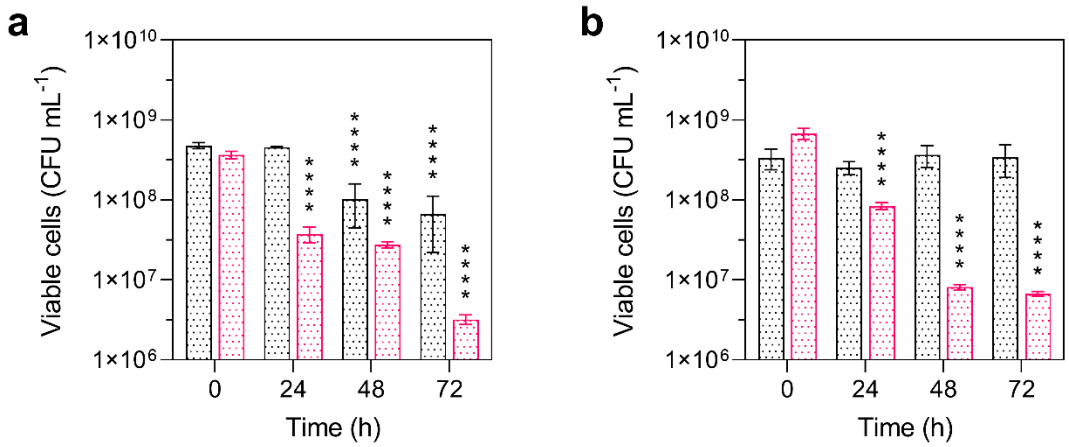

Figure 5.3 Freeze-thaw stress test. Viable cell count of strains **a** *Arthrobacter agilis* DSM 20550^T and **b** *Arthrobacter bussei* DSM 109896^T grown at 10 °C (black) and 30 °C (red) in tryptic soy broth after one (24 h), two (48 h) and three (72 h) freeze-thaw cycles. Values are means ± standard deviation (n = 3). Asterisks represent p values (*p < 0.001, **p < 0.0001, ***p < 0.00001, ****p < 0.000001) compared to the initial cell count at 0 h (colour figure online)

Conclusion

This work reveals the beneficial effect of the bacterioruberin content of pink-pigmented *Arthrobacter* species on membrane fluidity under low-temperature conditions. These results strengthen that bacterioruberin is a fatty acid-independent mechanism for regulating membrane fluidity and represents an additional adaptive response to low growth temperatures with a beneficial impact on membrane integrity, as demonstrated by the increased resistance to freeze-thaw stress. The beneficial effect of this rare C_{50} carotenoid on cells of *Arthrobacter* species and other bacterioruberin-producing bacteria may in part explain the successful colonization of low-temperature environments by these organisms.

2 Materials and methods

Materials

All chemical reagents and solvents were purchased from Alfa Aesar, Carl Roth, MilliporeSigma, Sigma-Aldrich, Thermo Fisher Scientific, and VWR. Solvents and water for analytics were of HPLC grade and used as received.

Bacterial strains, culture media, and cultivation

In this research, we examined two *Arthrobacter* strains. *A. agilis* DSM 20550^T was isolated in 1981, and *A. bussei* DSM 109896^T was isolated from cheese made of cow's milk in 2018. Both species belong to the "Pink *Arthrobacter agilis* group" within the "*Arthrobacter agilis* group" and showed a more intense pigmentation at low growth temperatures (Flegler *et al.* 2020).

All species were aerobically cultured in 100 mL tryptic soy broth (TSB). TSB contained 17.0 g peptone from casein L^{-1}, 3.0 g peptone from soy L^{-1}, 2.5 g D-glucose L^{-1}, 5.0 g sodium chloride L^{-1}, and 2.5 g dipotassium hydrogen phosphate L^{-1} using 300 mL Erlenmeyer flasks. Growth in the TSB was documented by optical density (OD) at 625 nm with a GENESYS 30 visible spectrophotometer (Thermo Fisher Scientific, USA). Cultures were prepared in independent replicates, inoculated with 1% (vol/vol) of overnight culture, and incubated on an orbital shaker at 10 or 30 °C and 150 rpm in the dark until late exponential phase (OD_{625nm} = 1–1.2). Cultures were harvested by centrifugation (10000 × *g* for 10 min) at growth temperature and washed thrice with sterile phosphate-buffered saline (PBS), which was adjusted to growth temperature, pH 7.4. Subsequently, this biomass was used for carotenoid analysis, membrane fluidity measurement, and freeze-thaw stress test. Colonies were cultivated on tryptic soy agar (TSA) containing 15.0 g peptone from casein L^{-1}, 5.0 g peptone from soy L^{-1}, 5.0 g sodium chloride L^{-1}, and 15.0 g agar-agar L^{-1} at 30 °C.

To determine colony-forming units (CFU) for the freeze-thaw stress test, serial dilutions were plated on TSA (90 mm Petri dish) using the exponential mode (ISO 4833-2, ISO 7218, and AOAC 977.27) of the easySpiral automatic plater (Interscience, France). After incubation for 48 h at 30 °C, the CFU were counted for the corresponding dilution steps, and the weighted average of enumerated *Arthrobacter* sp. was given in CFU mL^{-1}. The results for the temperature stress test were presented as viable cells (CFU mL^{-1}).

Statistical evaluation

Statistical analysis was performed using Prism (version 9.2.0; GraphPad Software, United States). Mean values (*M*) and standard deviations (SD) of *n* (see legends) biological replicates were calculated for all experiments. Two-way ANOVA was performed with the recommended post hoc test

($\alpha = 0.001$). Data are presented as $M \pm SD$; *$p < 0.001$, **$p < 0.0001$, ***$p < 0.00001$, ****$p < 0.000001$.

References

Bowman JP, McCammon SA, Brown MV, Nichols DS, McMeekin TA (1997) Diversity and association of psychrophilic bacteria in Antarctic sea ice. *Appl Environ Microbiol* 63:3068–3078

Busse H-J (2016) Review of the taxonomy of the genus *Arthrobacter*, emendation of the genus *Arthrobacter sensu lato*, proposal to reclassify selected species of the genus *Arthrobacter* in the novel genera *Glutamicibacter* gen. nov., *Paeniglutamicibacter* gen. nov., *Pseudoglutamicibacter* gen. nov., *Paenarthrobacter* gen. nov. and *Pseudarthrobacter* gen. nov., and emended description of *Arthrobacter roseus*. *Int J Syst Evol Microbiol* 66:9–37

Carlquist M, Fernandes RL, Helmark S, Heins A-L, Lundin L, *et al.* (2012) Physiological heterogeneities in microbial populations and implications for physical stress tolerance. Microb Cell Factories 11:94

Chattopadhyay MK, Jagannadham MV, Vairamani M, Shivaji S (1997). Carotenoid pigments of an antarctic psychrotrophic bacterium *Micrococcus roseus*: temperature dependent biosynthesis, structure, and interaction with synthetic membranes. *Biochem Biophys Res Commun* 239:85–90

Chaturvedi VK, Ramakrishna Kurup CK (1986) Interaction of lutein with phosphatidylcholine bilayers. *Biochim Biophysic Acta Biomembr* 860:286–292

Conn HJ, Dimmick I (1947) Soil bacteria similar in morphology to *Mycobacterium* and *Corynebacterium*. *J Bacteriol* 54:291–303

Flegler A, Runzheimer K, Kombeitz V, Mänz AT, Heidler von Heilborn D, *et al.* (2020) *Arthrobacter bussei* sp. nov., a pink-coloured organism isolated from cheese made of cow's milk. *Int J Syst Evol Microbiol* 70:3027–3036

Flegler A, Kombeitz V, Lipski A (2021) Menaquinone-mediated regulation of membrane fluidity is relevant for fitness of *Listeria monocytogenes*. *Arch Microbiol* 203:3353–3360

Fong NJC, Burgess ML, Barrow KD, Glenn DR (2001) Carotenoid accumulation in the psychrotrophic bacterium *Arthrobacter agilis* in response to thermal and salt stress. *Appl Microbiol Biotechnol* 56:750–756

Giani M, Martínez-Espinosa RM (2020) Carotenoids as a protection mechanism against oxidative stress in *Haloferax mediterranei*. *Antioxidants* 9:1060

Gruszecki WI (2004) Carotenoid orientation: Role in membrane stabilization. In: Krinsky NI, Mayne ST, Sies H (eds) *Carotenoids in health and disease*. CRC Press, Boca Raton

Hammond RK, White DC (1970) Inhibition of vitamin K_2 and carotenoid synthesis in *Staphylococcus aureus* by diphenylamine. *J Bacteriol* 103:611–615

Holt NE, Zigmantas D, Valkunas L, Li X-P, Niyogi KK, Fleming GR (2005) Carotenoid cation formation and the regulation of photosynthetic light harvesting. *Science* 307:433–436

Kaiser P, Surmann P, Vallentin G, Fuhrmann H (2007) A small-scale method for quantitation of carotenoids in bacteria and yeasts. *J Microbiol Methods* 70:142–149

Knothe G, Dunn RO (2009) A comprehensive evaluation of the melting points of fatty acids and esters determined by differential scanning calorimetry. *J Am Oil Chem Soc* 86:843–856

Lazrak T, Milon A, Wolff G, Albrecht A-M, Miehé M, *et al.* (1987) Comparison of the effects of inserted C_{40}- and C_{50}-terminally dihydroxylated carotenoids on the mechanical properties of various phospholipid vesicles. *Biochim Biophysic Acta Biomembr* 903:132–141

Mandelli F, Miranda VS, Rodrigues E, Mercadante AZ (2012) Identification of carotenoids with high antioxidant capacity produced by extremophile microorganisms. *World J Microbiol Biotechnol* 28:1781–1790

Miller NJ, Sampson J, Candeias LP, Bramley PM, Rice-Evans CA (1996) Antioxidant activities of carotenes and xanthophylls. *FEBS Lett* 384:240–242

Milon A, Wolff G, Ourisson G, Nakatani Y (1986) Organization of carotenoid-phospholipid bilayer systems. Incorporation of zeaxanthin, astaxanthin, and their C_{50} homologues into dimyristoylphosphatidylcholine vesicles. *Helv Chim Acta* 69:12–24

Rohmer M, Bouvier P, Ourisson G (1979) Molecular evolution of biomembranes: structural equivalents and phylogenetic precursors of sterols. *Proc Natl Acad Sci USA* 76:847–851

Seel W, Flegler A, Zunabovic-Pichler M, Lipski A (2018) Increased isoprenoid quinone concentration modulates membrane fluidity in *Listeria monocytogenes* at low growth temperatures. *J Bacteriol* 200:e00148–18.

Seel W, Baust D, Sons D, Albers M, Etzbach L *et al.* (2020) Carotenoids are used as regulators for membrane fluidity by *Staphylococcus xylosus*. Sci Rep 10:330

Shahmohammadi HR, Asgarani E, Terato H, Saito T, Ohyama Y, *et al.* (1998) Protective roles of bacterioruberin and intracellular KCl in the resistance of *Halobacterium salinarium* against DNA-damaging agents. *J Radiat Res* 39:251–262

Sleight SC, Wigginton NS, Lenski RE (2006) Increased susceptibility to repeated freeze-thaw cycles in *Escherichia coli* following long-term evolution in a benign environment. *BMC Evol Biol* 6:104

Strand A, Shivaji S, Liaaen-Jensen S (1997) Bacterial carotenoids 55. C_{50}-carotenoids 25.[†] revised structures of carotenoids associated with membranes in psychrotrophic *Micrococcus roseus*. *Biochem Syst Ecol* 25:547–552

Strzałka K, Gruszecki WI (1994) Effect of β-carotene on structural and dynamic properties of model phosphatidylcholine membranes. I. An EPR spin label study. *Biochim Biophysic Acta Biomembr* 1194:138–142

Subczynski WK, Markowska E, Gruszecki WI, Sielewiesiuk J (1992) Effects of polar carotenoids on dimyristoylphosphatidylcholine membranes: a spin-label study. *Biochim Biophysic Acta Biomembr* 1105:97–108

Subczynski WK, Markowska E, Sielewiesiuk J (1993) Spin-label studies on phosphatidylcholine-polar carotenoid membranes: effects of alkyl-chain length and unsaturation. *Biochim Biophysic Acta Biomembr* 1150:173–181

Sutthiwong N, Fouillaud M, Valla A, Caro Y, Dufossé L (2014) Bacteria belonging to the extremely versatile genus *Arthrobacter* as novel source of natural pigments with extended hue range. *Food Res Int* 65:156–162

Tobias AV, Arnold FH (2006) Biosynthesis of novel carotenoid families based on unnatural carbon backbones: a model for diversification of natural product pathways. *Biochim Biophys Acta Mol Cell Biol Lipids* 1761:235–246

Yabuzaki J (2017) Carotenoids database: structures, chemical fingerprints and distribution among organisms. *Database* 2017:bax004

Yabuzaki J (2020) Carotenoid database. http://carotenoiddb.jp/index.html. Accessed 18 Nov 2021

Chapter 6

Engineered CRISPR/Cas9 system for transcriptional gene silencing in *Arthrobacter* species indicates bacterioruberin is indispensable for growth at low temperatures

Pink-pigmented *Arthrobacter* species produce the rare C_{50} carotenoid bacterioruberin, which is suspected to be part of the cold adaptation mechanism. *In silico* analysis of the repertoire of genes encoded by the *Arthrobacter agilis* and *Arthrobacter bussei* genome revealed the biosynthetic pathway of bacterioruberin. Although genetic analysis is an essential tool for studying the physiology of *Arthrobacter* species, genetic manipulation of *Arthrobacter* is always time and labor-intensive due to the lack of genetic engineering tools. Here we report the construction and application of a CRISPR/deadCas9 system (pCasiART) for gene silencing in *Arthrobacter* species. The engineered system pCasiART is suitable for the Golden Gate assembly of spacers, enabling rapid and accurate construction of adapted systems. In addition, pCasiART has been developed to provide an efficient transcription inhibition system for genome-wide gene silencing. The gene silencing of the phytoene synthase (CrtB), the first enzyme in bacterioruberin biosynthesis, suppressed bacterioruberin biosynthesis in *Arthrobacter agilis* and *Arthrobacter bussei*, resulting in a lack of pink pigmentation, reduction of biomass production and growth rates at low temperatures.

Keywords: *Arthrobacter*; Bacterioruberin; CRISPR/Cas9 system; Transcriptional gene inhibition; Cold adaptation

This chapter is under review as a Short Communication in *Current Microbiology*:

Flegler A., Lipski A. (2022) Engineered CRISPR/Cas9 system for transcriptional gene silencing in *Arthrobacter* species indicates bacterioruberin is indispensable for growth at low temperatures.

Author contributions: AF conceived, designed, performed the experiments, analyzed the data, prepared all figures, and wrote the manuscript; AL reviewed and edited the manuscript.

1 Introduction

Carotenoids are among the most diverse natural pigments found in animals, plants, fungi, bacteria, and archaea. Currently, the Carotenoids Database provides information on 1204 natural carotenoids in 722 source organisms (Yabuzaki 2020). The biosynthesis pathway from isopentenyl pyrophosphate (IPP) and dimethylallyl pyrophosphate (DMAPP) to phytoene is present in most carotenoid-producing bacteria. IPP and its isomer DMAPP are the primary building blocks of carotenoids produced by the mevalonate and the 2-*C*-methyl-D-erythritol 4-phosphate (MEP) pathways in bacteria. Most carotenoids consist of long-chain polyenes synthesized by condensing two C_{20} geranylgeranyl pyrophosphate (GGPP) to phytoene using the phytoene synthase (CrtB). Transformation of phytoene by desaturation, isomerization, cyclization and other modifications leads to the production of various carotenoids (Moise *et al.* 2014). Although numerous bacteria produce carotenoids, and their genomes encode carotenoid biosynthetic pathways, only <10% of these pathways have been experimentally validated (Nupur *et al.* 2016).

The genus *Arthrobacter*, described by Conn and Dimmick (Conn & Dimmick 1947) and amended by Busse (2016), is a common group of bacteria isolated from various sources such as soil, air, food, water, and plants that can produce a wide variety of pigments of different colors, e.g., yellow, red, green and blue (Sutthiwong *et al.* 2014). The C_{50} carotenoid bacterioruberin and its glycosylated derivates are expected to play a crucial role in the cold adaptation of pink-pigmented *Arthrobacter* species, shown by supplementation experiments (Flegler & Lipski 2021; Fong *et al.* 2001). The rarely occurring bacterioruberin is derived from the C_{40} structure by adding two C_5 isoprene units, which may be modified by further desaturation and hydroxylation (Britton *et al.* 2004; Dummer *et al.* 2011; Yang *et al.* 2015). In addition, the production of the acyclic C_{50} carotenoid bacterioruberin is typical in extremely halophilic archaea and psychrophilic bacteria (Sutthiwong *et al.* 2014). Although some *Arthrobacter* species produce bacterioruberin, the biosynthetic pathway in these bacteria has not been elucidated. In addition to that, only a few *Arthrobacter* species have been genetically modified and were studied due to the few existing genetic engineering tools. Nevertheless, although transposon mutagenesis systems and homologous recombination systems have already been developed and performed to create mutants of *Arthrobacter* strains, genetic manipulation is always time-consuming and labor-intensive (Niu *et al.* 2020). For example, knocking out a gene via homologous recombination requires typically two separated crossover steps. First, the editing plasmid is integrated into the target locus by homologous recombination, which is achieved by incubating the cells at a nonpermissive temperature. Second, removal of the integrated plasmid is promoted by growing the cells at a permissive temperature, and loss of the editing

plasmid in the genome is facilitated by a counter-selection method. As a result, the entire genome editing takes a minimum of one week. The discovery of the CRISPR/Cas9 system provides a simple, sequence-specific platform to generate a double-stranded DNA break in the target genome, making it possible to select double-crossing events in one step (Doudna & Charpentier 2014). A previous study by Chen *et al.* (2017) demonstrated that CRISPR/Cas9 was successfully used for genome editing in *Staphylococcus aureus*. Additionally, by converting the active sites, Asp_{10} and His_{840} to Ala of the Cas9 protein, they constructed the highly efficient transcription-inhibition system pCasiSA. One significant advantage of using the CRISPR/Cas9 system for gene silencing is the fast and easy assembly of the genome-targeting module, the spacer, compared with other tools (Chen *et al.* 2017). In addition, a pool of spacers can be readily synthesized using the high-throughput DNA synthesis technique. Using the Golden Gate assembly, it is possible to simultaneously assemble a collection of spacers, enabling rapid and accurate construction of a library for genome-wide studies using the catalytically inactive dead Cas9 protein (Casi9).

Here we decipher in silico the biosynthetic pathway of bacterioruberin of *Arthrobacter* species. Furthermore, we report the construction and application of a CRISPR/deadCas9 system (pCasiART) for gene silencing in *Arthrobacter* species. The engineered system pCasiART is suitable for efficient transcription inhibition and gene silencing. The system was applied here for gene silencing *crtB*, producing the first enzyme in bacterioruberin biosynthesis to suppress bacterioruberin biosynthesis. With this approach, we demonstrated the role of bacterioruberin for growth under low-temperature conditions for pink pigmented *Arthrobacter* strains.

2 Results and discussion

Analysis of genes of the bacterioruberin biosynthetic pathway in the genome of *Arthrobacer agilis* and *Arthrobacter bussei*

The present study revealed in silico the biosynthetic pathway of the carotenoids present in *A. agilis* and *A. bussei* based on bioinformatics data (Fig. 6.1a). Function and pathway analysis was performed using the BlastKOALA web tool of the Kyoto Encyclopedia of Genes and Genomes (KEGG) database (Kanehisa *et al.* 2016). Genome analysis of *A. agilis* strain NCTC2676_1 (GCF_900631605.1) and *A. bussei* strain DSM 109896^T (GCF_009377195.2) revealed that both have all genes involved in the MEP pathway (Rohmer *et al.* 1996) for the synthesis of geranyl pyrophosphate from the isoprenoid precursors IPP, DMAPP and other carotenoid biosynthetic genes. The MEP pathway genes annotated in *A. agilis* are *dxs* (WP_087026194.1), *dxr* (WP_087030629.1), *ispD* (WP_087028001.1), *ispE* (WP_087030977.1), *ispF* (WP_087028003.1), *ispG*/*gcpE* (WP_087030618.1), *ispH* (WP_087029689.1), *idi* (WP_087030401.1), and two homologs

of *idsA* (WP_087025706.1, WP_087030119.1). The MEP pathway genes annotated in *A. bussei* DSM 109896^{T} are *dxs* (WP_152814802.1), *dxr* (WP_152816690.1), *ispD* (WP_152816505.1), *ispE* (WP_152815970.1), *ispF* (WP_152816409.1), *ispG/gcpE* (WP_055772581.1), *ispH* (WP_152812126.1), *idi* (WP_152812423.1), and two homologs of *idsA* (WP_152814964.1, WP_152812421.1).

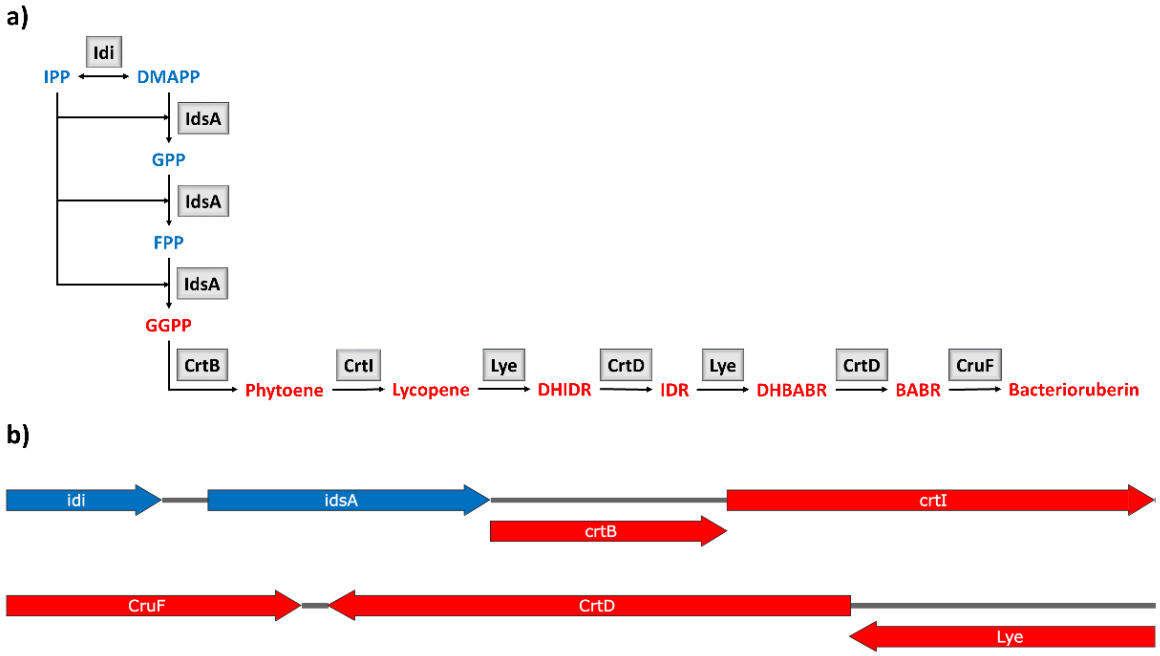

Figure 6.1 (a) Bacterioruberin biosynthesis pathway of *A. agilis* and *A. bussei* and (b) genetic organization of bacterioruberin genes. Intermediates from the 2-*C*-methyl-D-erythritol 4-phosphate (blue) and the bacterioruberin pathway (red) are isopentenyl pyrophosphate (IPP), dimethylallyl pyrophosphate (DMAPP), farnesyl pyrophosphate (FFP), geranylgeranyl pyrophosphate (GGPP), phytoene, lycopene, dihydroisopentenyldehydrorhodopin (DHIDR), isopentenyldehydrorhodopin (IDR), dihydrobisanhydrobacterioruberin (DHBABR), bisanhydrobacterioruberin (BABR) and bacterioruberin. Enzymes involved in different steps of the pathway are isopentenyl pyrophosphate isomerase (Idi), geranylgeranyl pyrophosphate synthase (IdsA), phytoene synthase (CrtB), phytoene desaturase (CrtI), lycopene elongase/hydratase (Lye), carotenoid-3,4-desaturase (CrtD), and bisanhydrobacterioruberin hydratase (CruF).

The functional analysis with BlastKOALA of coding DNA sequence (CDS) revealed genes for potential carotenoid biosynthesis in *A. agilis* and *A. bussei*. However, this analysis annotated only two genes encoding for bacterioruberin biosynthesis. Additional homology analysis, using standard protein BLAST with non-redundant UniProtKB/SwissProt sequences (Altschul *et al.* 1990), revealed candidate genes encoding enzymes for bacterioruberin biosynthesis. WP_158250107.1 (*A. agilis*) and WP_152813953.1 (*A. bussei*) are annotated as squalene/phytoene synthase family protein and had 35% and 36.1% amino acid sequence identity to CrtB of *Streptomyces griseus* and 26.3% and 26.8%, respectively, with that of *Pantoea agglomerans*. Furthermore, WP_179195224.1 (*A. agilis*) and WP_152812419.1 (*A. bussei*) are annotated as phytoene desaturase (CrtI) and had 43.1% and

42.4% amino acid identity with that of *Haloarcula japonica* strain DSM 6131 and 28.7% and 29.1%, respectively, from that of *Staphylococcus aureus* subsp. *aureus* MRSA252. The genes *idi*, *idsA*, *crtB*, and *crtI* cluster in that order on the genome of *A*. *agilis* and *A*. *bussei* (Fig. 6.1b). It is known that the genes related to carotenoid synthesis are arranged in clusters or neighborhoods in some bacteria (Giraud *et al.* 2004; Misawa *et al.* 1990). Based on the pathway annotation using KEGG Database, CrtI was involved in the multistep conversion of phytoene into lycopene. In addition, in the bacterioruberin biosynthetic pathway, lycopene is used as a precursor and converted to bacterioruberin by introducing two C_5 isoprene units, two double bonds, and four hydroxyl groups into lycopene. Pink-pigmented *Arthrobacter* species produce bacterioruberin-type carotenoids (Flegler *et al.* 2020; Fong *et al.* 2001), but the complete pathway for the biosynthesis of bacterioruberin in pink-pigmented *Arthrobacter* species is not yet known. Some coding sequences (CDS) were predicted to be candidate genes encoding enzymes for the biosynthesis of bacterioruberin. For example, lycopene elongase (Lye) catalyzes the committed step in bacterioruberin biosynthesis (Yang *et al.* 2015). Lye converts lycopene into dihydroisopentenyldehydrorhodopin (DHIDR). In the genome of *A*. *agilis* and *A*. *bussei*, WP_087030409.1 and WP_152813957.1 are annotated as UbiA family prenyltransferase showed 37.9% and 38.3% amino acid identity with Lye from *Dietzia* sp. strain CQ4 and 36.8% and 36.3%, respectively, of *Halobacterium salinarum* strain NRC-1. 1-Hydroxy-2-isopentenylcarotenoid 3,4-desaturase (CrtD) further converts DHIDR into isopentenyldehydrorhodopin (IDR), which is converted to dihydrobisanhydrobacterioruberin (DHBABR) by Lye. DHBABR is converted to bisanhydrobacterioruberin (BABR) by CrtD. Homology analysis revealed that WP_087030149.1 of *A*. *agilis* and WP_152812439.1 of *A*. *bussei* are annotated as a phytoene dehydrogenase-related protein had 27.4% and 28.7%, respectively, amino acid identity with CrtD from *Haloarcula japonica*. Bisanhydrobacterioruberin hydratase (CruF) is responsible for the final conversion of BABR into BR in various halophilic bacteria. The protein WP_158250106.1 of A. agilis and WP_191931588.1 of A. bussei are annotated as a carotenoid biosynthesis protein with 44.1% and 42.3%, respectively, amino acid identity with CruF from *H*. *japonica* strain DSM 6131. The genes of Lye, CrtD, and CruF cluster in that order in the genome of *A*. *agilis* and *A*. *bussei* (Fig. 6.1b). Homologs of the carotenoid 1,2-hydratase (CrtC), involved in the spirilloxanthin biosynthetic pathway, could not be found in the genome of *A*. *agilis* and *A*. *bussei*.

Engineering a CRISPR/Cas9 system for gene silencing in *Arthrobacer* species

As demonstrated by the success of Casi9 for transcriptional inhibition in *S*. *aureus* (Chen *et al.* 2017), we designed and constructed the transcription inhibition system pCasiART for use with *Arthrobacter* sp. (Fig. 6.2). Following the approach of Chen *et al.* (2017), we developed the

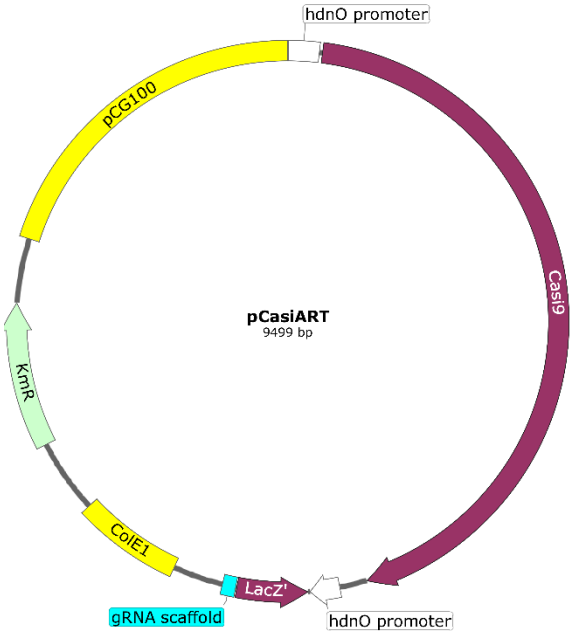

Figure 6.2 Annotated plasmid map of pCasiART. *hdnOp*, promoter of the 6-D-hydroxynicotine oxidase gene (*hdnO*) from plasmid pAO1 used for expression of catalytic inactive dead Cas9 (Casi9) and gRNA scaffold; Casi9, Cas9 protein from *Streptococcus pyogenes* with mutation of Asp_{10} and His_{840}, to Ala; *Bsa*I sites for Golden Gate assembly of the spacer; *lacZα*, a fragment of β-galactosidase for the blue-white screen, spacer insertion site; KmR, the kanamycin-resistance marker in *Escherichia coli* and *Arthrobacter* sp.; ColE1, a replication origin for *E. coli*; *pCG100*, a cryptic fragment from *Corynebacterium glutamicum* ATCC 13058 that can replicate autonomously in *Arthrobacter* species. Created with SnapGene® software (Insightful Science; available at snapgene.com).

analogous system pCasiART, with pART2 (Sandu *et al.* 2005) as the backbone, an effective tool for fast and accurate screening of genes and pathways of interest in *Arthrobacter* species. The detailed functionality of this CRISPR/deadCas9 system has been described previously (Chen *et al.* 2017). Therefore, we adapted the available *S. aureus* transcription inhibition system pCasiSA using the catalytically inactive dead Cas9 protein (Casi9) in *Arthrobacter* strains. An advantageous feature of this system is the presence of two seamless cloning sites. The *Bsa*I sites are used for one-step assembly of spacers by golden gate assembly, and the *Xba*I and *Xho*I sites are used for one-step Gibson assembly-mediated cloning of repair arms for homologous recombination-mediated repair after a DNA double-strand break (Gibson *et al.* 2009). Furthermore, the plasmid pCasSA contains the gene for the well-studied Cas9 protein from *Streptococcus pyogenes* (Anders *et al.* 2014; Nishimasu *et al.* 2014), in which its expression is driven by a strong *rpsL* promoter from *S. aureus*. On the other hand, the transcription of sgRNA is driven by the strong promoter *cap 1A*. Because the *rpsL* and *cap 1A* promoter in *A. agilis* and *A. bussei* has not been detected, we replaced both promoters with the well-studied strong promoter/operator of the 6-D-hydroxynicotine oxidase gene (*hdnO*) from *Arthrobacter oxidans* (Brandsch *et al.* 1986) to drive the expression of Casi9 and sgRNA. The functionality of pART2 was tested in advance with pART2-*gfp* in *A. agilis* DSM 20550^T and *A. bussei* DSM 109896^T. Both strains produced bright fluorescence when electroporated with pART2-*gfp*, confirming the functionality of the *hdnO* promoter for the mentioned purpose.

Silencing crtB reveals that bacterioruberin is indispensable for growth at low temperatures in pink-pigmented *Arthrobacter* species

Bacterioruberin is assumed to support cold adaptation in pink-pigmented *Arthrobacter* species, as indicated by suppression experiments (Flegler & Lipski 2021). Therefore, specific silencing of bacterioruberin synthesis is indispensable to demonstrate the impact of bacterioruberin on cold adaptation and to detect other phenotypes associated with the synthesis of bacterioruberin. So far, there has been no molecular suppression of the bacterioruberin content. Therefore, we silenced the *crtB* gene of *A. agilis* DSM 20550^T and *A. bussei* DSM 109896^T with pCasiART to disrupt the bacterioruberin production. The efficiency of this gene silencing system was evaluated by comparing the bacterioruberin content in cells carrying the empty pCasiART plasmid or the pCasiART plasmid with the *crtB* spacer (pCasiART-*crtB*). The total bacterioruberin was extracted and quantified as described previously (Flegler & Lipski 2021). As shown in Fig. 6.3, the bacterioruberin content in both strains was drastically reduced and below detection limit of 0.2 µg cell dry weight g^{-1} after introducing the spacers, demonstrating the effective transcriptional inhibition caused by the pCasiART system. In addition, colony formation and growth at 20 °C of both strains carrying pCasiART-*crtB* was slower than those carrying pCasiART. At a growth temperature of 10 °C, colony formation of both strains with pCasiART-*crtB* was utterly absent. Thus, these results demonstrate the importance of bacterioruberin biosynthesis at decreasing growth temperature for pink-pigmented *Arthrobacter* strains. After curing the plasmid on TSA plates without kanamycin, we observed that both strains regained their typical pink pigmentation. The experiments were not performed at 30 °C because both species grow very slowly with pCasiART or pART2-*gfp* on TSA with kanamycin at this temperature.

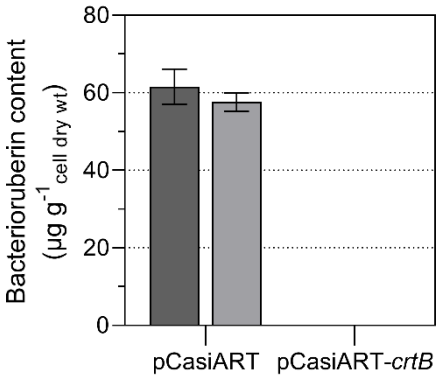

Fig. 6.3 Bacterioruberin content after CRISPR/Cas9-mediated transcription inhibition of *crtB*. Total bacterioruberin content of strains *Arthrobacter agilis* DSM 20550^T (dark grey) and *Arthrobacter bussei* DSM 109896^T (grey) grown at 20 °C. Values are means ± standard deviation (n = 3).

3 Material and methods

Bacterial strains, plasmids, and culture conditions

The bacterial strains and plasmids used in this study are listed in Table 6.1. Plasmids pART2, pART2-*gfp*, and pCasiSA were gratefully provided by Prof. Susanne Fetzner (University of Münster, Germany) and Prof. Dr. Quanjiang Ji (ShanghaiTech University, China), respectively. NEB 5-alpha

Competent *Escherichia coli* (New England Biolabs, UK) cells were used for the molecular cloning procedure and grown in lysogeny broth (LB) or on LB agar plates. Two *Arthrobacter* strains of two different species were examined. Both species belong to the "Pink *Arthrobacter agilis* group" within the "*Arthrobacter agilis* group," showing a more intense pigmentation at low growth temperatures (Flegler *et al.* 2020). *Arthrobacter agilis* DSM 20550^T and *Arthrobacter bussei* DSM 109896^T were aerobically cultured in 100 ml tryptic soy broth (TSB) containing 17 g peptone from casein L^{-1}, 3 g peptone from soy L^{-1}, 2.5 g D-glucose L^{-1}, 5 g sodium chloride L^{-1}, and 2.5 g dipotassium hydrogen phosphate L^{-1} using 300 ml Erlenmeyer flasks or on tryptic soy agar (TSA) plates. Growth in the TSB medium was documented by optical density (OD) at 625 nm with a GENESYS 30 visible spectrophotometer (Thermo Fisher Scientific, USA). Cultures were prepared in independent replicates, inoculated with 1% (vol/vol) of overnight culture, and incubated on an orbital shaker at 10 or 30 °C and 150 rpm in the dark until late exponential phase (OD_{625} = 1-1.2). When appropriate, kanamycin was added to the medium at final concentrations of 140 µg ml^{-1} for *A*. *agilis* or *A*. *bussei* strains after electroporation and 30 µg ml^{-1} for *E*. *coli* after transformation.

Table 6.1 Bacterial strains and plasmids used in this study.

Strains and plasmids	Relevant genotype and description or sequence	Reference or source
Plasmids		
pUC19	Ap^R, *lacZ'*, *ColE1* ori, MCS	Yanisch-Perron *et al.* (1985)
pART2	Km^R, *hdnO* promoter, *pCG100* ori, *ColE1* ori, MCS, His_8-tag	Sandu *et al.* (2005)
pART2-*gfp*	Km^R, *hdnO* promoter, *gfp*, *pCG100* and *ColE1* ori, MCS, His_8-tag	Sandu *et al.* (2005)
pCasiSA	Km^R, Cm^R, *repF* ori, *ColE1* ori, *cap 1A* promoter, *rpsL* promoter, sgRNA, dead Cas9	Chen *et al.* (2017)
pEX-K168_gblock	Synthesized gBlock with *Bsa*I sites containing *hdnO* promoter along with the sgRNA fragment, Km^R, *ColE1* ori	This study
pART2-Casi9	*Sal*I/*Avr*II fragment of PCR-amplified dead Cas9 from pCasiSA in Sali/AvrII of pART2	This study
pART2-Casi9gBlock	*Avr*II/*Bsu36*I fragment containing *hndo* promoter and sgRNA from pEX-K168_gblock in *Avr*II/*Bsu36*I of pART2-Casi9	This study
pART2-Casi9gBlockori*	Substitution in pCG100 ori a_{7320} to g_{7320} of pART2-Casi9gBlock	This study
pCasiART	*Bsa*I fragment of PCR-amplified *lacZ'*, from pUC19 in *Bsa*I of pART2-Casi9gBlockori*	This study
pCasiART-*crtB*	pCasiART with *crtB* spacer in *Bsa*I/*Bsa*I	This study
Strains		
E. coli NEB 5-alpha	*fhuA2Δ(argF-lacZ)U169 phoA glnV44 Φ80 Δ(lacZ)M15 gyrA96 recA1 relA1 endA1 thi-1 hsdR17*	New England Biolabs
Arthrobacter agilis DSM 20550^T	Wild type	Koch *et al.* (1995)
A. agilis pART2-*gfp*	Km^R, *A. agilis* DSM 20550^T carrying pART2-*gfp*	This study
A. agilis pCasiART	Km^R, *A. agilis* DSM 20550^T carrying pCasiART	This study
A. agilis pCasiART-*crtB*	Km^R, *A. agilis* DSM 20550^T carrying pCasiART-*crtB*	This study
Arthrobacter bussei DSM 109896^T	Wild type	Flegler *et al.* (2020)
A.bussei pART2-*gfp*	Km^R, *A. bussei* DSM 109896^T carrying pART2-*gfp*	This study
A. bussei pCasi	Km^R, *A. bussei* DSM 109896^T carrying pCasiART	This study
A. bussei pCasi-*crtB*	Km^R, *A. bussei* DSM 109896^T carrying pCasiART-*crtB*	This study

Construction of pCasiART

Standard DNA manipulation and cloning methods were used (Ausubel 1987). Plasmid Miniprep Kit, DNA Gel Extraction Kit, restriction enzymes, T4 ligase, Q5 High-Fidelity 2X Master Mix, and Q5 Site-Directed Mutagenesis Kit were obtained from New England Biolabs (Ipswich, UK) and used according to the manufacturer's instructions. Oligonucleotides and synthesized gBlock were obtained from Eurofins MWG (Ebersberg, Germany). Primers used in this study are listed in Table 6.2. The pCasiART plasmid was constructed using the following procedures: The gene encoding the catalytically inactive Cas9 was amplified from the pCasiSA plasmid (Chen *et al.* 2017) and inserted into the *Sal*I/*Avr*II sites of the pART2 plasmid (Sandu *et al.* 2005). Next, the hdnO promoter and the sgRNA fragment were synthesized as a gBlock and inserted into the *Bsu36*I/*Avr*II sites of the previously generated plasmid. Afterward, a single-base substitution a_{7320} to g_{7320} was performed to eliminate the hindering *Bsa*I site in the origin of replication *pCG100* for subsequent spacer insertion. Additionally, *lacZα*, *lac* operator, and lac promoter were amplified from the pUC19 plasmid (Yanisch-Perron *et al.* 1985) and inserted into the *Bsa*I/*Bsa*I sites for the blue-white screen of the successfully integrated spacer, resulting in the final pCasiART plasmid. The success of constructing the pCasiART plasmid was verified by PCR, enzyme digestion, and sequencing. Designing the spacers of interest for pCasiART (pCasiART-spacer) with related Golden Gate assembly is explained in detail in the supplementary information. Detailed cloning history of pCasiART is shown in Fig. S6.1.

Table 6.2 Primers used to construct pCasiART and pCasiART-*crtB*.

Name	Sequence (5'-3')	Description
Casi9_F	ATTAGTCGACatggataagaaatactcaataggc (*Sal*I)	amplification of *cas9* from pCasiSA
Casi9_R	TAATCCTAGGttcaccgtcatcaccgaaac (*Avr*II)	amplification of *cas9* from pCasiSA
Q5SDM_a7320g_F	gccaagagagGgaccctacgg	eliminate *Bsa*I site in *pCG100*
Q5SDM_a7320g_R	ctcctttctaggtcgggc	eliminate *Bsa*I site in *pCG100*
LacZ_F	GGAAATGAGACCctatgcggcatcagagcagattgta (*Bsa*I)	amplification of the *lacZ*' from pUC19 plasmid
LacZ_R	AAAACTGAGACCtttacactttatgcttccggctc (*Bsa*I)	amplification of the *lacZ*' from pUC19 plasmid
crtBspacer_F	GAAACGAGTAGCAGCGGATGACCT	spacer for gene silencing *crtB*
crtBspacer_R	AAACAGGTCATCCGCTGCTACTCG	spacer for gene silencing *crtB*

4 Conclusion

The development of the pCasiART system would enable accurate genome-wide and defined screening of gene libraries, which cannot be achieved with conventional screening tools such as transposon-mediated screening in *Arthrobacter* sp. We developed a highly efficient CRISPR/deadCas9-mediated transcriptional inhibition system for *Arthrobacter* sp., enabling fast and accurate screening of genes and pathways responsible for the phenotypes of interest. Furthermore, these results report the first gene silencing in *Arthrobacter* species by a CRISPR/Cas9 system.

Introducing modern DNA assembly techniques into the system would significantly reduce the time and effort required. Further use and optimizations of the pCasiART system should dramatically accelerate various studies in *Arthrobacter* sp. and related bacteria, such as enzymology, natural product extraction, gene characterization, and other basic science research in microbiology as well as interdisciplinary research in chemical biology and synthetic biology.

Supporting information

Detailed protocol concerning designing spacers of interest for pCasiART.

The pCasiART plasmids for transcriptional gene inhibition were assembled using the following protocol:

1. **Oligo Design**
   A 20 bp-spacer sequence was selected before 5'-NGG-3' (5'-NGG-3' was not included in the spacer) the target gene. A ratio of 40~60% GC is the best. The two oligos were synthesized in the following form:
   Oligo I: 5'- GAAANNNNNNNNNNNNNNNNNNN -3'
   Oligo II: 3'-NNNNNNNNNNNNNNNNNNNCAAA -5'

2. **Phosphorylation**

2 µl	Oligo I (50 µM)
2 µl	Oligo II (50 µM)
5 µl	T4 DNA Ligase Buffer (10x) (NEB)
1 µl	T4 Polynucleotide Kinase (NEB)
40 µl	Nuclease-free H_2O
50 µl	

   Incubated at 37 °C for 1 h.

3. **Annealing**
   2.5 µl of 1 M NaCl was added to the phosphorylated oligo pairs, incubated at 95 °C for 3 min, and slowly cooled down to room temperature using a thermocycler. Next, the annealed oligos were diluted 20 times using Nuclease-free H_2O.

4. **Golden Gate assembly**

xx µl	20 fmol pCasi9ART plasmid	
1 µl	diluted annealed oligos (100 fmol)	
0.5 µl	T4 DNA Ligase Buffer (10x) (NEB)	
0.5 µl	T4 Polynucleotide Kinase (NEB)	
xx µl	Nuclease-free H_2O	
10 µl		
37 °C	2 min	} 25 cycles
16 °C	5 min	
50 °C	5 min	
80 °C	15 min	
10 °C	infinite	

5. **Transformation**

   10 µl product of Golden Gate assembly was transformed into 100 µl 5-alpha Competent *E. coli* cells (NEB). White colonies were selected via blue/white screening on an LB agar plate containing 80 µg X-gal ml^{-1}, 0.3 mM IPTG, and 30 µg kanamycin ml^{-1}. The success of constructing the pCasiART-spacer plasmid was verified by PCR or sequencing.

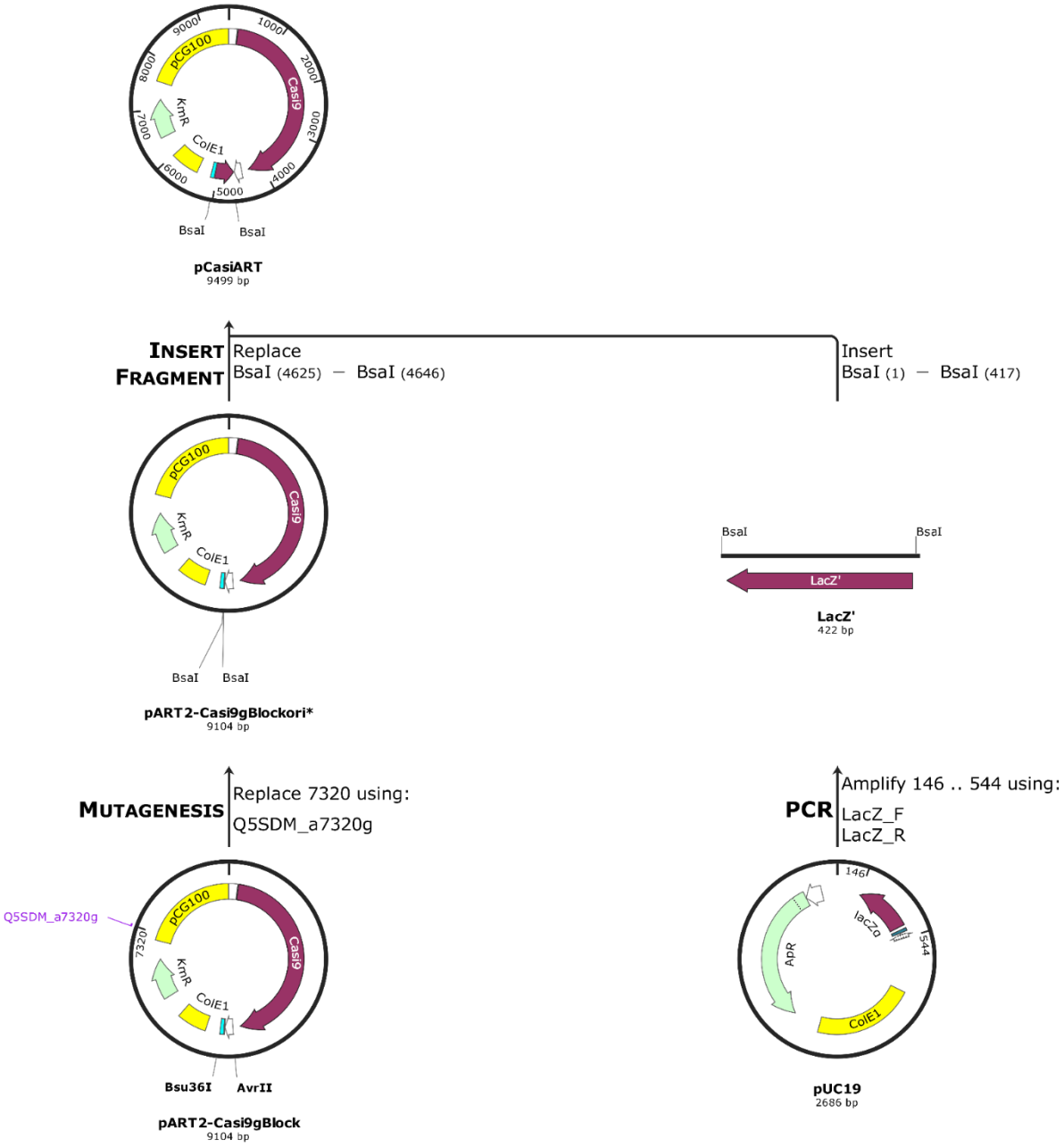

Fig. S6.1 Construction history of pCasiART with pART2 as the backbone. Created with SnapGene® software (Insightful Science; available at snapgene.com)

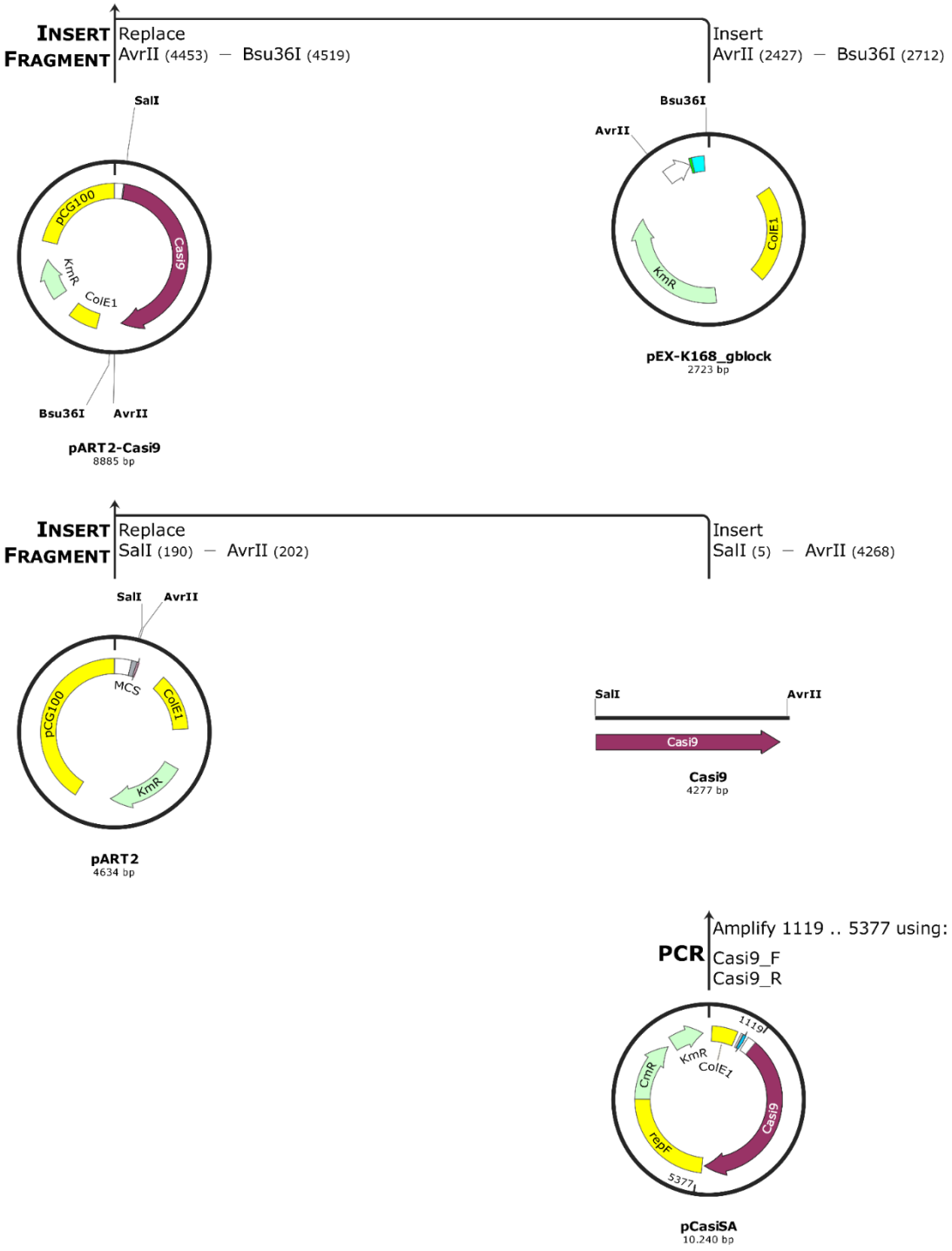

(continued) Fig. S6.1 Construction history of pCasiART with pART2 as the backbone. Created with SnapGene® software (Insightful Science; available at snapgene.com)

References

Altschul SF, Gish W, Miller W, Myers EW, Lipman DJ (1990) Basic local alignment search tool. *J Mol Biol* 215:403–410

Anders C, Niewoehner O, Duerst A, Jinek M (2014) Structural basis of PAM-dependent target DNA recognition by the Cas9 endonuclease. *Nature* 513:569–573

Ausubel FM (1987) *Current protocols in molecular biology*. Wiley, New York

Brandsch R, Faller W, Schneider K (1986) Plasmid pAO1 of *Arthrobacter oxidans* encodes 6-hydroxy-D-nicotine oxidase: cloning and expression of the gene in *Escherichia coli*. *Mol Gen Genet* 202:96–101

Britton G, Liaaen-Jensen S, Pfander H (2004) *Carotenoids*. Birkhäuser, Basel

Busse H-J (2016) Review of the taxonomy of the genus *Arthrobacter*, emendation of the genus *Arthrobacter sensu lato*, proposal to reclassify selected species of the genus *Arthrobacter* in the novel genera *Glutamicibacter* gen. nov., *Paeniglutamicibacter* gen. nov., *Pseudoglutamicibacter* gen. nov., *Paenarthrobacter* gen. nov. and *Pseudarthrobacter* gen. nov., and emended description of *Arthrobacter roseus*. *Int J Syst Evol Microbiol* 66:9–37

Chen W, Zhang Y, Yeo W-S, Bae T, Ji Q (2017) Rapid and efficient genome editing in *Staphylococcus aureus* by using an engineered CRISPR/Cas9 system. *J Am Chem Soc* 139:3790–3795

Conn HJ, Dimmick I (1947) Soil bacteria similar in morphology to *Mycobacterium* and *Corynebacterium*. *J Bacteriol* 54:291–303

Doudna JA, Charpentier E (2014) Genome editing. The new frontier of genome engineering with CRISPR-Cas9. *Science* 346:1258096

Dummer AM, Bonsall JC, Cihla JB, Lawry SM, Johnson GC, Peck RF (2011) Bacterioopsin-mediated regulation of bacterioruberin biosynthesis in *Halobacterium salinarum*. *J Bacteriol* 193:5658–5667

Flegler A, Lipski A (2021) The C_{50} carotenoid bacterioruberin regulates membrane fluidity in pink-pigmented *Arthrobacter* species. *Arch Microbiol* 204:70

Flegler A, Runzheimer K, Kombeitz V, Mänz AT, Heidler von Heilborn D *et al.* (2020) *Arthrobacter bussei* sp. nov., a pink-coloured organism isolated from cheese made of cow's milk. *Int J Syst Evol Microbiol* 70:3027–3036

Fong NJC, Burgess ML, Barrow KD, Glenn DR (2001) Carotenoid accumulation in the psychrotrophic bacterium *Arthrobacter agilis* in response to thermal and salt stress. *Appl Microbiol Biotechnol* 56:750–756

Gibson DG, Young L, Chuang R-Y, Venter JC, Hutchison CA, Smith HO (2009) Enzymatic assembly of DNA molecules up to several hundred kilobases. *Nat Methods* 6:343–345

Giraud E, Hannibal L, Fardoux J, Jaubert M, Jourand P *et al.* (2004) Two distinct *crt* gene clusters for two different functional classes of carotenoid in *Bradyrhizobium*. *J Biol Chem* 279:15076–15083

Kanehisa M, Sato Y, Morishima K (2016) BlastKOALA and GhostKOALA: KEGG tools for functional characterization of genome and metagenome sequences. *J Mol Biol* 428:726–731

Koch C, Schumann P, Stackebrandt E (1995) Reclassification of *Micrococcus agilis* (Ali-Cohen 1889) to the genus *Arthrobacter* as *Arthrobacter agilis* comb. nov. and emendation of the genus *Arthrobacter*. Int J Syst Bacteriol 45:837–839

Misawa N, Nakagawa M, Kobayashi K, Yamano S, Izawa Y, *et al.* (1990) Elucidation of the *Erwinia uredovora* carotenoid biosynthetic pathway by functional analysis of gene products expressed in *Escherichia coli*. *J Bacteriol* 172:6704–6712

Moise AR, Al-Babili S, Wurtzel ET (2014) Mechanistic aspects of carotenoid biosynthesis. *Chem Rev* 114:164–193

Nishimasu H, Ran FA, Hsu PD, Konermann S, Shehata SI, *et al.* (2014) Crystal structure of Cas9 in complex with guide RNA and target DNA. *Cell* 156:935–949

Niu H, Sun X, Song J, Zhu C, Chen Y, *et al.* (2020) Knockout of *pde* gene in *Arthrobacter* sp. CGMCC 3584 and transcriptomic analysis of its effects on cAMP production. *Bioprocess Biosyst Eng* 43:839–850

Nupur LNU, Vats A, Dhanda SK, Raghava GPS, Pinnaka AK, Kumar A (2016) ProCarDB: a database of bacterial carotenoids. *BMC Microbiol* 16:96

Rohmer M, Seemann M, Horbach S, Bringer-Meyer S, Sahm H (1996) Glyceraldehyde 3-phosphate and pyruvate as precursors of isoprenic units in an alternative non-mevalonate pathway for terpenoid biosynthesis. *J Am Chem Soc* 118:2564–2566

Sandu C, Chiribau C-B, Sachelaru P, Brandsch R (2005) Plasmids for nicotine-dependent and -independent gene expression in *Arthrobacter nicotinovorans* and other *Arthrobacter* species. *Appl Environ Microbiol* 71:8920–8924

Sutthiwong N, Fouillaud M, Valla A, Caro Y, Dufossé L (2014) Bacteria belonging to the extremely versatile genus *Arthrobacter* as novel source of natural pigments with extended hue range. *Food Res Int* 65:156–162

Yabuzaki J (2020) Carotenoid Database. http://carotenoiddb.jp/index.html. Accessed 10 January 2022

Yang Y, Yatsunami R, Ando A, Miyoko N, Fukui T *et al.* (2015) Complete biosynthetic pathway of the C_{50} carotenoid bacterioruberin from lycopene in the extremely halophilic archaeon *Haloarcula japonica*. *J Bacteriol* 197:1614–1623.

Yanisch-Perron C, Vieira J, Messing J (1985) Improved M13 phage cloning vectors and host strains: nucleotide sequences of the M13mpl8 and pUC19 vectors. *Gene* 33:103–119

Concluding remarks

Due to widespread low temperatures on Earth, both natural and anthropogenic, and the concomitant need for bacteria to survive and persist, adaptation of their membranes is challenging. Since bacterial membranes are adapted to distinct temperatures, shifting to cold temperatures can lead to physiological arrest. Therefore, it is of utmost importance to identify the underlying adaptive mechanisms of living nature, understand them and subsequently control them for applied biotechnology, food microbiology, and food safety. Furthermore, because bacterial cold adaptation relies primarily on the restricted mechanism of *de novo* synthesis of endogenous fatty acids, other adaptive mechanisms may likely alter the physicochemical state of membranes. In this thesis, unusual cold adaptation mechanisms by exogenous fatty acids (Chapter 2) or menaquinones (Chapter 3) in *L. monocytogenes* and carotenoids (Chapters 5 and 6) in the novel pink pigmented *Arthrobacter* sp. (Chapter 4) were investigated to assess the effects on their membranes.

Effects of exogenous fatty acids in *Listeria monocytogenes*

According to the current state of research, membrane adaptation to low temperatures is accomplished by changing the fatty acid composition endogenously. This system has been studied for several decades and provides an established functional description of cell membrane adaptation to constantly changing environmental factors such as pressure, acidity or basicity, osmolarity, and temperature. Endogenous fatty acids with low melting temperatures are incorporated into the membrane at low temperatures, thus maintaining an active physiological membrane for membrane-dependent processes. Depending on the nature of the fatty acid modification in question, adaptation requires modification of pre-existing fatty acids, such as insertion of a double bond by desaturases, or, in most cases, changing the chain length or degree of branching by *de novo* synthesis of the corresponding lipids. However, the latter point represents an energy-intensive process. Moreover, considering the limiting environmental factors for bacteria during growth, the constant re-synthesis of lipids should be a significant disadvantage since biomass is not continuously rebuilt. Another way of membrane adaptation has been described for some bacteria by uptake and incorporating fatty acids from the environment. This adaptation mechanism has not been suspected for *L. monocytogens*, as most publications have argued against it.

The survival nature of *L*. *monocytogenes* seems to depend highly on its ability to survive at a wide temperature range. It also possesses various molecular adaptation mechanisms to survive at low temperatures. Part of the cold adaptation occurs by altering the fatty acid composition, or what is known as homeoviscous adaptation, as mentioned earlier, to maintain optimal membrane fluidity. The foodborne pathogen responds to the temperature change by inserting fatty acids with a low melting point into the membrane to correspondingly lower the transition temperature from the liquid-crystalline phase to the gel phase. Although this modification of the fatty acid profile usually involves only endogenous fatty acids, this does not rule out the possibility of incorporating exogenous fatty acids into the membrane. Some Gram-positive bacteria were found to be able to insert certain fatty acids in their membrane, which eventually led to a change both in the lipid composition and the fluidity of the membrane. Polysorbate 80 was already known as an essential growth factor for some Gram-positive bacteria because primarily it consists of a polyoxyethylene sorbitan derivative of oleic acid, which happens to be the source of the required low-melting temperature fatty acid. Due to the bound oleic acid, the latest findings showed that Polysorbate 80 is a beneficial compound under cold and anaerobiosis in *B*. *cereus*. Therefore, the oleic acid in Polysorbat 80 is also expected to impact the cold adaptation of *L*. *monocytogenes*. Polysorbate 60 was chosen because it possesses a high content of fatty acids with a high melting temperature, for instance, palmitic and stearic acid. Additionally, Polysorbate 60 and Polysorbate 80 were supplemented as an equimolar mixture to determine the selectivity and extent of *L*. *monocytogenes* in terms of incorporating only fatty acids with a low melting temperature from the medium. In addition, lipid extracts from foods such as smoked salmon, minced meat, and milk, which are often contaminated by *L*. *monocytogenes*, were also tried as possible fatty acid-supplying additives.

Surprisingly, all tested *L*. *monocytogenes* strains could incorporate exogenous fatty acids from the environment, revealing significant complementation in the fatty acids profile when exogenous fatty acids were present, regardless of their source and the temperature (Chapter 2). This result is consistent with previous findings showing that the successful incorporation of exogenous fatty acids into the bacterial membrane requires much less energy and metabolic building material than the very energy- and material-intensive biosynthesis of the fatty acids. The remaining energy can therefore be used for other cellular functions. The exogenous supply of fatty acids can influence the endogenous fatty acid profile. Furthermore, additional research demonstrated that exogenous fatty acids could not bypass the inhibition of FASII in *Bacillales* because branched-chain *anteiso*-$C_{15:0}$ fatty acids are essential for proper membrane function. On the one hand, the decrease in *anteiso*-$C_{15:0}$ could be due to this partial inhibition. On the other hand, there is also a high probability that this phenomenon is actually due to the production of *anteiso*-$C_{17:0}$. Furthermore, incorporating

exogenous fatty acids modified the menaquinone content, changing membrane fluidity and growth properties of *L*. *monocytogenes*. Depending on the exogenous fatty acids present, this improves membrane fluidity and cell viability at low growth temperatures. Acyl chain composition has been shown to play a crucial role in *L*. *monocytogenes* survival, and an increase in straight-chain fatty acids reduces the organism's fitness. The influence of external fatty acids from the food matrix significantly impacts the contamination dynamics of chilled foods and should be considered in future food preservation and stability against *L. monocytogenes* colonization.

Fatty acid independent cold adaptation of *Listeria monocytogenes*

The sheer diversity of survival and adaptation mechanisms to low temperatures is also common in other life forms. Thus, homoiothermic eukaryotic cells have evolved a different type of membrane adaptation that is known. The melting point is varied using different fatty acids, but the phase transition is significantly broadened by incorporating sterols such as cholesterol or ergosterol. These lipophilic compounds are present in 20–40 mol% concentrations in eukaryotic plasma membranes but are absent in bacterial membranes. This lipophilic compound reduces the melting point, thus ensuring sufficient membrane fluidity at low temperatures and at the same time ensuring the mechanical robustness of the membrane. This liquid-ordered phase, which can be considered between the gel and liquid-crystalline phase, reinforces the membrane order due to the incorporation of lipophilic substances but still preserves the lateral mobility of the lipids so that the membrane functions are not affected. For cold adaptation, it has already been suspected that menaquinones and carotenoids, as lipophilic molecules of the bacterial membrane, maintain membrane fluidity at low temperatures.

Disruption of menaquinone-dependent membrane fluidization under low-temperature conditions resulted in the overall reduced fitness of *L*. *monocytogenes* (Chapter 3). These results indicate that this fatty acid-independent mechanism for regulating membrane fluidity represents an additional adaptive response to low growth temperatures that positively affects membrane integrity, growth rate, and resistance of bacterial cells to temperature stress. The results suggest that food constituents such as aromatic amino acids and menaquinone, respectively, may influence the growth rates and fitness of certain *L*. *monocytogenes* strains at low temperatures and should be considered in future modeling of food stability to *L*. *monocytogenes* colonization.

Fatty acid-independent cold adaptation in pink-pigmented *Arthrobacter* species

Increased production of pigments at low temperatures has been observed in the past for several bacterial species. Some authors associated this phenomenon with a potential cold adaptation mechanism. However, there has been no experimental evidence for the involvement of the C_{50} carotenoid bacterioruberin in the modification of membrane fluidity at low-temperature conditions and thus in cold adaptation. Although an association of bacterioruberin in bacterial membranes with cold adaptation has been suggested, this has not been investigated. The search for model organisms resulted in a novel bacterioruberin-producing species isolated from cold-stored, ready-to-eat cheese (Chapter 4). Thus, pink-pigmented *Arthrobacter* species were suitable as model organisms producing bacterioruberin for determining the effect of a fatty acid-independent cold adaptation and their influence on membrane fluidity, as was previously done for menaquinones in *L*. *monocytogenes* and carotenoids in *S*. *xylosus*.

This work demonstrates for the first time that bacterioruberin is part of the cold adaptation in pink-pigmented *Arthrobacter* sp. by altering membrane fluidity and fitness by increasing the bacterioruberin content in the membrane (Chapter 5). This improved membrane fluidity at low temperatures and is consistent with previous findings in artificial liposomes and *S*. *xylosus*. A significant increase in bacterioruberin incorporation was observed for pink-pigmented species *A*. *bussei* and *A*. *agilis*., showing a fatty acid-independent cold adaptation of the cell membrane, as previously shown for menaquinones.

Additionally, the pCasiART system's development would enable accurate genome-wide and defined screening of gene libraries, which cannot be achieved with conventional screening tools such as transposon-mediated screening in *Arthrobacter* sp. (Chapter 6). The highly efficient CRISPR/deadCas9-mediated transcriptional inhibition system for *Arthrobacter* sp. enables fast and accurate screening of genes and pathways responsible for the phenotypes of interest. Introducing modern DNA assembly techniques would significantly reduce the time and effort required. Further use and optimizations of the pCasiART system should dramatically accelerate various studies in *Arthrobacter* sp. and related bacteria, such as enzymology, natural product extraction, gene characterization, and other interdisciplinary research fields.

Acknowledgments

At this point, I would like to express my special thanks to all the people who accompanied and supported me during my doctoral studies at the Department of Microbiology and Hygiene at the University of Bonn, although I am only able to name a choice.

First and foremost, I would like to thank Prof. Dr. André Lipski for the opportunity to work in his department and on this thesis's topics to gain deeper insights into the world of microorganisms. Furthermore, I appreciate the freedom and support with always inspiring and helpful advice and creative discussions, and his trust over the last years.

Furthermore, I would like to thank Priv.-Doz. Dr. Christiana Dahl for being my second supervisor, Prof. Dr. Lukas Schreiber, and Prof. Dr. Ute Weisz for participating in the examination committee.

A special thanks to all students who contributed to this thesis with their enthusiastic support in the laboratory work and the data analysis. Thanks to Katharina, Alicia, Tabea, Janice, Vanessa, Tatjana, Frieda, and Wanda. You have confirmed my conviction that teaching is fun.

A big thanks to all my colleagues, including Mareike, Waldemar, Julia, David, Eva, Bettina, Hildegard, Paula, and Sabine, for the great teamwork and all collaborations and conversations of both a professional and private nature. Thank you for the many great moments, for the many kind words, support, advice, and shared knowledge and friendships. Great gratitude goes to my office colleagues of the past years, Waldemar, David, and Julia, for all our conversations and a working atmosphere in which one always felt comfortable.

Of course, life is not all work. Finally, I want to thank my family and friends for their love and constant support and remind me of life's essential things.